CORE FLOODING STUDY OF CO_2-SOLUBLE POLYMERS FOR IMPROVED MOBILITY CONTROL AND CONFORMANCE CONTROL

by

Husain Zaberi

B.S. in Petroleum Engineering, University of Tulsa, Oklahoma, 2011

Submitted to the Graduate Faculty of

Swanson School of Engineering in partial fulfillment

of the requirements for the degree of

M.S. in Petroleum Engineering

University of Pittsburgh

2016

UNIVERSITY OF PITTSBURGH

SWANSON SCHOOL OF ENGINEERING

This thesis was presented

by

Husain Zaberi

It was defended on

November 17, 2016

and approved by

Robert Enick, Ph.D., Professor, Department of Chemical and Petroleum Engineering

Badie Morsi, Ph.D., Professor, Department of Chemical and Petroleum Engineering

Sachin Velankar, Ph.D., Professor, Department of Chemical and Petroleum Engineering

Thesis Advisor: Robert Enick, Ph.D., Professor, Department of Chemical and Petroleum Engineering

CORE FLOODING STUDY OF CO_2-SOLUBLE POLYMERS FOR IMPROVED MOBILITY CONTROL AND CONFORMANCE CONTROL

Husain Zaberi, M.S.

University of Pittsburgh, 2016

Despite its success in recovering oil as an enhanced oil recovery (EOR) solvent over the past 50 years, the effectiveness of CO_2 is hindered by its low viscosity relative to the oil and water being displaced. This results in an unfavorable mobility ratio that promotes viscous fingering and gravity override, thereby reducing oil recovery. The initial focus of the research was to decrease CO_2 mobility through a long-term injection of a dilute solution of a high molecular weight polyfluoroacrylate (PFA) thickener in CO_2 capable of quadrupling the viscosity of CO_2. However, when thickened CO_2 was used to displace pure CO_2 from sandstone or limestone cores at a constant volumetric flow rate, the pressure drop increased by factors significantly greater than four. Coupled with increased hydrophobicity of the core and the recovery of polymer downstream of the core, it became apparent that some of the polymer remained dissolved in CO_2 solution and passed through the core as desired, but some of the PFA adsorbed onto the core surfaces and dramatically reduced permeability while enhancing hydrophobicity. Therefore, the notion of using PFA as a CO_2 mobility control agent that remains dissolved in CO_2 solution while propagating hundreds of feet from an injection well without suffering adsorption loss was deemed unrealistic. However, the PFA-induced permeability reduction makes PFA an excellent candidate as the first CO_2-soluble conformance control agent. During conformance control, the

intent is to inject a small slug of (CO_2+PFA) solution into the near-wellbore region of a high permeability, watered-out, oil-depleted thief zone, especially if the zone can be temporarily isolated during injection of the PFA solution. If the PFA solution is successful in reducing the permeability of the thief zone, subsequent injection of CO_2 into all zones should result in a much smaller proportion of the CO_2 going into the thief zone and a larger proportion of the CO_2 entering the oil-rich zones. Numerous CO_2-displacing-brine core flooding tests were then conducted to test this hypothesis and conformance control was often achieved with (CO_2+PFA) solutions, especially in parallel sandstone cores.

TABLE OF CONTENTS

LIST OF TABLES

LIST OF FIGURES

LIST OF EQUATIONS

ACKNOWLEDGMENTS

First and foremost, I would like to thank my research supervisor, Dr. Robert Enick. Without his assistance and dedicated involvement in every step throughout this research, this paper would have never been accomplished.

I would also like to thank my lab partner, Jason Lee, for his constructive support and useful comments throughout the lab work in this research.

I would also like to thank the rest of my thesis faculty committee, Dr. Badie Morsi and Dr. Sachin Velankar, for their insightful feedback and thoughtful questions.

Most importantly, none of this could have happened without my family. Everything I am and everything I accomplish are thanks to their unconditional love and infinite support.

I dedicate this work to my twin sister, who has always been and will always be my anchor in life.

NOMENCLATURE

CO_2	Carbon Dioxide
EOR	Enhanced Oil Recovery
USDOE	United States Department of Energy
ROS	Residual Oil Saturation
WAG	Water Alternating with Gas
SAG	Surfactant Alternating with Gas
HCPV	Hydrocarbon Pore Volume
HCPV	Pore Volume
HAP	Hydrophobically Associative Polymer
Wt.%	Weight Percentage
PVT	Pressure Volume Temperature
BPR	Back Pressure Regulator
DSC	Differential Scanning Calorimeter
σ	Interfacial Tension
S_w	Water Saturation
S_{wirr}	Irreducible Water Saturation
S_o	Oil Saturation
S_{CO2}	Carbone Dioxide Saturation

M_w	Molecular Weight
θ_c	Contact Angle
bbl	Barrel of Oil
scf	Standard Cubic Foot
τ	Shear Stress
γ	Shear Rate
η	Coefficient of Viscosity
V_t	Terminal Velocity
γ_c	Shear Rate of a Falling Cylinder
γ_b	Shear Rate of a Falling Ball
r_c	Radius of a Falling Cylinder
r_t	Radius of a Tube
A_c	Area of a Falling Cylinder
$V_{t,sol}$	Terminal Velocity of a Thickened CO_2 Solution
$V_{t,o}$	Terminal Velocity of a Pure CO_2 Solution
μ_{sol}	Viscosity of a Thickened CO_2 Solution
μ_o	Viscosity of a Pure CO_2 Solution
C_i	Polymer's Initial Concentration
C_n	Polymer's New Concentration
$V_{CO_2 injected}$	Volume of CO_2 Injected into a Mixer
V_{mixer}	Volume of a Mixer
K_{e,CO_2}	Effective Permeability of a Rock to CO_2
$K_{e,w}$	Effective Permeability of a Rock to water

W	Weight of a Falling Ball
F_D	Drag Force
F_B	Buoyant Force
C_D	Drag Coefficient
Re	Reynolds Number
μ	Viscosity of a Fluid
ρ_f	Density of a Fluid
ρ_b	Density of a Falling Ball
d_b	Diameter of a Falling Ball

1.0 INTRODUCTION

1.1 CO_2 EOR HISTORY

For many years, the petroleum industry devoted time and efforts for research and development to apply EOR technologies targeting residual oil after waterflooding. The use and implementation of CO_2 as a displacing fluid in EOR programs has been recognized as one of the most promising technologies in the United States with remarkable results over the years. The first utilization of CO_2 in EOR programs was in 1972 by the Scurry Area Canyon Reef Operator Committee (SACROC) Unit of the Kelly Snyder Field in Texas. Due to limited CO_2 sources at the time, the SACROC field was divided into three areas, or phases, of similar hydrocarbon pore volume (HCPV), which were CO_2 flooded consecutively. Ever since that CO_2 EOR program commenced in that field, significant amounts of crude oil were recovered which were mainly attributed to CO_2 injection (Ghahfarokhi, Pennell, Matson, Linroth, & Kinder, 2016).

The United States is still leading the world in the number of implemented CO_2 EOR programs due to the country's favorable geology of the reservoirs and the close proximity between oil fields and regions with CO_2 resources (Gulf Coast, Mid-Continent, Rocky Mountains and Permian Basin). For any EOR program, the possible sources for CO_2 are: 1) natural sources where reservoirs produce gas that is primarily CO_2, 2) natural gas processing sources where reservoirs produce significant amount of CO_2-contaminated methane and 3)

industrial sources where CO_2 is produced as a by-product during the manufacture of CO_2 chemical processing or capturing, and sold to the operators of natural CO_2 pipelines (Verma, 2015).

1.2 CO_2 EOR ECONOMICS

Even though CO_2 EOR technology has demonstrated significant success over the past 50 years in the petroleum industry, it is important to note that there are numerous costs associated with processing both CO_2 and water needed in EOR programs. However, the increasing trend on the number of CO_2 EOR programs suggests a marginal profit involved on the implementation of this technology (Figure 1). In 2012, the United States Department of Energy (USDOE) reported that the US used 2995 MMCF/D of purchased CO_2 to produce 282 MBBL/D of oil, and is predicted to use up to 6418 MMCF/D of CO_2 to produce 615 MBBL/D of oil by the year of 2020 (Wallace & Kuuskraa, 2014).

Currently CO_2 operators in several states are paying roughly $45/ton for high pressure CO_2, which is equivalent to $2.50/1000 scf. This price is typically ratcheted in contracts to New York Mercantile Exchange (NYMEX) crude oil price using factors of 1-3% (e.g. for an oil price of $100/bbl, the CO_2 price would be $1-3/1000scf).

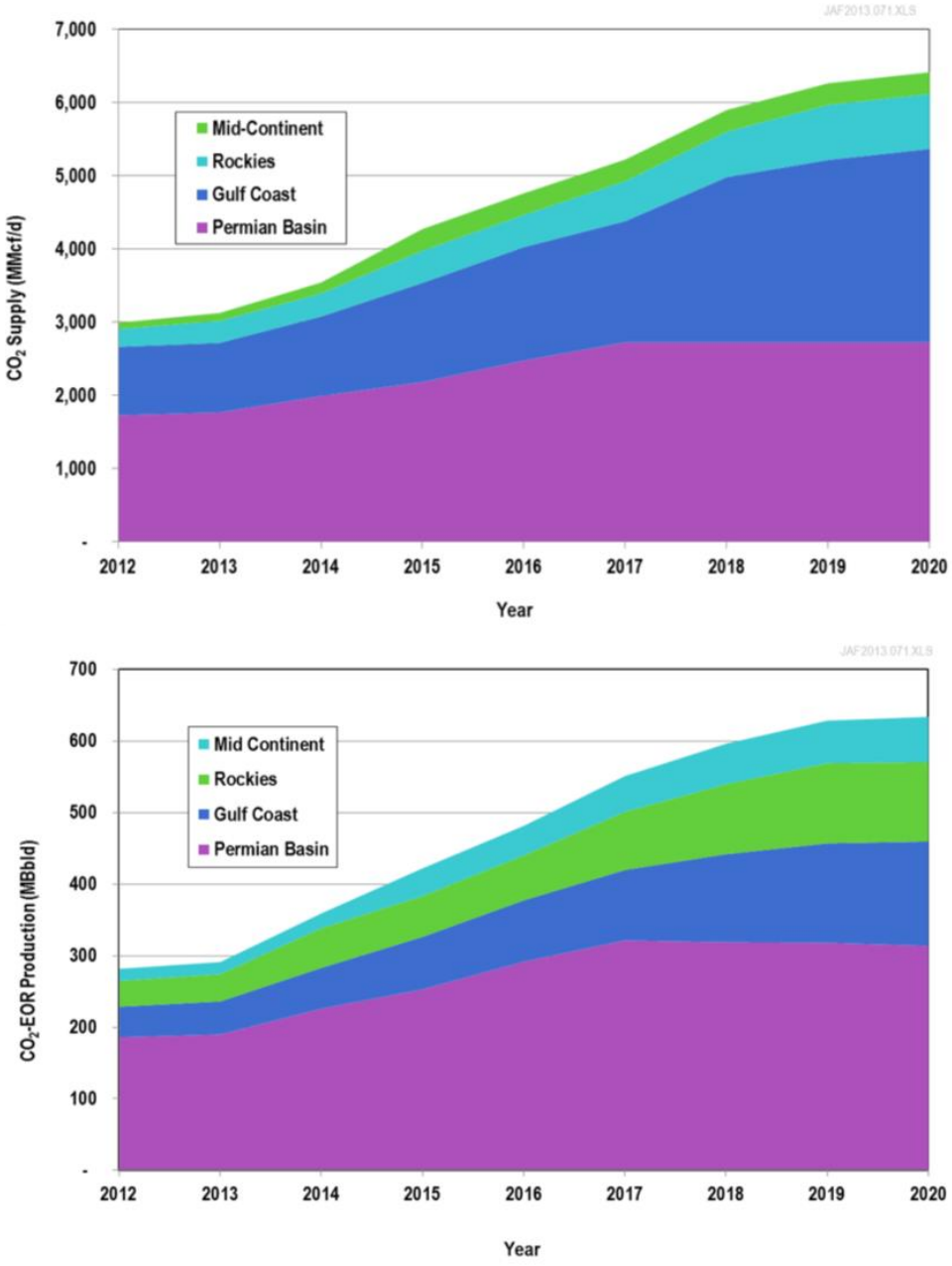

Figure 1. Annual CO_2 EOR Oil Production from EOR Projects **(Wallace & Kuuskraa, 2014)**

1.3 CO_2 EOR PHYSICAL PROPERTIES

The phase diagram for CO_2 (Mw = 44.01 g/mol) is shown in (Figure 2). At ambient conditions, CO_2 is a colorless, odorless gas. The critical pressure and critical temperature values for CO_2 are 1070 psia (72 atm) and 31 °C, respectively. Above the critical temperature, CO_2 is in a supercritical state forming a dense phase with liquid-like density and gas-like low viscosity, both of which are pressure-adjustable (Ennin, Grigg, Center, & Technolog, 2016).

Since most light oil reservoirs are in the (25-125 °C) range and pressures of several thousand psi, the CO_2 injected in these formations is commonly in the supercritical state. Even though CO_2 has a liquid-like density at this state (0.4-0.7 g/cm^3), it is still less dense than the crude oil and brine in the formation, which promotes CO_2 gravity override of the oil. Moreover, the viscosity of CO_2 at these conditions (0.05-0.10 mPa s) is significantly less than typical light oil viscosity (0.5-5.0 mPa s), which leads to an unfavorable mobility ratio, viscous fingering (especially in uniform formations), low oil recovery, high ratios of CO_2 produced to oil produced, and high rates of CO_2 re-cycle and re-compression.

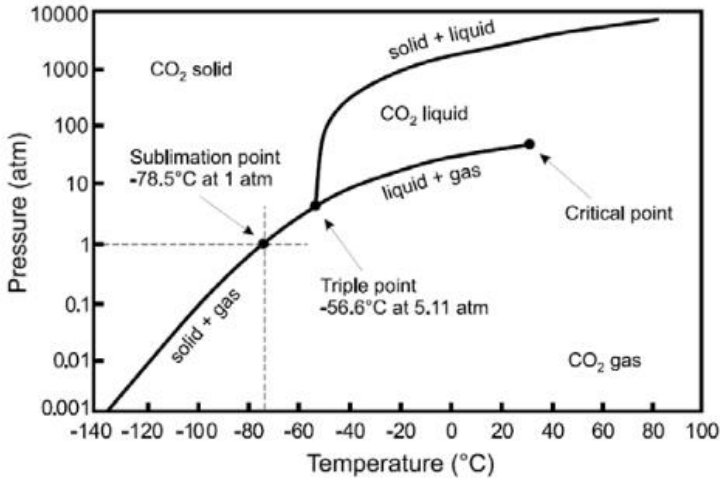

Figure 2. CO_2 Phase Diagram **(Alabdulkarem, Hwang, R.Radermacher, & Maryland, 2012)**

1.4 CO_2 EOR APPLICATIONS

CO_2 EOR process is usually conducted after primary and secondary oil recoveries, where residual oil saturation (ROS) is between 55 to 65% of original oil in-place (OOIP). Because CO_2, unlike water, is a good solvent for oil, CO_2 EOR enables recovery of the residual oil by changing its physical characteristics. CO_2 and oil can develop miscibility at high pressure, which eliminates the interfacial tension (σ) between CO_2 and oil. On the other hand, CO_2 is only slightly soluble in water, which results in small losses of CO_2 to the aqueous phase in the pores. This strong oil solvent strength and low solubility in brine or water make CO_2 an excellent candidate in EOR to displace nearly all of the residual oil left behind by waterfloods as long as the CO_2 effectively seeps through the formation. However, CO_2 has much lower viscosity and density than oil, promoting gravity override and viscous fingering that results in very low sweep efficiency (i.e. the CO_2 "misses" substantial portions of the formation). Although it is not easy to increase the density of CO_2, it is possible to increase its viscosity or apparent viscosity or decrease its mobility. This "mobility control" is the subject of many previous and ongoing research programs seeking to:

(1) Decrease CO_2 mobility by increasing the viscosity of the injected CO_2, becoming "thickened" CO_2, for mobility control (research).

(2) Decrease CO_2 mobility by decreasing CO_2 relative permeability via water alternating with gas (WAG) for mobility control (commercialized).

(3) Divert CO_2 flow to layers with lower permeability by placing water-based gels in the highest permeability layers; for conformance control (commercialized).

(4) Use CO_2-in-brine foams for mobility and/or conformance controls (pilot tests).

The design of a thickener (program 1 in the preceding list) that can easily dissolve in CO_2 and effectively decrease the mobility of the injected CO_2 solution would eliminate viscous fingering, reduce the fluid processing costs (as water co-injection would no longer be needed), and increase oil recovery. However, the economics of a CO_2 thickener must be considered. If one assumes a price of \$40/ton CO_2 (\$0.02/lb of CO_2), the addition of 0.1 wt.% of a polymer costing \$80/lb (the fluoroacrylate monomer cost is \$40/lb) to the CO_2 would result in the cost of thickened CO_2 being \$200/lb. If the polymer was an effective thickener at 0.01 wt.%, the thickened CO_2 would cost about \$56/lb (Table 1). The operator and reservoir engineers would then have to assess if the increased recovery expected from the lower viscosity of the thickened CO_2 warranted its implementation. In 2012, engineers at Denbury Resources, Kinder Morgan, Tabula Rasa and Conoco Phillips indicated to Dr. Enick and coworkers that if the CO_2 could be altered to have the same viscosity as the oil being displaced; the cost of the thickened CO_2 would need to be roughly less than \$56 per ton (e.g. \$8/lb at 0.1wt.%; \$80/lb at 0.01wt.%); otherwise they would tend to favor injection of larger volumes of pure CO_2 while attempting to attain mobility control via the WAG process. This research initially targeted a polymer for mobility control. As will be shown in the results, the agent actually proved to have significant problems as a mobility control agent while displaying remarkable conformance control capabilities.

Table 1. Thickened CO_2 Feasible Economics Based on Industry Feedback

Cost of CO_2	**[\$/ton]**	40	40	40
Cost of CO_2	**[\$/lb]**	0.02	0.02	0.02
Cost of Polymer	**[\$/lb]**	80	80	8
Polymer Concentration	**[wt.%]**	0.1	0.01	0.1
Cost of Thickened CO_2	**[\$/ton]**	200	56	56

* 1 ton ~ 2000 lb

2.0 LITERATURE REVIEW

2.1 WAG FOR MOBILITY CONTROL

WAG injection process, where the gas is supercritical CO_2, has been increasingly applied as an EOR method during CO_2 miscible displacement, particularly in reservoirs that have been waterflooded. It has been widely applied to improve mobility control where water and gas, including CO_2, are injected alternately (program 2 in the preceding list). The alternating injection of water and CO_2 does not result in an increase in the viscosity of CO_2, rather it increases water saturation (S_w) and reduces CO_2 saturation (S_{CO2}) in the pore space of the rock, which directly reduces CO_2 relative permeability and, as a result, reduces CO_2 mobility (Equation 1). After using WAG process in many EOR projects over the years, the industry noted several disadvantages associated with this technique. First, corrosion problems arise as CO_2 mixes with water forming carbonic acid (pH ~ 3), especially in injection and production wells. Second, injectivity losses occur with undesirable low injection rates of both CO_2 and water during WAG process, especially if the injection is simultaneous rather than alternating. Third, optimal values of the WAG ratio and slug size can be difficult to determine. Lastly, blocking of oil contact by CO_2 may occur as water shields pores occupied with residual oil saturation and CO_2 can no longer reach these pores accordingly (Rogers & Grigg, 2000).

$$M = \frac{M_{Displacing\ Phase\ (Gas)}}{M_{Displaced\ Phase\ (Oil)}} = \frac{\frac{Kr_g}{\mu_g}}{\frac{Kr_o}{\mu_o}} = \frac{Kr_g \mu_o}{Kr_o \mu_g}$$ Equation 1

2.2 GELS FOR CONFORMANCE CONTROL

CO_2 EOR is usually conducted in numerous layers of a rock with widely varying permeability values (program 3 in the preceding list). Conformance control refers to using gels in the near-injection well region to inhibit or block the entrance of CO_2 into high permeable zones that have been extensively waterflooded and CO_2 flooded; these "thief zones" retain little recoverable oil yet consume the majority of injected CO_2. Gels are elastic and semisolid materials that are usually formed chemically by mixing water-soluble polymers and cross-linkers in an aqueous solution; the gelation typically occurs after the solution has been injected into the parallel zones. Although costlier to conduct, the best results are obtained by isolating the offending layer and injecting the polymer solution into only the thief zone. Gels are effective the most in projects with considerable amount of residual oil-rich accumulating in low permeability zones. Gels are often used along with WAG and CO_2 flooding which contribute to better conformance control and mobility control.

2.3 FOAMS FOR CONFORMANCE CONTROL AND MOBILITY CONTROL

CO_2-in-brine foams are another method that has been used in about 20 pilot-scale tests as a conformance control and/or mobility control agent. They typically contain a continuous low

volume fraction aqueous phase, which contains dissolved surfactant, and a high volume fraction, high pressure, discontinuous CO_2 bubble phase. Each surfactant is composed of two segments: polar (hydrophilic and CO_2-phobic) and non-polar portion (hydrophobic and CO_2-philic). Upon mixing the surfactant solution and dense CO_2, the surfactant reduces interfacial tension and promotes foam formation in the pores of the rock. Foams have very high apparent viscosity (i.e low mobility) in porous media.

"Strong foams" are effective the most in heterogeneous reservoirs with multiple producing layers of different permeabilities, and they are generated by surfactant solution alternating with gaseous CO_2 (SAG). These foams are often de-stabilized by crude oil, which is beneficial if one intends to block high permeability oil-depleted zones while promoting flow into lower permeability oil-rich zones. The objective is to inject small volumes of highly concentrated surfactant and CO_2 into the high permeability, oil-depleted zones in the near wellbore region (within ~100 ft). This diverts the flow towards a low permeability zone, that contains the residual oil saturation.

On the other hand, injecting "weak foams" are effective the most in single layered reservoirs where large volumes of very dilute surfactant solutions are injected via SAG in an attempt to form foam with a mobility comparable to the oil such that viscous fingering is inhibited hundreds of feet from the injection. Therefore, they are particularly effective mobility control agents, especially if they are resilient to the presence of oil. However, it is important to note that foams, in general, are dependent on rock properties, oil and gas saturations and fluid properties, which make predicting their flow behavior in reservoir conditions very challenging. Further, the surfactant solutions are susceptible to surfactant losses to adsorption, which can greatly diminish the efficacy of either conformance control or mobility control.

2.4 WATER-SOLUBLE POLYMER ADSORPTION FOR CONFORMANCE CONTROL

Polymer adsorption, which can occur during thickened CO_2 floods, the placement of gels, or the injection of thickened water during secondary recovery, is the adhesion of polymer molecules to the rock surface, creating a film-layer of polymer that coats the pore space and rock surface. In mobility control, the adsorbed layer potentially depreciates the polymer's value in the solution and acts as a flow barrier. However, in conformance control, the adsorbed layer may efficiently reduce permeability and thereby divert the flow to unswept zones. Therefore, understanding polymer adsorption and retention is extremely vital in EOR applications that involve the flow of polymer solutions through the porous medium. The following section details multiple factors that were attributed to polymer adsorption and retention.

Zaitoun and coworkers examined and reported many findings on the effect of adsorption on polymer propagation and flow in rocks. In 1987, Zaitoun and coworkers claimed that high molecular weight water-soluble polymers are capable of increasing the viscosity of water flowing through a porous rock, although the macromolecule may be larger than a rock pore. At a high shear rate, hydrodynamic forces are strong enough to realign and uncoil the polymeric macromolecules in the direction of the flow (shear thinning behavior), which in turn allows the larger macromolecules to pass through the smaller pores. In conformance control polymer treatments, the polymer is often injected, close to the wellbore, at a high shear rate. But far away from the wellbore, the hydrodynamic forces are too weak for the polymer macromolecules to pass through the pores (Zaitoun & Kohler, 1987). Furthermore, they claimed that weakly anionic (negatively charged) water-soluble polymers, surprisingly, adsorbed onto rocks with negative surface charge, such as sandstone. They attributed this high affinity of polymer adsorption to

either positively charged clay minerals originally contained in the rock, or the formation of a hydrogen bond with silica, or silicon dioxide (SiO_2). They also speculated that the activity of one strong group from the polymer might cause the polymer macromolecule to be entirely linked to a mineral in the surface. Furthermore, the summation of linkages from several weak groups of the same polymer might produce a single strong force linking the polymer macromolecule to the mineral in the surface.

In 1995, Zaitoun and coworkers examined the effects of heterogeneity, residual oil saturation and injection rate on polymer adsorption. They identified a new type of water-soluble, nonionic polyacrylamide-based gel polymer to study flow-induced retention for near-wellbore treatments. A series of core flooding experiments showed that adsorbed macromolecules previously stretched under elongation forces bridged pore throats and caused polymer retention (at high shear rate and low-to-medium permeability). They claimed that the polymer would penetrate more deeply into a high-permeability oil-depleted zone than a low-permeability oil-rich zone, and therefore improve the resistance to flow, or viscosity, in the high-permeability zone. When used in an injection well, the polymer would reduce subsequent water flow in the high-permeability zone and, as a result, facilitate more water flowing in the low-permeability zone. When used in a production well, the polymer would reduce the relative permeability to water much more than the relative permeability to oil. Therefore, in zones flooded by the polymer, the resulting water viscosity would be stronger than the oil viscosity (Zaitoun, Zitha, & Chauveteau, 1995).

In 1998, Zaitoun and coworkers again used polyacrylamide to examine the effect of residual oil saturation and pore structure heterogeneity on bridging adsorption. A series of core flooding experiments on Berea sandstone, with and without residual oil, indicated that for a

given injection rate, the intensity of core plugging is higher at residual oil saturation than at 100% water saturation. Cores with residual oil saturation decreased the size of pore channels and, therefore, increased bridging adsorption at lower injection rate. Furthermore, a low-permeability Berea sandstone at residual oil saturation and low injection rate, resulted in plugged progressive upstream pore throats due to polymer retention (Zaitoun & Chauveteau, 1998).

Again in 2002, Zaitoun and coworkers used the polyacrylamide polymer to investigate the origin of the bridging adsorption effect. Their research found that when the water-soluble polymer was injected at low shear rates, the adsorbed film-layer thickness was independent of the injection rate. But when the polymer was injected at high shear rates, the adsorbed film-layer thickness increased as the injection rate increased. They referred to this mechanism as flow-induced adsorption (Zaitoun, Chauveteau, & Denys, 2002).

Several research pursuits have followed the standards set by Zaitoun and coworkers, one of which was done by Ogunberu and Asghari. Their research investigated the influence of flow-induced-adsorption in reducing water permeability during near-wellbore polymer treatments. They concluded that flow-induced adsorption happened above a certain critical shear rate, which significantly decreased water permeability (Ogunberu & Asghari, 2005).

Broseta and coworkers examined the influence of wettability and oil saturation on polymer adsorption and retention. They argued that nonionic polyacrylamide and polysaccharides water-soluble polymers exhibited stronger adsorption than anionic polyacrylamide onto hydrophobic surfaces. Furthermore, polymer adsorption under residual oil saturation was different than adsorption under 100% water saturated porous medium. In a water-wet system, an increase in adsorption was expected due to an additional adsorbing oil surface. In

an oil-wet system, a decrease in adsorption was expected due to limited access to the rock surface (Broseta, Medjahed, Lecourtier, & Robin, 1995).

Mungan and coworkers examined the effects of polymer adsorption on displacement efficiency. The author argued that the conventional polymer flooding method involving the use of a slug process would cause a slug breakdown. The slug process consists of injecting polymer-treated water followed by untreated-water. At the leading flood front of the slug, the effectiveness of the polymer solution is continuously diminished due to dilution with encountered connate water and polymer adsorption on the rock surfaces. On the trailing flood front of the slug, at most minimal adsorption occurs and, consequently, viscous fingering takes place due to an unfavorable mobility ratio (Mungan, 1970).

Meister and coworkers defined and attributed polymer adsorption to three main mechanisms: hydrodynamic retention, entrapment and surface adsorption. First, hydrodynamic retention occurs when the polymer is continuously contained within a recirculating flow vortex created by a rapid flow through an orifice passage. Second, adsorption due to entrapment occurs when large polymer molecules plug smaller sized pore throats. This adsorption mechanism could be reversed by stopping flow where some of the larger polymer molecules would diffuse into larger pore throats and eventually be produced when flow is resumed. Third, surface adsorption occurs due to the retention of a polymer on a surface, which is controlled by the nature of the surface, the polymer and the solvent. Meister and coworkers analyzed this adsorption mechanism in their research (Meister, Pledger Jr., Hogen-Esch, Butler, & Florida, 1980).

Meister and coworkers studied and reported many findings on the influence of surface charge and surface area on polymer retention. They tested retention of the same polyacrylamide polymer by Berea sandstone, sodium kaolinite and Baker dolomite. For positively charged

surfaces, such as dolomite, hydrolysis of polyacrylamide increased retention. On the other hand, for negatively charged surfaces, such as sandstone and constant surface areas, polyacrylamide decreased retention. In general, they concluded that any type of additives that form a less effective solvent increased retention. With water, increasing salinity or adding non-solvents (such as alcohols) made it a less effective solvent for polyacrylamide and, therefore, increased retention (Meister, Pledger Jr., Hogen-Esch, Butler, & Florida, 1980).

Using different salinities, polymer concentrations and degrees of hydrolysis, their analysis showed that Berea sandstone and sodium kaolinite were able to retain over 50% and 90%, respectively, of the polyacrylamide polymer. Compared to sodium kaolinite, Berea sandstone has minimal traces of kaolinite (7-10%). However, Baker dolomite was able to retain only 17.9% of an unhydrolyzed polyacrylamide polymer. It was concluded that clay content, determined by kaolinite composition, has a major effect on polymer retention (Meister, Pledger Jr., Hogen-Esch, Butler, & Florida, 1980).

By flocculating sodium kaolinite, they were able to decrease its surface area by over 80%, which, in turn, decreased retention by 70%. It was concluded that reducing surface area would reduce polymer retention, especially when adsorption is the main mechanism during the retention process (Meister, Pledger Jr., Hogen-Esch, Butler, & Florida, 1980).

All previous results from aqueous polymer solutions indicate that polymer adsorption and retention may have significant effect on fluid viscosity and on rock properties. Therefore, the adsorption of CO_2-soluble polymers dissolved in high pressure CO_2 flowing through cores may also occur.

2.5 SMALL MOLECULE CO_2 THICKENERS FOR MOBILITY CONTROL

Many attempts have been made in designing small molecule thickeners. Each small molecule is composed of a nonpolar segment that is CO_2 philic to promote dissolution, and an associative polar or hydrogen bonding segment(s) that is CO_2 phobic but promotes the formation of viscosity enhancing supramolecular structures. When dissolved in CO_2, the CO_2 philic segments arrange themselves to interact with the surrounding CO_2 solvent and, therefore, promotes solubility in CO_2 solution. The CO_2 phobic segments interact with other similar segments leading to the increase in CO_2 viscosity (Figure 3). Enick and coworkers developed small molecule CO_2 thickeners, such as a fluorinated telechelic ionomer and a tri (semi-fluorinated alkyl) tin fluoride, which had multiple concerns: 1) did not dissolve completely in CO_2, 2) dissolved in CO_2 for a short time, then came out of the solution, 3) resulted in a minimal increase in CO_2 viscosity, a factor of 2–4, 4) is expensive to design and 5) required high concentration, 3–6 wt.% (Enick & Olsen, 2012) and (Enick, et al., 2016). As of now, there are no affordable small molecule thickeners for CO_2.

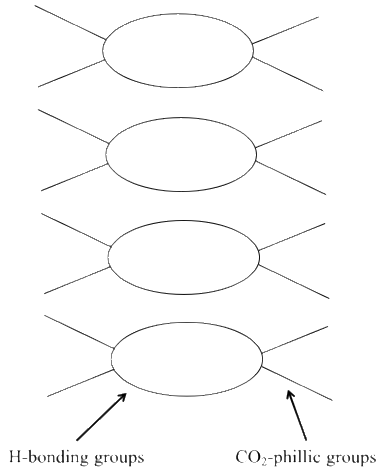

Figure 3. Small Molecule CO_2 Thickener

2.6 POLYMERIC CO_2 THICKENERS FOR MOBILITY CONTROL

Polymers are formed by chemical reactions in which a large number of small molecules, known as monomers, are linked sequentially, forming a chain. When the polymer's chain of molecules is perfectly aligned and uncoiled, the polymer develops a "shear thinning" and becomes less effective thickener. Moreover, if the polymer's chain of molecules is made of a single monomer, it is called a homopolymer, and if the polymer's chain of molecules is made of two different monomers, it is called a copolymer. Depending on the arrangement of the two monomers, a copolymer is classified as: 1) an alternating copolymer where the two monomers are arranged in an alternating fashion, 2) a random copolymer where the two monomers are arranged in any order, 3) a block copolymer where monomers are arranged in distinctive groups, or 4) a graft copolymer where a polymer made of one monomer is grafted, planted, onto another polymer made of the second monomer (Figure 4).

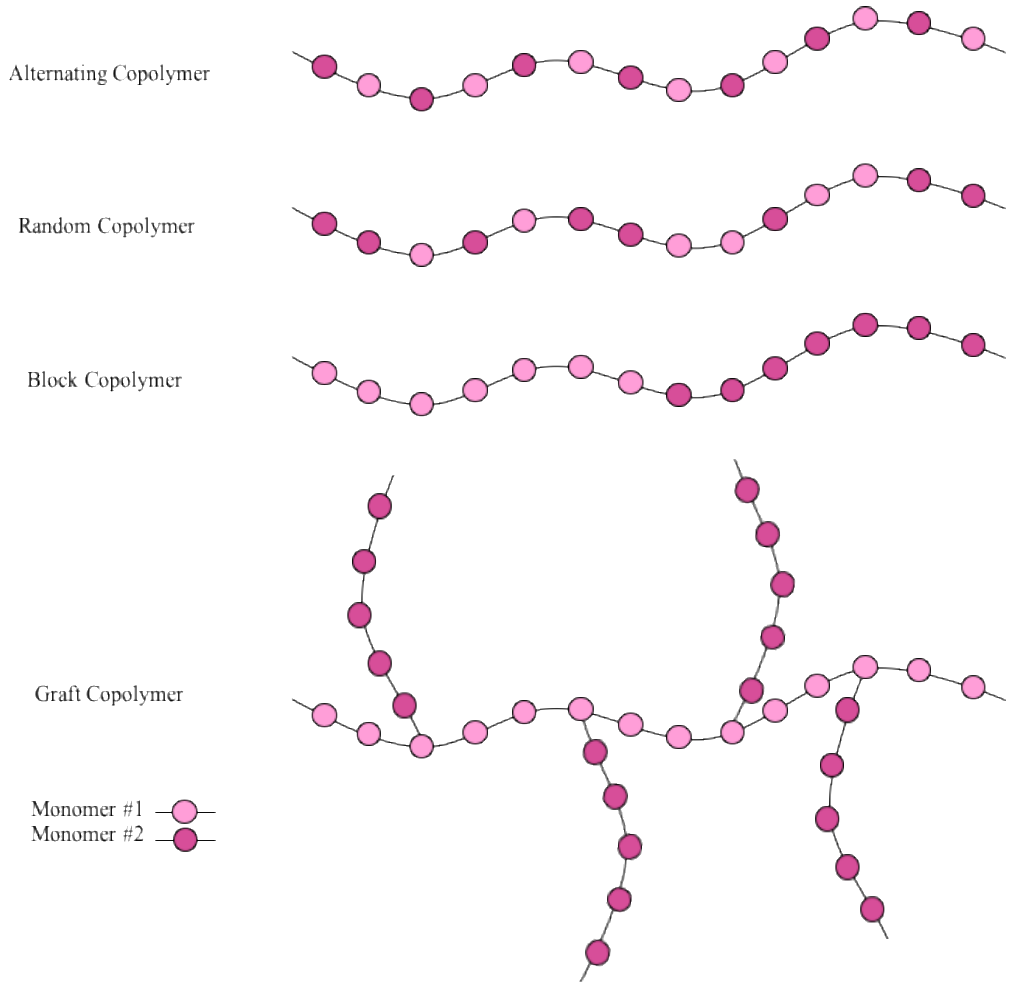

Figure 4. Types of Copolymers based on Monomers' Arrangements

Attempts have been made to increase the viscosity of CO_2 via dissolution of a polymer rather than decreasing CO_2 relative permeability via WAG or decreasing CO_2 mobility with thermodynamically unstable foams. However, high molecular weight (M_w) polymers are difficult to dissolve in CO_2 at concentrations great enough to cause significant increases in viscosity. Therefore, many attempts have been made to design polymers that have strong favorable thermodynamic interactions specifically with CO_2 because a thermodynamically stable, transparent CO_2 polymer solution, that has the same viscosity as the oil being displaced, has the potential to eliminate viscous fingering, delay CO_2 breakthrough, and eliminate the need for

WAG. Further, any of the water shielding effects associated with WAG would be minimized because water would not be co-injected with the thickened CO_2.

Previous research works in thickening CO_2 has focused on the identification of an appropriate polymer, which can be used as a thickener to effectively increase the viscosity of CO_2. This viscosity increase is achieved by varying the polymer's concentration in the solution which typically consists of CO_2 polymer and co-solvent (Enick & Olsen, 2012). In the following section, a thorough review of the literature related to previous attempts and efforts to identify the appropriate CO_2 thickeners is highlighted and used as a guideline of all the research works that have been dedicated over the years to enhance this technology. Refer to (0) for all polymer details in this section.

The initial attempts to thicken CO_2 were primarily associated with assessments of substances used to thicken hydrocarbons and oils because CO_2 is miscible with many light hydrocarbon components but only slightly miscible with water. Therefore, it was anticipated that non-polar organic polymers that were crude oil-soluble would be more likely to dissolve in CO_2 than water-soluble polymers (Enick, et al., 2014). Heller and coworkers measured the solubility of 53 commercially available polymers in CO_2 and identified a total of 18 polymers that exhibited solubility values of (0.24-1.1) wt.% at temperatures of (20-58) °C and pressures of (1700-3100) psia. Using windowed Falling Cylinder experiments to measure CO_2 viscosity, none of the polymers were capable of inducing significant viscosity increases. It is important to note that those polymers had very low molecular weight ($M_w < 1000$) and that their research team reported less than 25% increase in viscosity (Heller & Dandge, 1987). However, Zhang and coworkers used two of Heller's low molecular weight polymers in their experiments and, using Capillary Viscometer, reported a substantial increase in viscosity, a (1300%-1400%) increase

(Zhang, She, & Gu, 2011). The polymers they used from Heller's experiments were (0.6-0.8) wt.% of poly (vinyl ethyl ether) (PVEE) with a M_w = 3800 g/mol and poly(1-decene) (P1D) with a M_w = 910 g/mol. This claim was examined by Enick and coworkers using a Falling-Ball Viscometer as they discovered that even a 1 wt.% of those polymers did not increase the viscosity as reported by Zhang and coworkers (Enick, et al., 2014), thereby confirming the result that these low molecular weight polymers were not viable thickeners.

Bullen and co-workers issued a patent and claimed that their CO_2 liquid solution which contained a copolymer, polycarbonate, with (1.5-3) wt.% and M_w = (20,000-150,000) g/mol was able to increase the viscosity of CO_2 significantly at (1450-3625) psia and 22 °C (United States Patent No. 4,701,270, 1987). This claim was examined by Enick and coworkers for polycarbonate copolymers and they discovered that at 1 wt.%, M_w = 16,000 g/mol, 2030 psia and 22 °C, the polycarbonate copolymer did not increase CO_2 viscosity drastically as Bullen and coworkers claimed (Enick, Beckman, Huang, Shi, & Kilic, 2000) and (Enick, et al., 2014).

Bae and coworkers found that CO_2 can also be substantially thickened by using a silicone polymer, polydimethysiloxane (PDMS), together with an organic co-solvent, toluene. The specific effects of different co-solvents on the solubility of the silicone polymers in CO_2 were studied as well (Bae & Irani, 1993). Using a Capillary Viscometer, they discovered that with 4 wt.% of PDMS, M_w =197,000 g/mol, 20 wt.% of toluene and 76 wt.% of CO_2 was able to increase the viscosity of CO_2 by a factor of 30 at 4500 psia and 50 °C (Bae & Irani, 1995). On the other hand, Rousseau and coworkers examined CO_2 mobility control in terms of polymer-oil and polymer-rock interactions based on modeling results from core experiments using polymer-thickened CO_2 (Rousseau, Renard, Prempain, Fejean, & Betoulle, 2012). The polymer used as a thickener in their analysis was the PDMS, due to its solubility in supercritical CO_2 along with a

co-solvent, and its wide industrially availability. The mixture used in their analysis was composed of 4 wt.% PDMS, 20 wt.% toluene and 76 wt.% CO_2 performed at 54 °C and 2900 psia. The PDMS used has a kinematic viscosity of 600,000 cSt and a M_w = 260,000 g/mol. This mixture has very close characteristics to one of the mixtures examined by (Bae & Irani, 1993), highlighted above, which had the same PDMS/toluene/CO_2 ratio. In their analysis, Rousseau and coworkers emphasized the importance of these polymer-oil and polymer-rock interactions and their great influence on viscosity, particularly, when thickened CO_2 flows through an oil saturated zone in a reservoir. As PDMS/toluene-thickened, CO_2 interacts with that oil saturated zone, they claim that a high percentage of ineffective PDMS stays behind in cores while toluene remains unaffected. Their analysis concludes that more studies and models are needed to bring insights on feasibility of PDMS/toluene-thickened CO_2 interaction (Rousseau, Renard, Prempain, Fejean, & Betoulle, 2012).

McClain and co-workers developed a polymer, poly (1-,1-, dihydroperfluorooctyl acrylate (PFA), with 3.7 wt.% and M_w = 1,400,000 g/mol which was able to increase the viscosity of CO_2 by a factor of 2.5 at 4500 psia and 50 °C (McClain, et al., 1996). The PFA was a major discovery regarding the development of polymers, with high molecular weight, that could dissolve in CO_2 without the need of a co-solvent. Enick and coworkers commended this discovery and wanted to develop a polymer that could: dissolve in CO_2 at a concentration less than 3.7 wt.% and achieve a much greater increase in viscosity. Therefore, Enick and coworkers then developed an associative copolymer based on the PFA in the hope of reducing the polymer's concentration needed to attain a certain viscosity (Enick & Xu, 2001), (Enick, Beckman, Huang, Shi, & Kilic, 2000) and (Enick, Xu, & Walschin, 2003).

From all previous research, it has been demonstrated that the viscosity of CO_2 can be, indeed, increased with a high molecular weight polymer. However, the considerable addition of co-solvent (approximately 90% CO_2 and 10% co-solvent) to the solution is expensive in a field scale compared to a core lab sample scale. This challenge led USDOE to conduct a research solely on identifying the only known thickener that does not require a co-solvent and dissolves in CO_2 at low concentrations (less than 1 wt.%) and typical CO_2 flooding reservoir conditions; this copolymer is a fluoroacrylate-styrene (PolyFAST), which was designed by Enick and coworkers (Enick & Olsen, 2012). Using Berea sandstone cores, PolyFAST successfully increased the viscosity of CO_2 at 1.5 wt.% concentration by a factor of 19 (an 1800% increase) at a superficial velocity of 1 ft/day, a factor of 12 at 10 ft/day, and a factor of 3 at 50 ft/day. However, the significant cost of the fluoroacrylate monomer prevented the PolyFAST to be applied on a field scale (Enick, et al., 2014). Then, Enick and co-workers attempted to design a non-fluorinated version of the PolyFAST polymer in the hope of identifying a cost-effective thickener. They successfully developed a benzoyl-vinyl acetate (PolyBOVA) polymer with 3.7 wt.% and M_w = 1,400,000 g/mol which was able to increase the viscosity of CO_2 by 80% at 9300 psia and 25 °C. As noted, unlike the PolyFAST, the PolyBOVA dissolved in CO_2 at a much higher pressure (Enick & Tapriyal, 2008).

Therefore, the only known CO_2-thickening polymers capable of dissolving to several weight percent in CO_2 at EOR conditions without the need for a co-solvent are high molecular weight polyfluoroacrylate homopolymers (PFA) and fluoroacrylate-co-styrene (PolyFAST) copolymers. Consequently, these polymers (PFA and PolyFAST) were used in this study of mobility control in single cores and, after an unexpected discovery, conformance control for parallel cores.

3.0 EXPERIMENTAL PROCEDURE

3.1 METHODOLOGY

An ideal CO_2 thickener is inexpensive, environmentally safe, water-insoluble additive that can dissolve in CO_2 solution, without a co-solvent, at typical reservoir conditions and enhance the viscosity of CO_2. As discussed previously, liquid CO_2 at or above the supercritical state has high density and low viscosity, and has been widely used for many years as an EOR displacing fluid due to that relatively dense CO_2 displacing residual oil more efficiently than gaseous CO_2. This experimental work will detail the initial efforts for designing a CO_2-soluble polymer to be used as a mobility control agent, and the subsequent effective use of the same polymer as a conformance control agent. In general, this experimental work will illustrate the following steps:

(1) Designing a (high) molecular weight polymer.

(2) Dissolving a (1 wt.%) of that polymer in liquid CO_2 solution.

(3) Flowing the CO_2 and polymer solution through sandstone or limestone cores at temperatures of (23-25 °C) and pore pressures of (1850-3000 psi).

(4) Developing an increase in the pressure drop which corresponds to an increase in the viscosity of CO_2 attributable to the polymer that remains in solution (mobility control), and a decrease in the relative permeability of CO_2 due to polymer adsorption and retention (conformance control).

3.2 POLYMER DESIGN

When conducting a polymer-thickened CO_2 core flood, a high molecular weight polymer is designed to dissolve in the pure CO_2, increase the viscosity of the CO_2 solution and decrease the mobility of CO_2, which will result in favorable sweep efficiency. In polymer flooding core tests, the pure CO_2 is pumped at a certain superficial and frontal velocities into a mixer, which has the thickened CO_2 solution (Figure 5). The slowly diluted polymer in the CO_2 solution is then displaced into the core. The expected pressure drop behavior for the thickened CO_2 solution flowing inside the core is illustrated in (Figure 6).

In this work the PFA and PolyFAST were selected because they exhibited particularly high CO_2 solubility, without the need of a co-solvent, while effectively increasing the viscosity of CO_2. High purity of the PFA homopolymer and PolyFAST copolymer were obtained as a gift from a fluorchemical supplier.

It is important to note that the fluoroacrylate monomer in PFA and PolyFAST copolymer originally contained eight fluorinated carbons (C_8F_{17}). Despite the success of PolyFAST copolymer, extensive studies conducted recently on fluorinated polymers have confirmed that, depending on the number of fluorinated carbons, some are considered environmentally persistent and bio-accumulative substances (e.g. perfluorooctanoic acid, PFOA). Polymers with less than seven fluorinated carbons are not considered bio-accumulative (Pricharda, Thomasb, Kauschb, & Vogta, 2011). In this experimental work, fluoroacrlyate monomers with only 6 fluorinated carbons were used (Table 3); the degradation product associated with this polymer is perfluorohexanoic acid. In this experimental work, polymer dissolution for mobility control and polymer adsorption for conformance control were discussed accordingly.

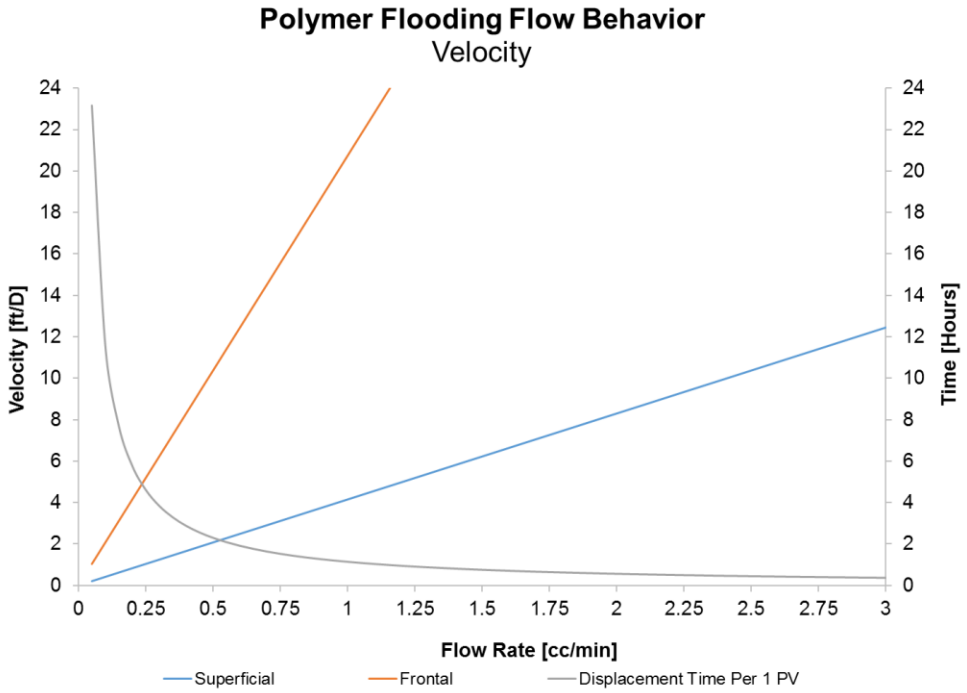

Figure 5. Expected Superficial and Frontal Velocities during CO_2-Polymer Flooding (Φ=20%)

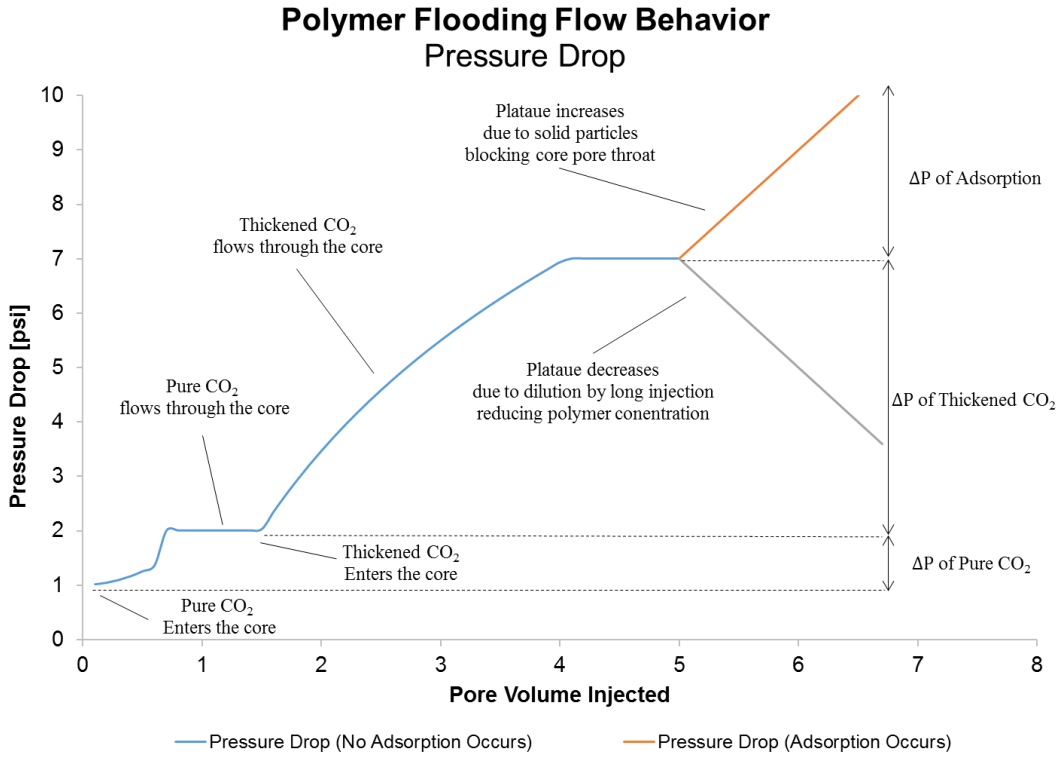

Figure 6. Expected Pressure Drop during Polymer Flooding

3.3 PHASE BEHAVIOR

The key factor to ensure that a polymer is completely dissolved in the CO_2 solution is by the determination of a cloud point pressure, which is the lowest pressure for which the polymer is mixed and obtained solubility in the CO_2 solution through a chained process using a Pressure-Volume-Temperature (PVT) apparatus within controlled parameters. Therefore, below this cloud point pressure, the polymer is expected to come out of the solution and CO_2 solubility is not achieved. The PVT apparatus consists of several components: a vent, air bath, magnetic stirrer, PVT cell, sight glass window, piston, back pressure regulation system, high pressure positive displacement pumps and a computer to control the pumps for accurate setting of fluid injection rates (Figure 7).

A predetermined amount of a desired polymer sample is contained within a transparent glass tube, which is placed on top of the piston, inside the sight glass window. The annulus space between the glass tube and the sight glass window is filled with a transparent fluid, silicon oil, which serves to apply an overburden pressure on the glass tube. As CO_2 is injected using the positive displacement pump where: 1) the piston moves downward and a space is created in the top portion of the glass tube at a volumetric rate equal to the withdrawn oil silicon space below the piston, and 2) CO_2 slowly starts occupying the created space in the top portion of the glass tube.

The mixer inside the sight glass window cell is used to accelerate the dissolving process between the polymer and CO_2, forming a thickened CO_2 solution. Therefore, the pressure of the

desired sample can be increased or decreased by pumping or withdrawing silicon oil, accordingly. Initially, a sample is set at a relatively high pressure, between 5000 and 4000 psi. Next, pressure is reduced until a two phase region occurs. Then, the sample pressure is slowly increased until a one transparent phase region occurs, marking the cloud point pressure of the thickened CO_2 solution.

In this experimental work, cloud point pressures were measured in a laboratory to determine whether the thickened CO_2 solution was saturated, in a two-phase region, or under-saturated, at a much higher pressure than the two-phase region. Moreover, core and polymer flooding tests were conducted at a pressure equal to or greater than the cloud point pressure to ensure that the polymer is completely dissolved in the CO_2 solution.

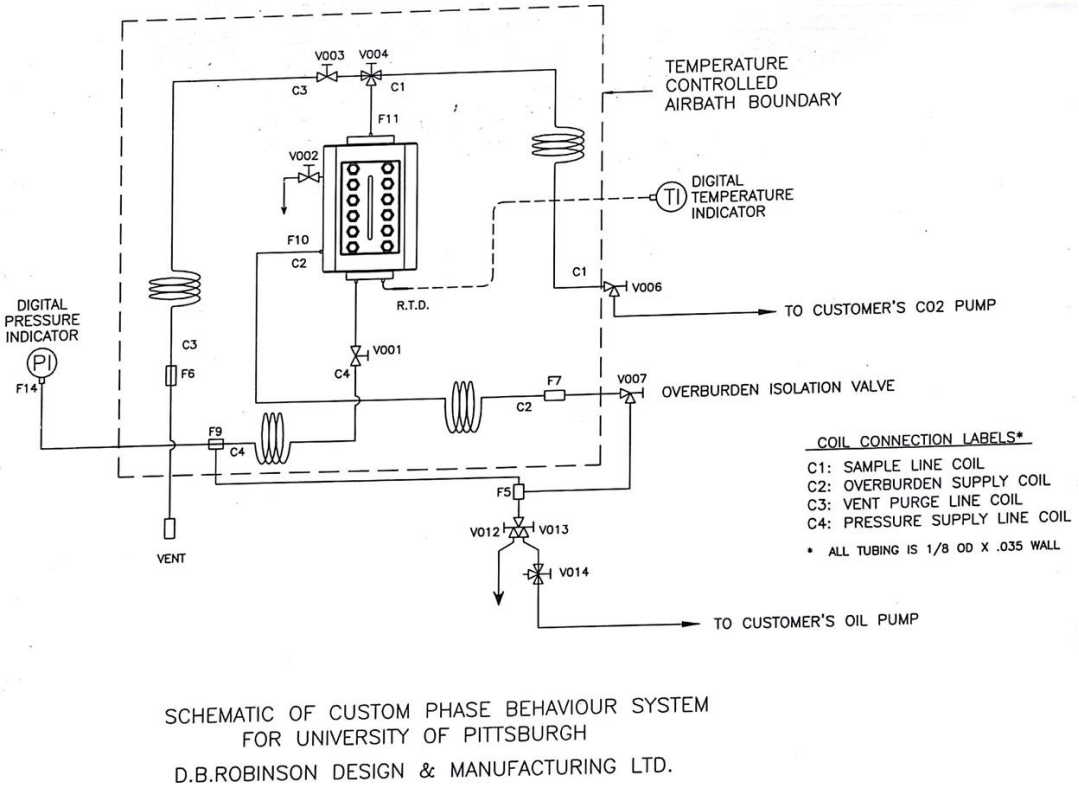

Figure 7. A Schematic of the PVT Apparatus (Robinson Cell)

3.4 VISCOSITY

Fluids tend to deform when they are exposed to forces or stresses, and viscosity is the one property that describes how fluids behave under this deformation. It is a property that demonstrates an internal resistance of a fluid to motion, and is generated due to the movement of particles within the fluid. A fluid with a high viscosity has stronger tendency to resist motion. Newton's law described the flow behavior of fluids with a simple relation between shear stress (τ) and shear rate (γ) with a proportionality constant (η) which is the coefficient of viscosity (Equation 2). Shear rate is also referred to as a velocity gradient, which is the mathematical slope of the fluid's velocity profile in the flow direction. If (η) is constant, then shear stress is independent of the shear rate, ($\eta = \mu$) and the fluid is said to be Newtonian. However, if (η) is not constant, then shear stress depends on shear rate, ($\eta = f(\gamma)$) and the fluid is said to be non-Newtonian.

For Newtonian fluids, the viscosity is independent of the shear rate that the fluid is undergoing. That is, no matter how fast they are forced to flow, the viscosity of Newtonian fluids will remain constant. As for non-Newtonian fluids, the viscosity shows shear thinning or thickening behavior when undergoing high or low shear rates. In other words, at a given pressure and temperature, the viscosity does not change for Newtonian fluids, but it decreases with increasing shear rates for non-Newtonian fluids. For example, at 25 °C and 4930 psi, PolyFAST copolymer flowing through a core showed a shear thinning behavior (Enick & Xu, 2001), that is as the shear rate increased, the viscosity of the thickened CO_2 decreased (Figure 8 and Figure 9). In this experimental work, all polymers dissolved in the CO_2 solution were recognized to be non-Newtonian fluid. However due to the impracticality of obtaining enough high pressure data over

wide ranges of shear rates to generate a model of non-Newtonian behavior, the dilute polymer solutions were considered to be Newtonian fluids.

$$\tau = \eta\gamma \qquad \text{Equation 2}$$

There are two methods used in this study to determine fluid viscosity: 1) a capillary viscometer where a fluid flows through a resistive component, and 2) a falling ball or cylinder viscometer where a solid object moves through a fluid. In this experimental work, the thickened CO_2 solution's viscosity was determined via capillary viscometer (Figure 11) at no cost by Praxair, and a falling ball viscometer (Figure 13).

For the capillary viscometer, the measured viscosity is correlated with the time taken for a specific quantity of fluid to flow through a capillary tube with a predetermined diameter and length sizes. For the falling ball or cylinder viscometer, the measured viscosity correlates with the time required for the object to drop to a certain distance, which is basically a terminal velocity (V_t). In order to estimate the increase in viscosity of the thickened CO_2 solution using either falling ball viscometer or falling cylinder viscometer, (Equation 3) was derived and used to describe the relationship between the terminal velocity of the falling object and the viscosity of the fluid.

$$\mu = K\frac{(\rho_s - \rho_f)}{V_t} \qquad \text{Equation 3}$$

Enick and coworkers indicated that there is only one paper published by (Doffin, Perrault, & Garnaud, 1984) which presented an expression for the average shear rate on the surface of a falling ball flowing at a certain terminal velocity in a column of a Newtonian fluid contained in a tube. That paper specified the maximum shear rate (γ_{max}) on a surface of a sphere occurs at the position along the equatorial plane where the gap between the ball and sphere is the smallest. Moreover, the paper failed to provide any mathematical derivation or enough supports

validating the claim that the average shear rate (γ_{avg}) is actually equal to half of the maximum shear rate. Enick and coworkers took a different approach in order to approximate the shear rate of a falling object through a Newtonian fluid, which is illustrated in the following section.

Using a falling cylinder viscometer, Enick and coworkers obtained the shear rate of a falling cylinder (γ_c) at the cylinder's radius, the tube's radius and the recorded terminal velocity of the cylinder (Equation 4). Using a falling ball viscometer, Enick and coworkers modeled the ball as an aggregated stack of thin coaxial horizontal cylinders falling through at the same terminal velocity as the falling ball (Figure 10). For each individual cylinder, a shear rate at the radius of the cylinder (γ_c), a surface area of the cylinder (A_c) and the terminal velocity needed to sustain a constant volumetric flow rate in the annular gap are measured accordingly. The product of the shear rate and surface area of each cylinder are summed and divided by the summation of all individual cylindrical areas to obtain the shear rate of a falling ball (γ_b), which is referred to as a "surface area" average shear rate. The maximum shear rate is obtained at the falling ball's radius, the tube's radius and the recorded terminal velocity of the ball (Equation 4) (Enick, et al., 2016). In this experimental work, shear rates and terminal velocities were calculated using Enick and coworkers' approach.

$$\gamma_c = V_t \left[\frac{-2r_c - \left(r_t{}^2 - r_c{}^2\right)\dfrac{1}{r_c \ln\left(\dfrac{r_c}{r_t}\right)}}{\ln\left(\dfrac{r_c}{r_t}\right)\left(r_t{}^2 + r_c{}^2\right) + \left(r_t{}^2 - r_c{}^2\right)} + \frac{1}{r_c \ln\left(\dfrac{r_c}{r_t}\right)} \right] \qquad \text{Equation 4}$$

$$\gamma_b = \frac{\sum_{i=1}^{n} \gamma_{c,i} A_{c,i}}{\sum_{i=1}^{n} A_{c,i}}$$

Similar to cloud point pressure tests, a predetermined amount of a thickened CO_2 solution sample, which is contained at or above the cloud point pressure, is placed inside a cell within a transparent glass tube. The rest of the glass tube is filled with a transparent fluid, silicon oil,

which serves to apply an overburden pressure on the thickened CO_2 solution sample. The ball or the cylinder is submerged inside the thickened CO_2 solution sample resting on top of a sliding piston, which separates the thickened CO_2 solution sample from the silicon oil. As the entire glass tube is inverted, the ball or the cylinder falls through the thickened CO_2 solution sample, the silicon oil slowly pushes the piston and a terminal velocity is recorded. This procedure is repeated 5–10 times and an average terminal velocity is recorded per a thickened CO_2 solution sample ($V_{t,sol}$). At the same pressure and temperature, the same procedure is conducted once using a pure CO_2 solution in order to report the terminal velocity of the pure CO_2 ($V_{t,o}$). Using Newton's law of motion and Stokes law, a simplified equation is found for calculating the viscosity of the thickened CO_2 solution relative to the known pure CO_2 viscosity. In this experimental work, the primary focus was on determining the ratio of the viscosity of the fluid with a dissolved polymer (μ_{sol}) to the viscosity of the pure fluid (μ_o), which is referred to as the relative viscosity (Equation 5). Furthermore, relative viscosities were calculated using Enick and coworkers' approach. For all steps and assumptions used to determine (Equation 3 and Equation 5), refer to (0).

$$\text{Relative Viscosity} = \frac{\mu_{sol}}{\mu_o} = \frac{V_{t,o}}{V_{t,sol}} \qquad \text{Equation 5}$$

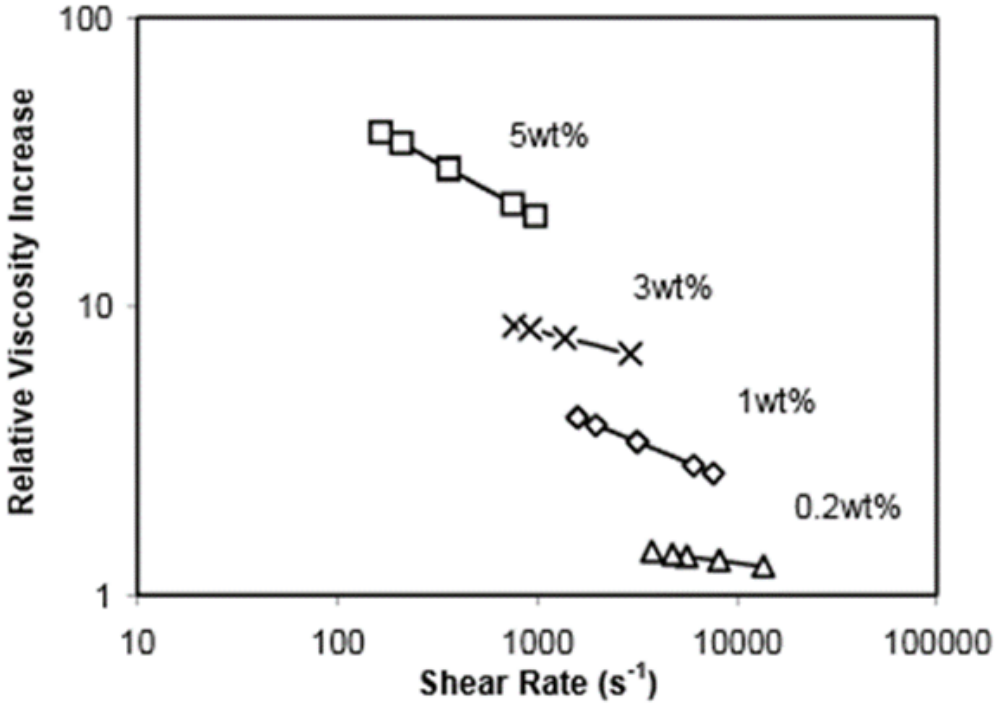

Figure 8. Relative Viscosity vs. (γ) using Falling Cylinder Viscometer **(Enick & Xu, 2001)**

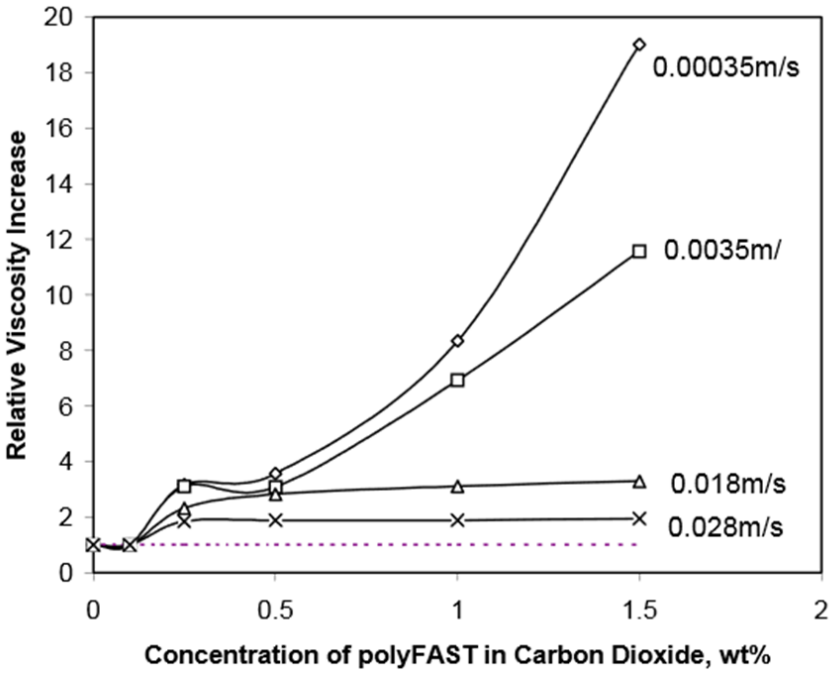

Figure 9. Relative Viscosity vs. (wt.%**)** using Flow through Porous Media **(Enick & Xu, 2001)**

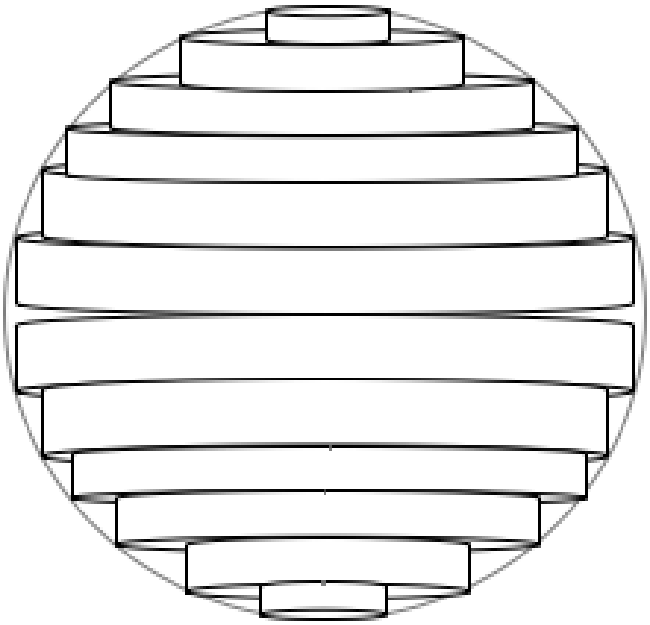

Figure 10. Multiple Cylinders Fitted inside a Sphere used to Estimate Falling Ball Shear Rate

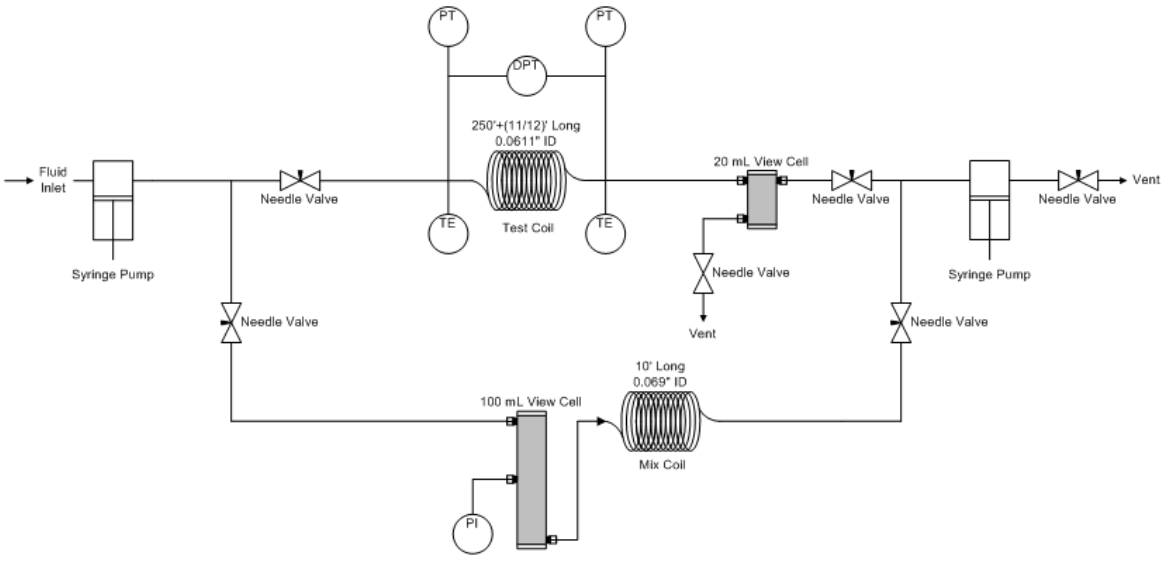

Figure 11. A Schematic of the Capillary Viscometer (Praxair, 2016)

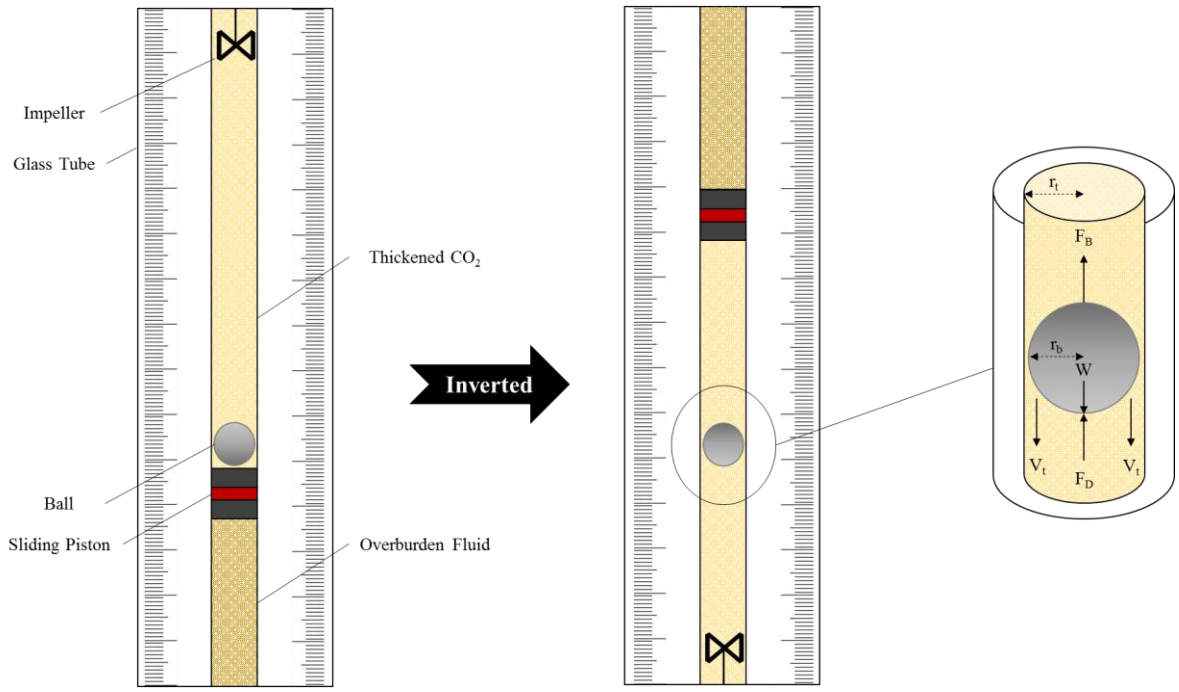

Figure 12. A Schematic of the Falling Ball Viscometer Used in This Study

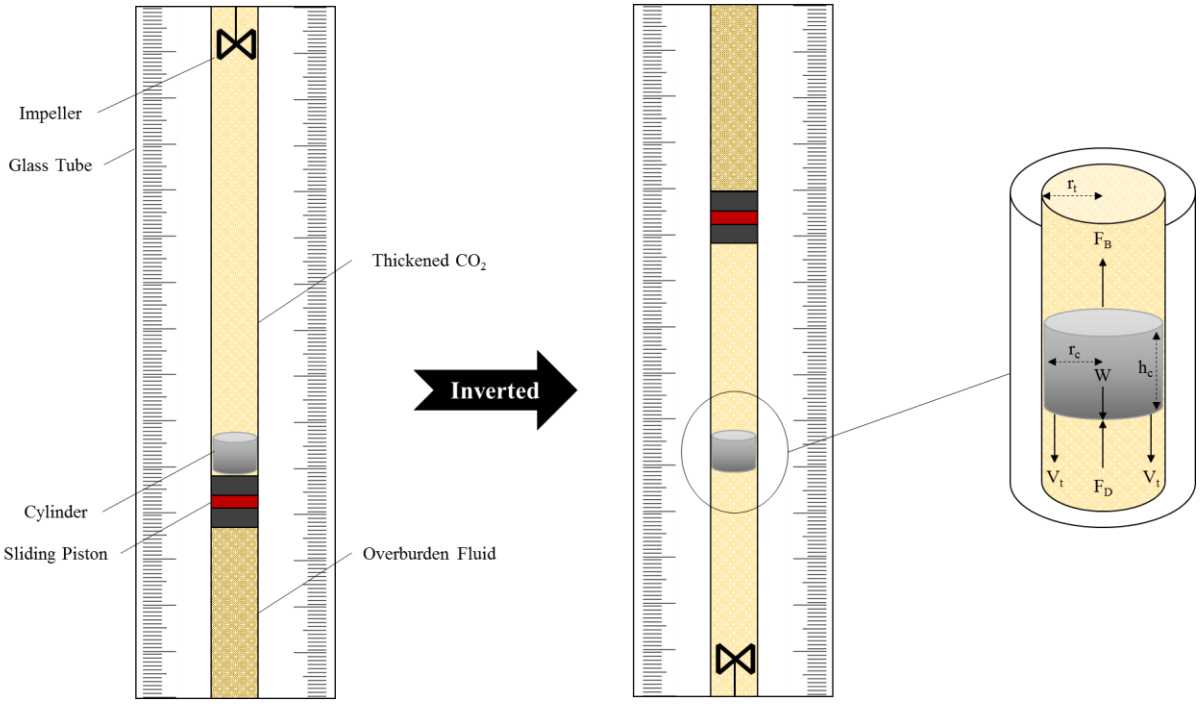

Figure 13. A Schematic of the Falling Cylinder Viscometer Used in Prior Studies

3.5 CORE FLOODING

Core flooding tests are often used to simulate a certain reservoir environment and determine how well various fluids flow through a rock sample from that reservoir. First, a cylindrical core is cut from an outcrop to a predetermined length and diameter size. Next, the core sample is placed in a core holder with the cylindrical outer surface of the core sealed with a pressurized sleeve that prevents fluid flow around the core and forces the fluid to flow through the core. Fluid flow is governed by Darcy's law (Equation 6). Typically, fluid is injected into the core at a constant volumetric flow rate. The pressure drop across the core is measured and then permeability is calculated. Note that a high pressure mixer is placed after the CO_2 pump but before the core holder. The pure CO_2 is displaced into the mixer, which contains the polymer, and the solution is thereby displaced into the core. In this experimental work, core flooding tests have gone through the above process under two configurations (Figure 14 and Figure 15). In one option, the outlet pressure of the core is maintained at a constant value by a back pressure regulator (as long as that regulator is not compromised by polymer deposits). In the other option, the fluid exiting the core is received by a positive displacement pump that gathers the effluent at the same volumetric rate as the pump displacing fluid into the core.

$$Q = \frac{-KA\Delta P}{\mu L} \qquad \text{Equation 6}$$

Core flooding tests are completed in various ways depending on the purpose of the test. In this experimental work, core tests were conducted either through a single core flood, where the tested fluid was injected into one core sample, or parallel core floods, where the tested fluid was injected into two core samples. Furthermore, the initial polymer concentration in CO_2 (C_i) was diluted slowly during each experiment according to (Equation 7). Moreover, all core

flooding tests were carried out roughly at temperature = 25 °C, pore pressure = 3000 psi, confining load (overburden) pressure = pore pressure + 500 psi (but not above 5000 psi). The core flooding tests involved thickened CO_2 displacing CO_2 from a CO_2-saturated core, CO_2 or thickened CO_2 displacing brine from a brine-saturated core(s), or CO_2 or thickened CO_2 displacing dead SACROC crude oil from a crude oil-saturated core. The core floods were conducted with a multiphase steady state core flooding apparatus in collaboration with Special Core Analysis Laboratories (SCAL) Incorporation (Table 2) or the National Energy Technology Laboratory (NETL).

$$C_n = C_i e^{-V_{CO_2\ injected}/V_{mixer}} \quad \text{Equation 7}$$

Table 2. SACROC Fluid and Rock Properties **(Ghahfarokhi, Pennell, Matson, Linroth, & Kinder, 2016)**

Date of Discovery	November 1948	**Reservoir Temperature, [°C]**	54
Formation	Canyon Reef Limestone	**Reservoir Pressure, [psig]**	3300
Depth, [ft]	6200-7000	**Viscosity, [cp]**	0.33
OOIP, [BSTB]	2.8	**API Gravity, [°]**	42
Average (Φ), [%]	7.6	**MMP, [psig]**	1850
Average (K), [mD]	19	**Bubble Point Pressure, [psig]**	1800

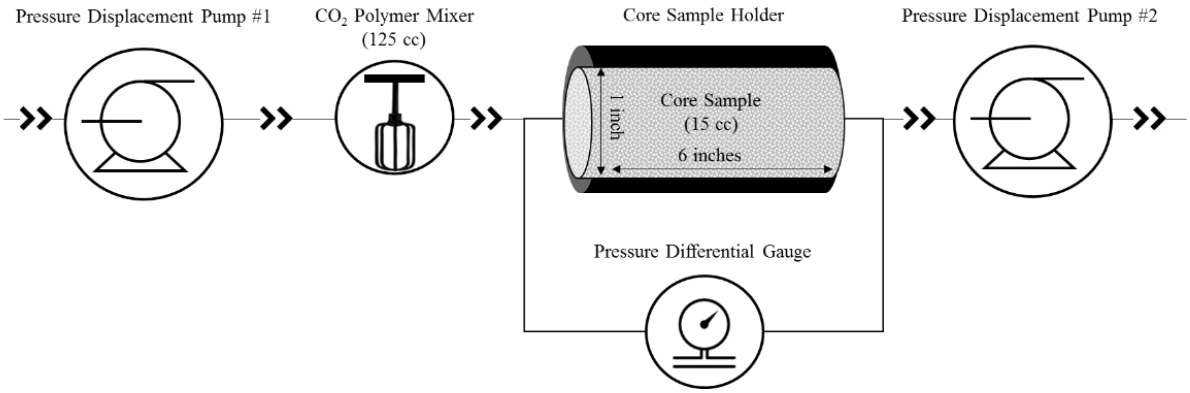

Figure 14. Core Flooding Test (Configuration #1)

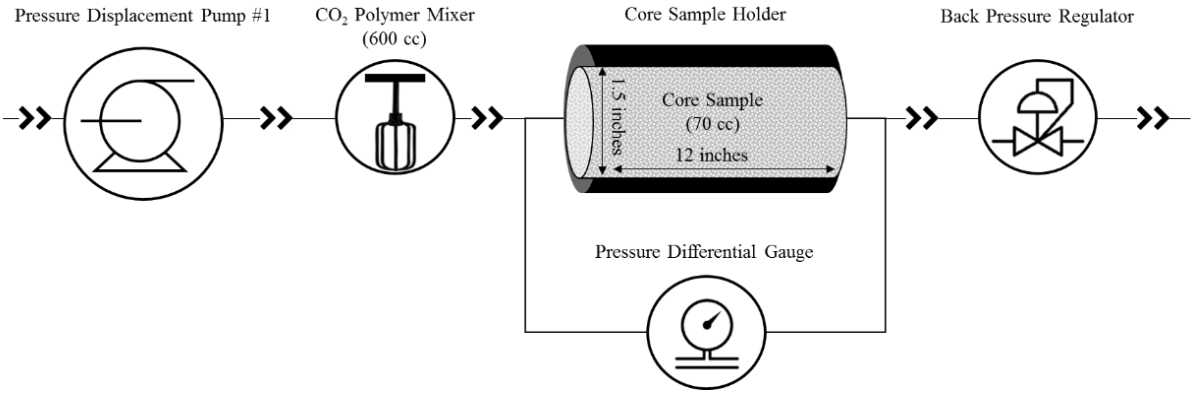

Figure 15. Core Flooding Test (Configuration #2)

4.0 RESULTS AND DISCUSSION

4.1 POLYMER DESIGN

The molecular weight of the PFA homopolymer has been estimated by the supplier as 250,000 g/mol. A higher molecular weight version of the PFA homopolymer was also synthesized and used in core flooding tests. Furthermore, a high molecular weight version of the PolyFAST was designed with six fluorinated carbons (Table 3).

Table 3. Designed Polymers for Core Flooding Tests

Polymer	Type	M_w [g/mol]
PFA	Polyfluoroacrylate Homopolymer	250,000
PFA	Polyfluoroacrylate Homopolymer	> 250,000
PFAST-C6	Polyfluoroacrylate Styrene Copolymer	> 250,000

4.2 PHASE BEHAVIOR

Cloud point pressures were measured for mixtures of the highest molecular weight PFA and CO_2 (Table 3). Based on these phase behavior results, core floods were later conducted at pressures of 3000 psi in order to assure the solubility of a 1 wt.% of the PFA in the CO_2 solution (Figure 16).

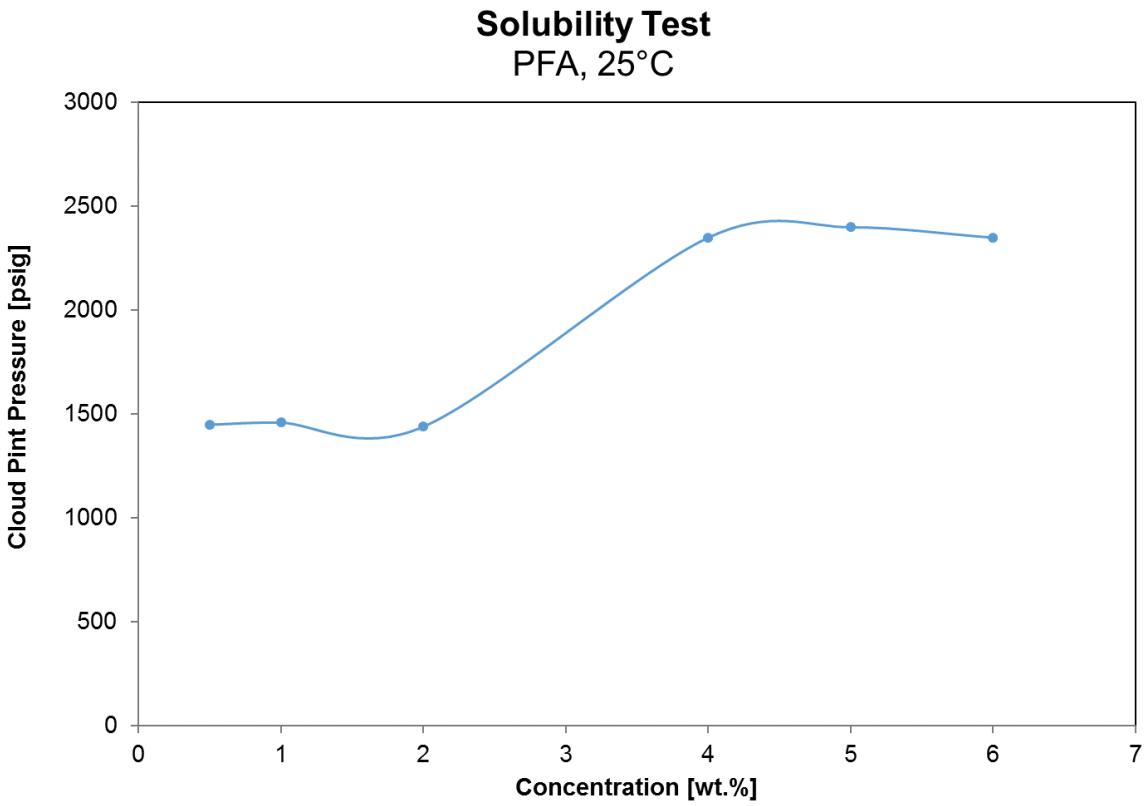

Figure 16. Solubility Test on the PFA Homopolymer

Ideally, the CO_2 thickener would not precipitate when CO_2 extracts light hydrocarbons from the crude oil as miscibility is developed in the layer of a rock via a multiple-contact extraction process (Figure 17). The ability for CO_2 to extract light hydrocarbons and form a mixture that becomes miscible with crude oil is what makes it an excellent solvent for EOR. However, fluoroacrylate homopolymers are known to be insoluble in hydrocarbon solvents. Therefore, several phase behavior experiments were conducted to determine if the presence of light alkanes in a CO_2-rich solution would render the PFA insolubility. If the PFA does precipitate, this would be an unfavorable attribute of using the PFA for mobility control because it would tend to make the polymer come out of the solution in the CO_2-crude oil mixing zone within the formation. Consequently, mixtures of light alkanes were prepared to represent the

lighter alkanes that are commonly extracted into the CO_2-rich phase during EOR (Figure 18). The alkane mixtures were composed of: n-Hexane, n-Decane, n-Tetradecane, n-Hexane and n-Octane. An analysis, conducted on SACROC crude oil composition during CO_2 extraction at 76 °F (22 °C), was used to form the composition of the light hydrocarbon mixture (alkane makeup) in several tests and determine if the light hydrocarbons act as a PFA anti-solvent (Table 4).

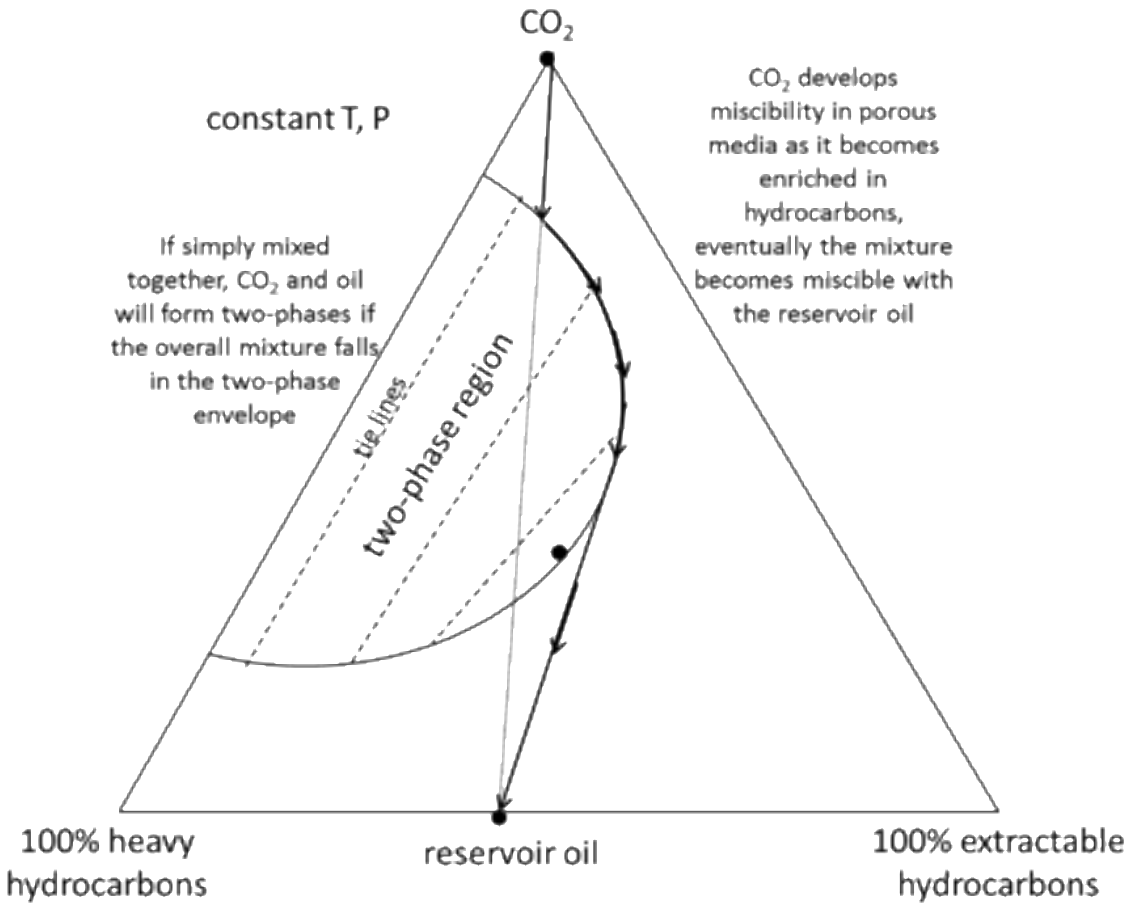

Figure 17. Ternary Diagram of Miscibility between CO_2 and Hydrocarbon Components

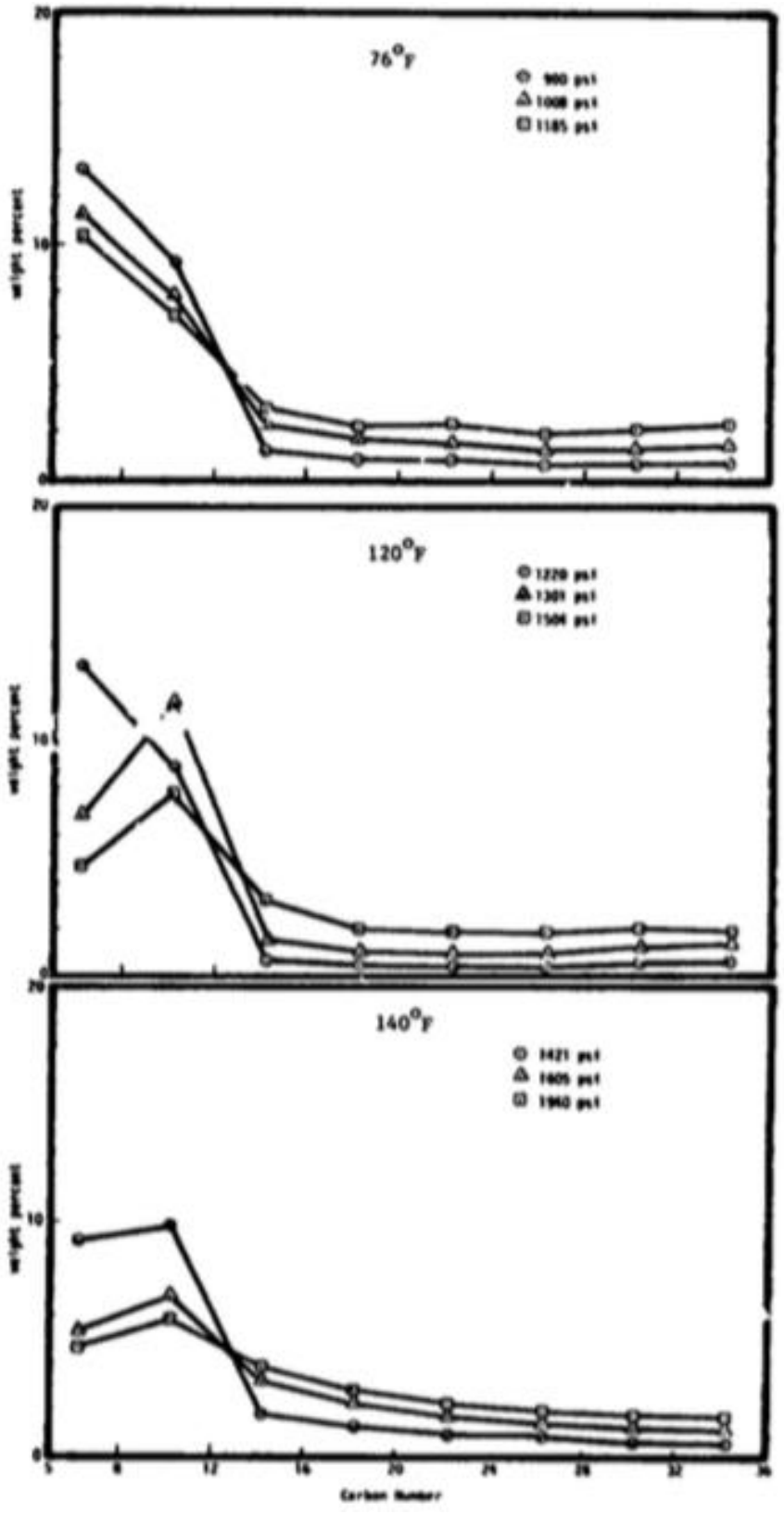

Figure 18. Chemical Composition of CO_2 using SACROC crude oil **(Wang & Alabama, 1986)**

At 1 wt.%, the PFA could not dissolve in a CO_2-rich solution containing 30 wt.% of the light alkane mixture, even at pressures as high as 9000 psi (Table 4). However, at 0.5 wt.% PFA in a CO_2-rich solution containing 15 wt.% mixed light alkanes, a solubility was achieved at a cloud point pressure lower than 3000 psi (Table 4). As expected, these solubility test results indicated that the polymer's solubility in a CO_2-rich solution diminished as the alkane contents in the solution increased.

Table 4. Solubility Tests of mixtures of light alkanes, PFA Homopolymer and CO_2

Light Alkane	**Alkane Makeup**	**Wt.%** *Not Soluble*	**Wt.%** *Soluble*
C6	40.0%	12.0%	6.0%
C10	26.7%	8.0%	4.0%
C14	13.3%	4.0%	2.0%
C16	6.7%	2.0%	1.0%
C18	6.7%	2.0%	1.0%
C20	6.7%	2.0%	1.0%
Alkanes		30.0%	15.0%
PFA		1.0%	0.5%
CO_2		69.0%	84.5%
		100.0%	**100.0%**

4.3 VISCOSITY

4.3.1 Falling Ball Viscometer

The viscosity of the thickened CO_2 was measured for all polymers in (Table 3) using a falling ball viscometer. All the thickened CO_2 viscosities were measured using (Equation 5) for an average terminal velocities reported per single polymer. As discussed previously, the shear rate

is not constant everywhere around the submerged ball, it is the highest along the annulus gap. For a falling ball, the shear rates were measured using (Equation 4) and showed an average shear rate of 7000 s^{-1}. However, a fluid flowing through a rock has a much lower shear rate.

At relatively high concentration, the PFA homopolymer exhibited (15-40) fold increase in the viscosity of the CO_2 solution at pressure higher than 3000 psig (Figure 20). For practical purposes, the PFA was tested at a much lower concentration, exhibited better results and was found to have (1.5-3) fold increase in the viscosity of the CO_2 solution at pressure higher than 3000 psig (Figure 19). Consequently, the PFA homopolymer was considered an excellent candidate for core flooding tests.

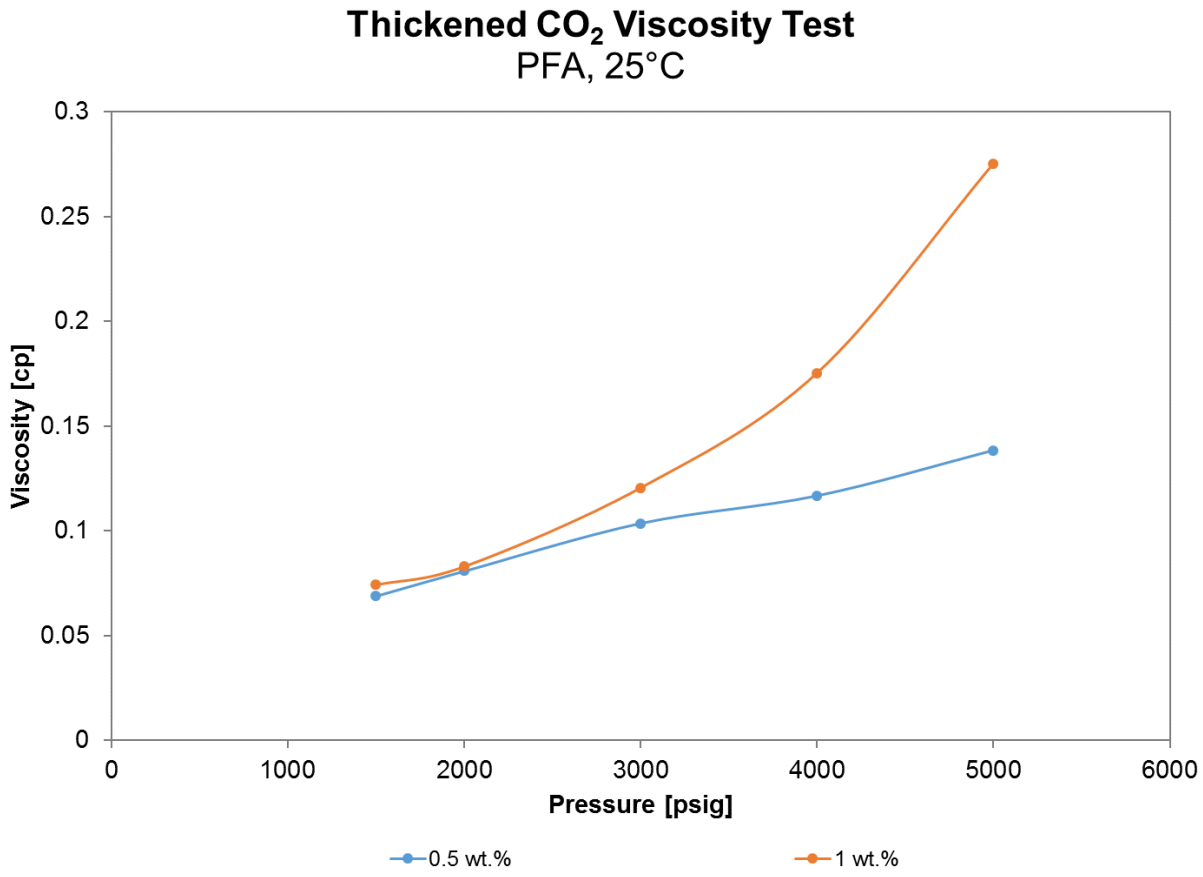

Figure 19. Viscosity Test on 0.5 wt.% and 1 wt.% PFA Homopolymer

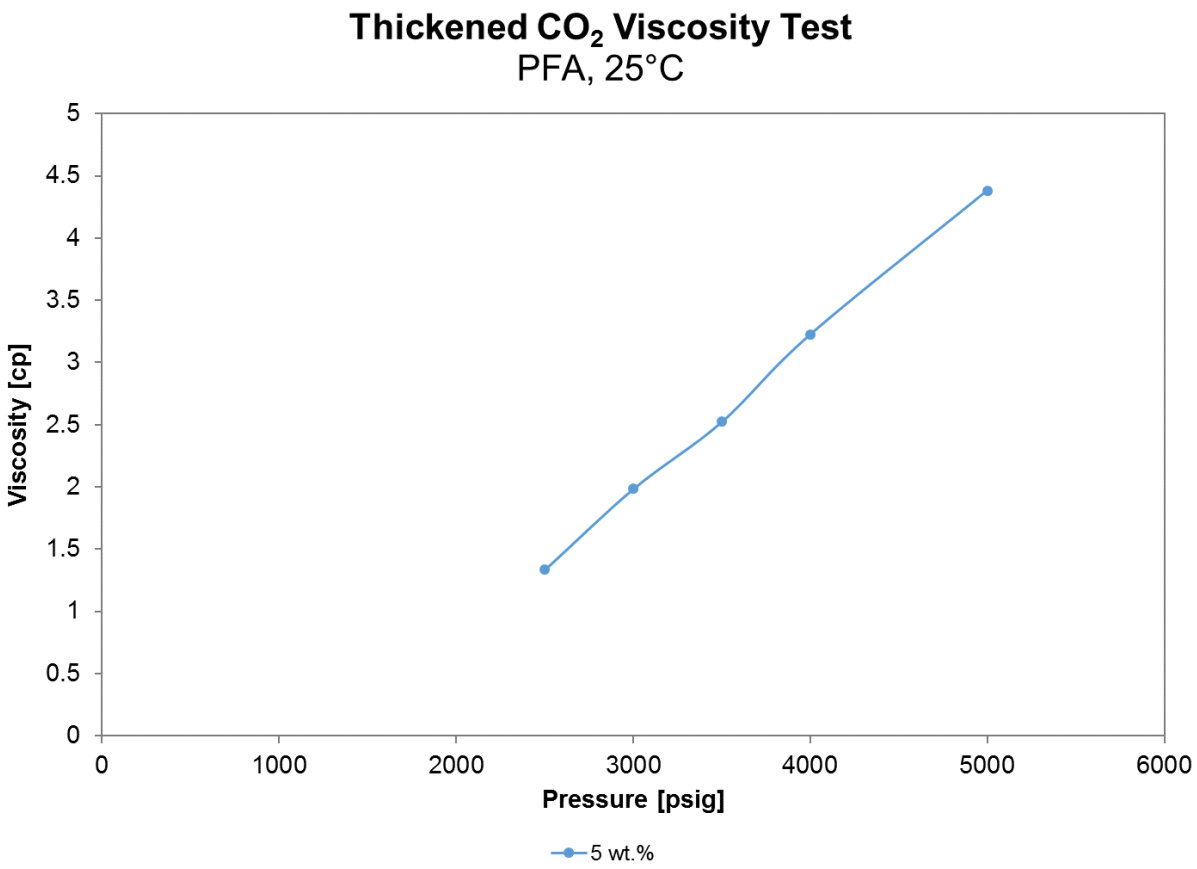

Figure 20. Viscosity Test on 5 wt.% PFA Homopolymer

4.3.2 Falling Cylinder Viscometer

The viscosity of the thickened CO_2 was measured for the PFA homopolymer using a falling cylinder viscometer. All the thickened CO_2 viscosities were measured using (Equation 5) for a maximum terminal velocity reported per single polymer. Again, it is important to note that the falling ball viscometer failed to provide a realistic representation of a shear rate of a fluid flowing through a pore throat, which is greatly less than 7000 s^{-1}. Therefore, the falling cylinder viscometer was used with five cylinders and different sizes to estimate a single maximum shear

rate at the edge of their radiuses using (Equation 4). Ideally, this approach would confirm the expected degree of viscosity enhancement at low shear rate.

In one hand, a narrow cylinder would fall quickly through a tube filled with Newtonian fluid and will develop a low shear rate due to the large annulus gap between the cylinder and the tube. On the other hand, a wide cylinder would fall slowly and develop a high shear rate due to the limited annuls space between the cylinder and the tube. Two of the narrow cylinders rattled, turned and did not fall nicely through the tube and, therefore, they were excluded from the analysis. The three remaining cylinders (cylinder #1, #2 and #3) fell nicely and showed a shear thinning behavior with a relative viscosity increase between (2-4) fold increases at low shear rates less than 7000 s^{-1} (Table 5 and Figure 21).

Table 5. Falling Ball and Falling Cylinder Viscometers Specifications

Falling Ball Viscometer		
Material	Pyrex	
Specific Gravity	2.23	g/cc
Diameter	31.587	cm
Traveling Distance	14	cm
Falling Cylinder Viscometer		
Material	Aluminum	
Specific Gravity	2.7	g/cc
Diameter	3.1618 (Cylinder #1) 3.1466 (Cylinder #2) 3.1313 (Cylinder #3)	cm
Length	2.192	cm
Traveling Distance	5-12	cm

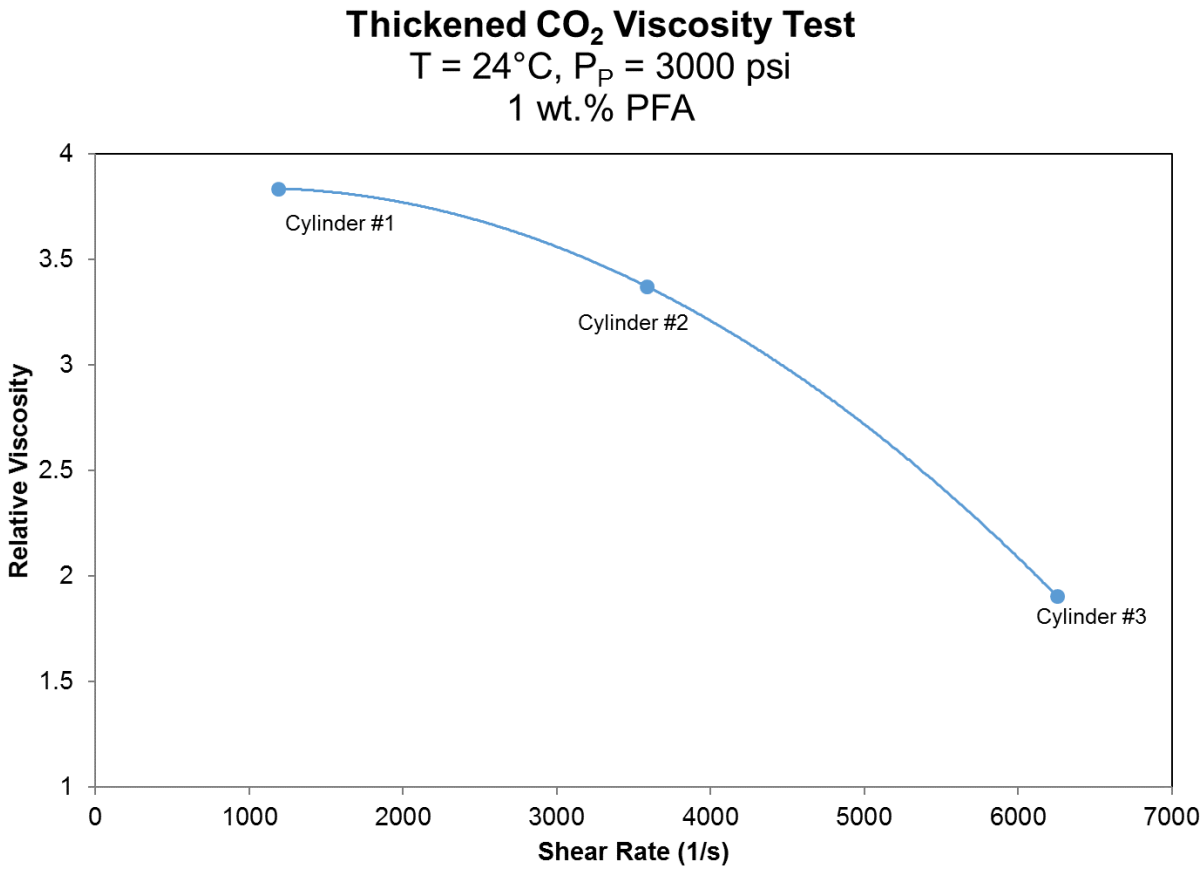

Figure 21. PFA Homopolymer Relative Viscosity vs. (γ) using Falling Cylinder Viscometer

4.3.3 Capillary Viscometer

The following experiment was conducted by Praxair. Approximately 1 wt.% (7.53 grams) of the PFA homopolymer was added to a 756 mL of CO_2 at 3000 psig. The polymer sample was loaded into a 100 mL view cell and dissolved by passing CO_2 across the sample using two syringe pumps. The two pumps were used to deliver and receive CO_2 across the sample in back-and-forth repetitive motion. Once the fluid in the delivery pump was exhausted, the flow is reversed using the other pump. The fluid was mixed for approximately 5 hours by passing the CO_2 and the

polymer solution back-and-forth between the two syringe pumps. The mixed solution was then set to rest for 48 hours, after which another 2 hours of mixing was completed using the same back-and-forth motion.

The pressure drop of the fluid was then measured by routing the mixed solution through 250 feet of 1/8 inch tubing with an internal diameter of 0.061 inches. The pressure drop was measured across the tubing using a differential pressure transducer. Various shear rates were achieved by changing the flow rate in the tubing using the syringe pumps. The results are displayed with measurements using water, at 100 psig, methanol, at 100 psig, and neat CO_2, at 3000 psig, using the same pressure transducer. The polymer showed a shear thinning behavior with a relative viscosity increase between (2.5-3.5) fold increases at low shear rates between (1150-50) s^{-1} (Figure 22).

These two different methods for estimating the viscosity enhancement associated with the PFA in CO_2 were in relatively close agreement with each other. In fact, the viscosity of the CO_2-rich polymer solution has not been previously reported using two different apparatuses. These results indicate that 1 wt.% PFA is expected to increase the viscosity of CO_2 by a factor of (3-4) at very low shear rates. Therefore, if viscosity enhancement was the only factor associated with the polymer dissolution, one would expect that in a test involving the displacement of the thickened CO_2 into a core previously saturated with only CO_2, flowing at a constant low flow rate, the pressure drop would increase by a factor of (3-4).

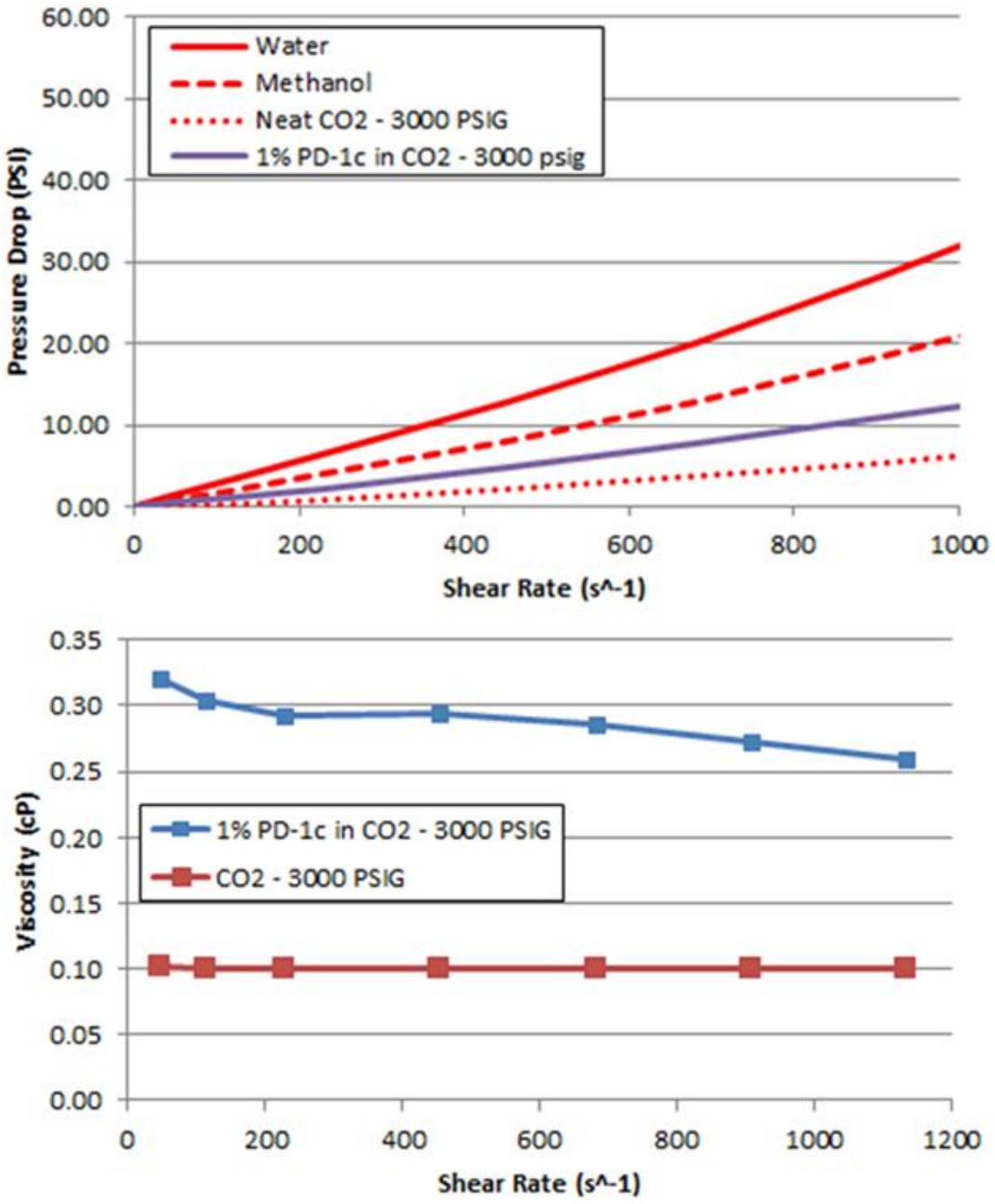

Figure 22. PFA Homopolymer Viscosity vs. (γ) using Capillary Viscometer (Praxair, 2016)

4.4 CORE FLOODING

4.4.1 Cores Flooded with Pure CO_2 and Brine (No Thickened CO_2 or Oil)

4.4.1.1 Single: Pure CO_2 Displacing Brine (Screening Tests)

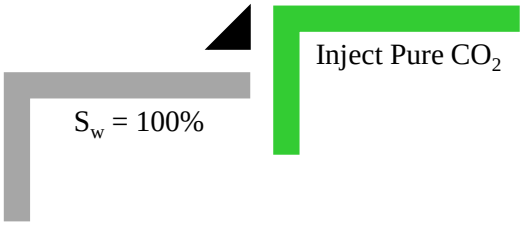

In this stage, the objective was to determine which types of commercially available standard outcrop cores yielded relatively low recovery of brine by injected CO_2. This was done in order to identify cores that would be likely to show the improvement in brine recovery (brine displacement) by CO_2 when a thickener was added. A control test, consisted of injecting pure CO_2, was conducted on brine water saturated single cores (S_w = 100%). In this experiment, all core samples listed in (Table 6) were tested. After comparing production performances, core samples with lower water production at a given volume of injected CO_2 were selected as viable core flooding candidates. Therefore, Berea sandstone, Carbon Tan sandstone, Indiana limestone (70 mD) and Edwards Yellow limestone core samples were selected for subsequent core flooding tests (Figure 23).

Table 6. Core Samples Analyzed for CO_2 and Polymer Flooding Feasibility

#	Core Sample	Rock Type	K_{Brine} [mD]	Φ [%]	Rock Formation
1	Berea	Sandstone	40	20	Kipton
2	Carbon Tan	Sandstone	11	15	Utah
3	Kirby	Sandstone	9	21	Edwards Plateau
4	Indiana	Limestone	9	18	Bedford
5	Indiana	Limestone	70	19	Bedford
6	Edwards Yellow	Limestone	40	22	Edwards Plateau
7	Guelph	Dolomite	10	17	Niagara

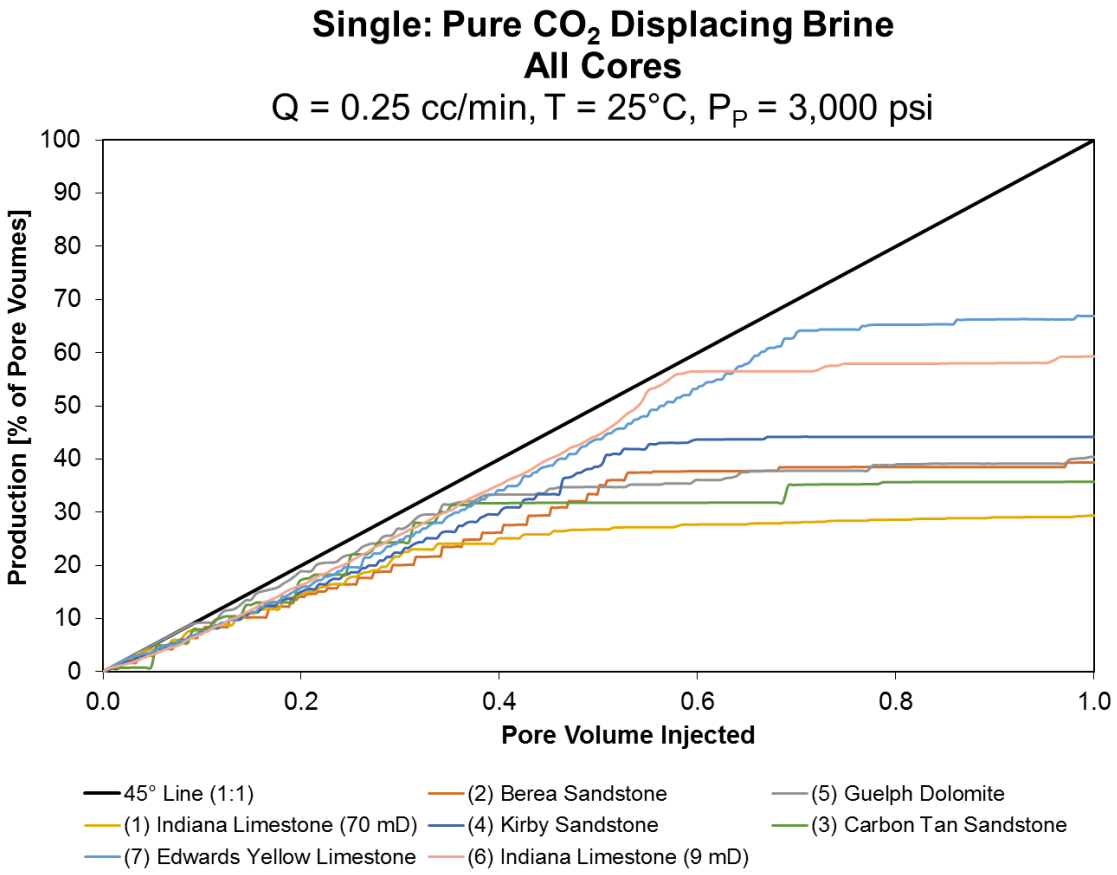

Figure 23. Single Core, Control Test, Production Performance on All Core Samples

4.4.1.2 Lessons Learned

(1) Mobility control analysis can be examined through single Berea, Carbon Tan sandstone, Indiana (70 mD) or Edwards limestone core floods. Even on this small

scale, viscous fingering and gravity override can occur. However, conformance control analysis is best determined with two parallel cores of differing permeability.

(2) For sandstone, Berea and Carbon Tan cores have productivity contrast suitable for parallel flooding with the Berea sandstone being the most permeable.

(3) For limestone, Indiana and Edwards Yellow cores have productivity contrast suitable for parallel flooding with Indiana limestone being the most permeable.

At this point, the most suitable core samples were selected to test the PFA for mobility control.

4.4.2 Cores Flooded with Pure CO_2, Thickened CO_2 or Oil (No Brine)

4.4.2.1 Single: Pure CO_2 vs. Thickened CO_2 Displacing Oil

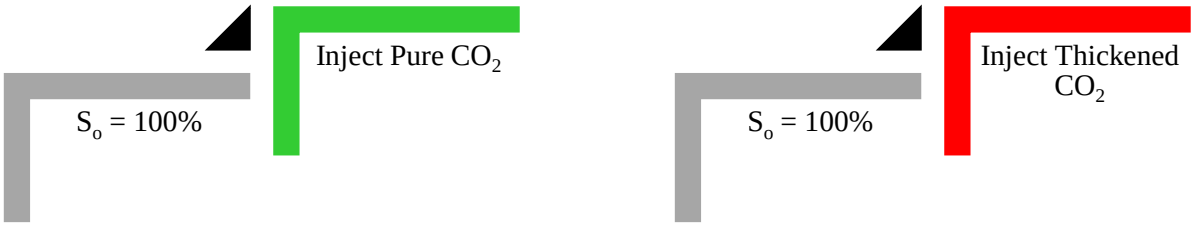

In this stage, a control test involving pure CO_2 displacing oil was followed by a test in which 1 wt.% PFA-thickened CO_2 displaced oil from a similar core. The cores were initially oil saturated (S_O = 100%). Oil recovery and pressure drop were recorded throughout the displacement.

Experiment #1. Berea Sandstone

First, pure CO_2 was injected into the Berea sandstone which was saturated with oil (S_o = 100%). Production performance indicated that after 2 pore volumes (PV) of injected pure CO_2, 79% of oil was recovered. The pressure drop increased and gradually plateaued at 10 psi. While the pressure drop performance showed that the pressure was fluctuating, injecting additional pure CO_2 caused the pressure drop to decrease to almost 6 psi (Figure 24 and Figure 25).

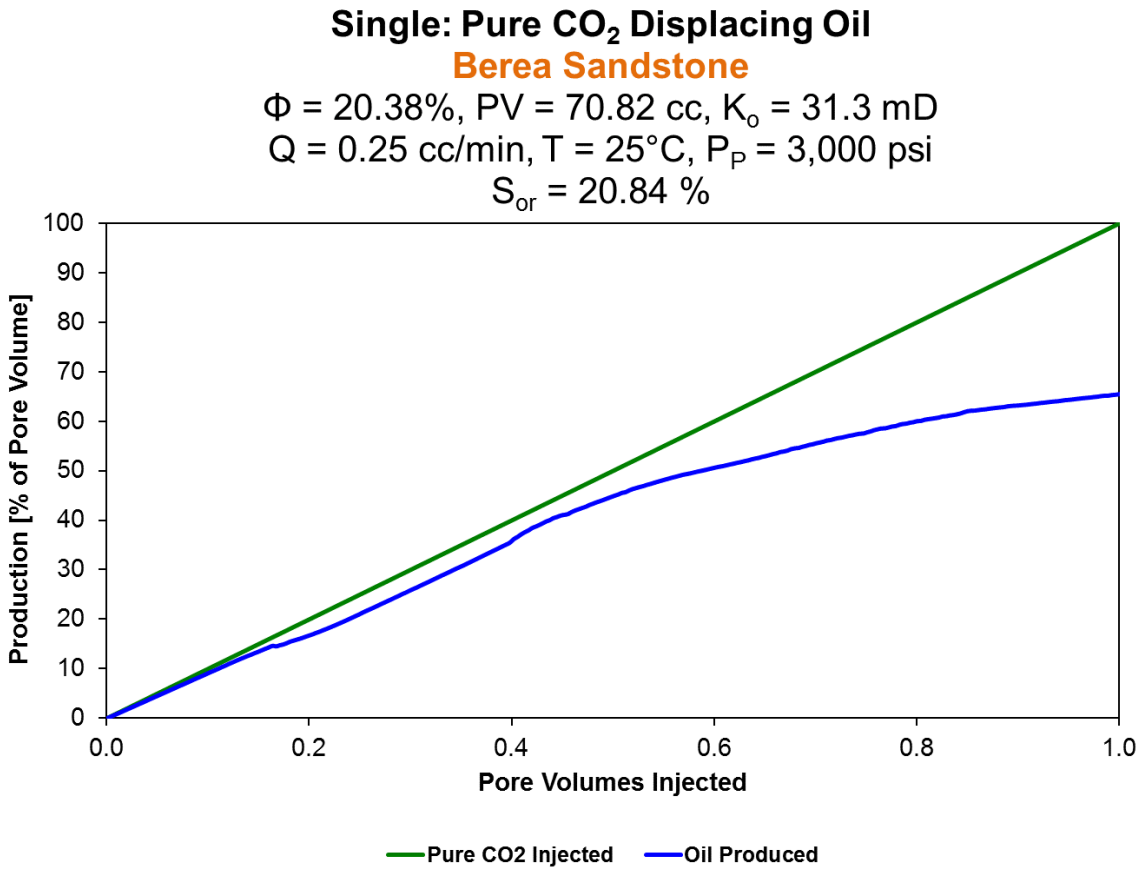

Figure 24. Single Core, Control Test, Production Performance

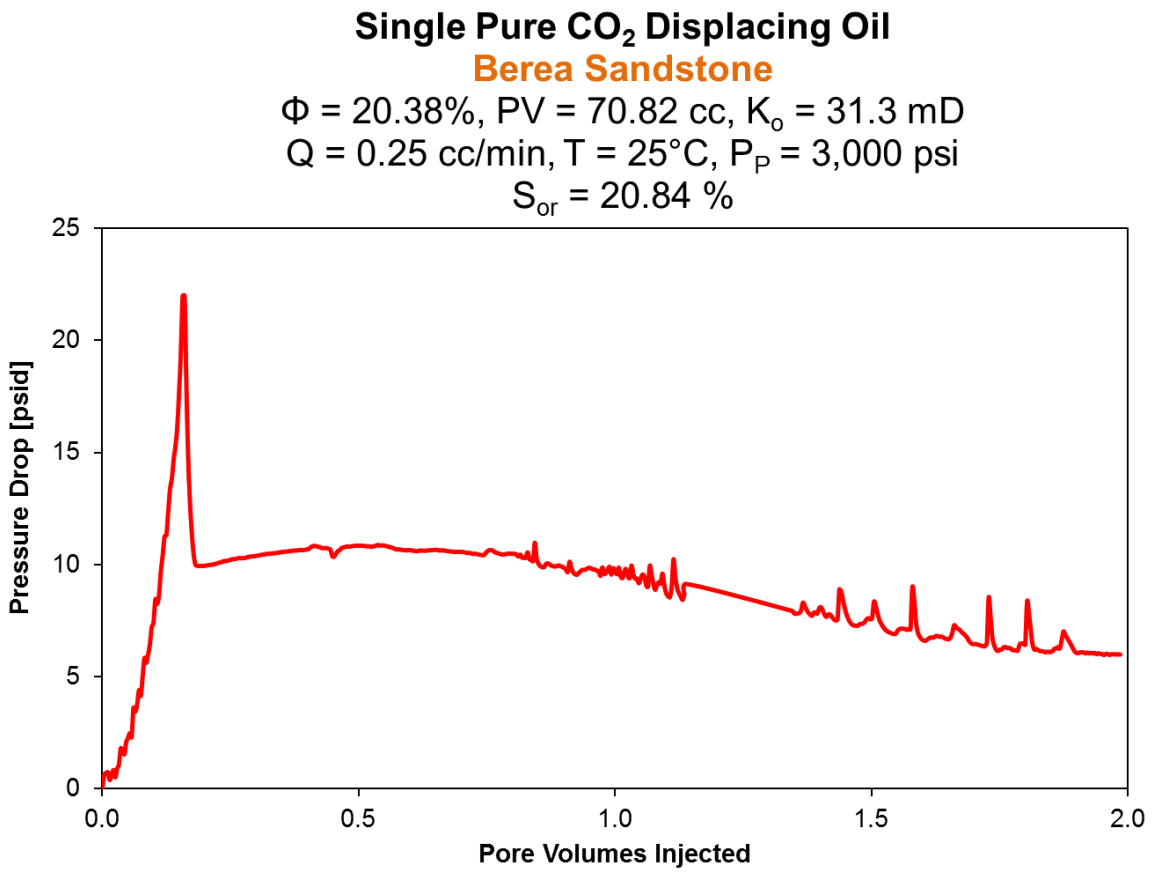

Figure 25. Single Core, Control Test, Pressure Performance

Experiment #2. Berea Sandstone

Next, thickened CO_2, composed of the PFA homopolymer and a CO_2 solution, was injected into the same Berea sandstone which was saturated with oil (S_o = 100%). Production performance indicated that after 2 PV of injected thickened CO_2, 95% of oil was recovered. While the pressure drop performance showed an initial 3-fold increase in pressure drop, injecting additional thickened CO_2 caused the pressure drop to increase drastically to almost 160 psi, which is 27-fold increase (Figure 26 and Figure 27).

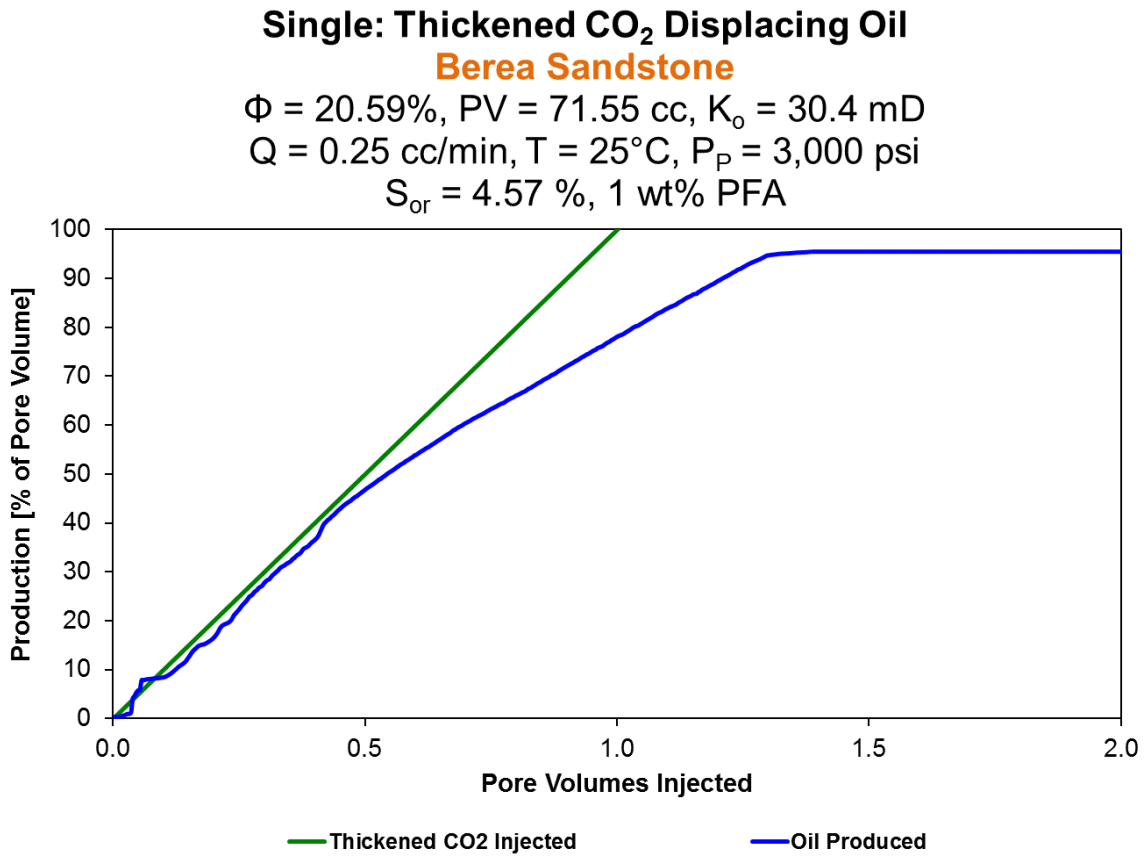

Figure 26. Single Core, Polymer Test, Production Performance

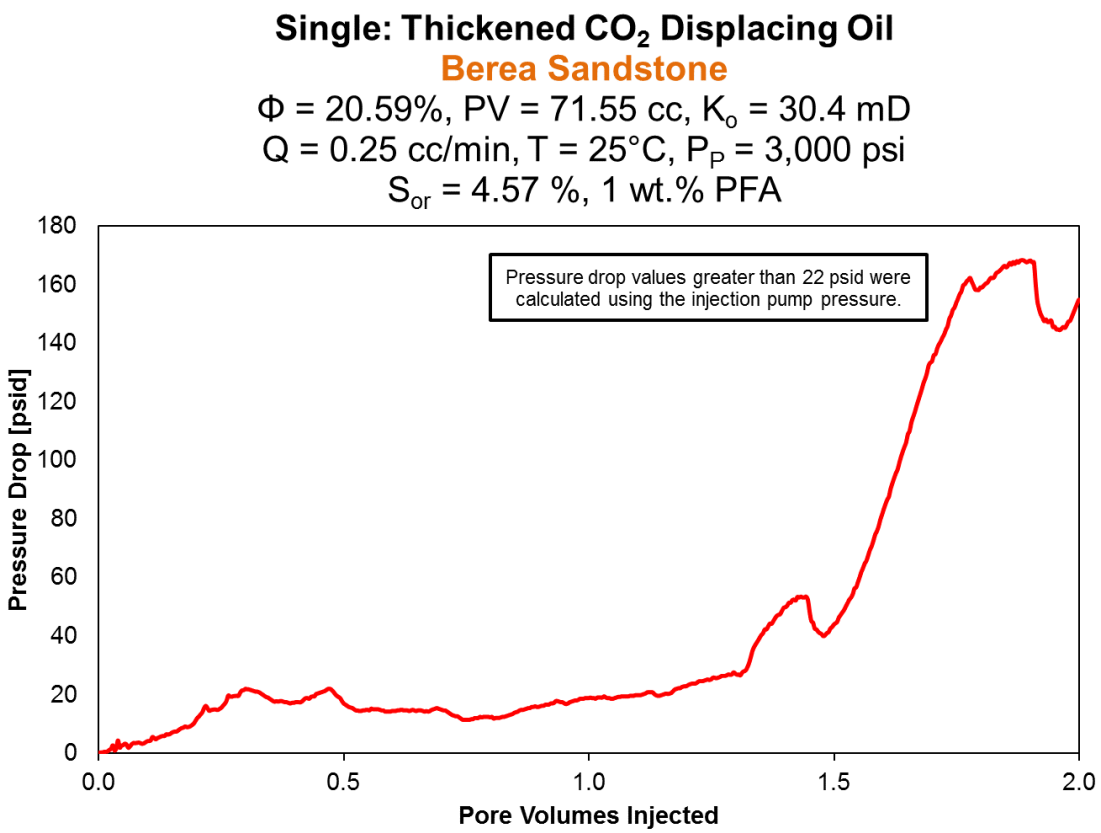

Figure 27. Single Core, Polymer Test, Pressure Performance

4.4.2.2 Lessons Learned

(1) The initial 3-fold increase in pressure drop, from 6 psi to 18 psi, was within the expected (3-4) fold increase. Therefore, the PFA was truly able to thicken CO_2 which resulted in an improvement in mobility control and oil recovery.

(2) However, the subsequent drastic increases in pressure drop suggested some additional phenomena, other than viscosity enhancement, caused the pressure drop to increase far beyond the expected (3-4) fold increase.

At this point, results indicated that the PFA provided the desired increase in oil recovery that appeared to be related to increased viscosity for the initial PVs of injected thickened CO_2. But the dramatic increase in pressure drop thereafter was indicative that the PFA was altering the porous media in some manner that was reducing its permeability.

4.4.3 Cores Flooded with Pure CO_2 and Thickened CO_2 (No Oil or Brine)

4.4.3.1 Single: Thickened CO_2 Displacing Pure CO_2

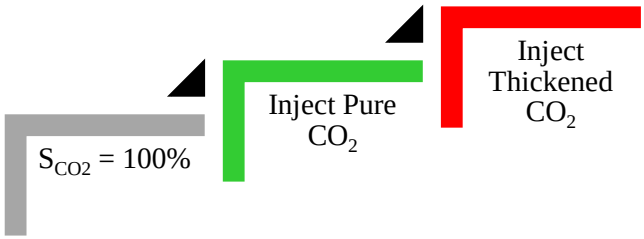

In this stage, the simplest core floods were conducted on cores initially saturated with only pure CO_2 (S_{CO2} = 100%). The control test consisted of injecting pure CO_2, while the PFA polymer test consisted of injecting thickened CO_2. In the following experiments, a 1 wt.% of either the PFA homopolymer or copolymer in the CO_2 solution was injected into the Berea sandstone and Indiana limestone to investigate viscosity change due to pressure drop increase during each core flooding.

Experiment #1. Berea Sandstone

Thickened CO_2 solution was injected into a single core which was saturated with pure CO_2 (S_{CO2} = 100%). In this experiment, the PFA copolymer in a CO_2 solution was injected into a

relatively high permeability Berea sandstone, 285 mD, and the following observations and attempts were considered (Figure 28):

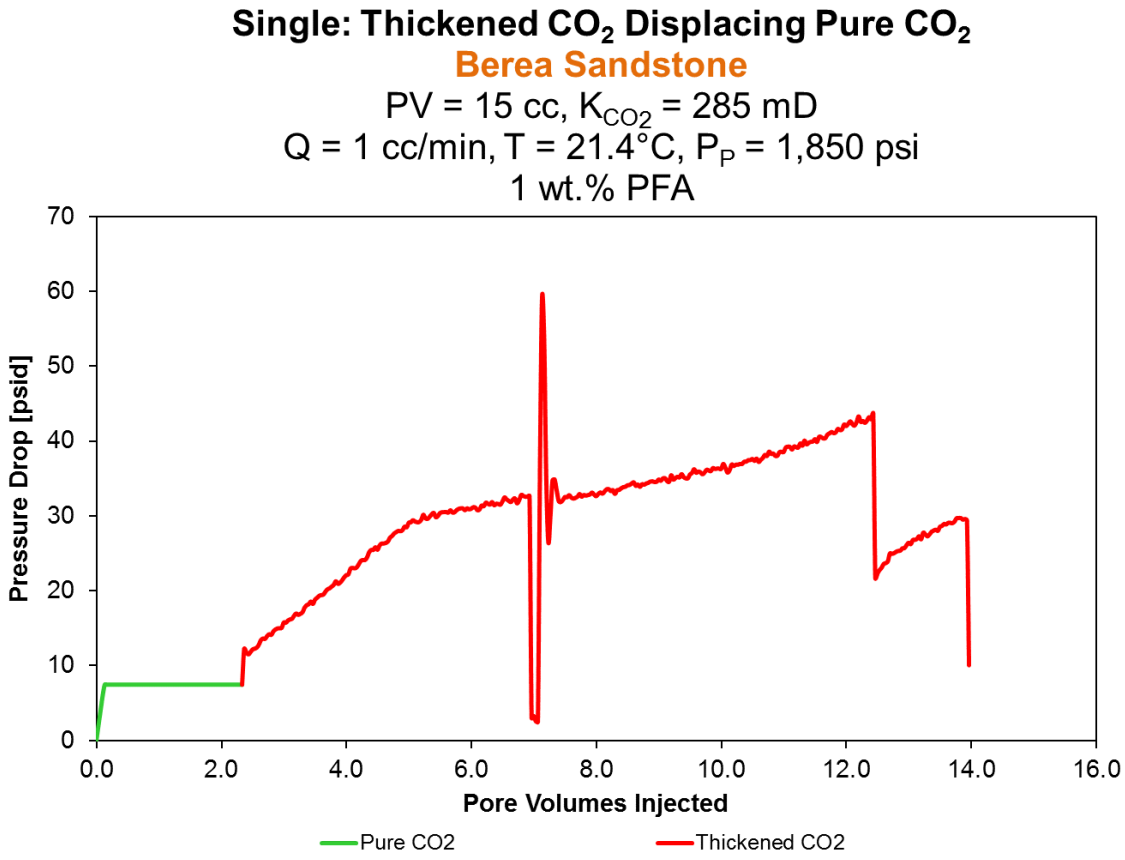

Figure 28. Single Core, Polymer Test, Pressure Performance (Experiment #1)

- *Observations:*

(1) Pure CO_2 was injected at 1 cc/min into the core and a baseline of 7.5 psi pressure drop was developed across the core.

(2) Next, thickened CO_2 solution, composed of pure CO_2 and the PFA copolymer, was injected at 1 cc/min, entered the core at 2.5 PV and a gradual increase in pressure drop was observed. After 4.5 PV of thickened CO_2 solution was injected,

the pressure drop increased to 30 psi, which is 4-fold increase in pressure drop. Similar to previous experiments, it was assumed that the pressure drop increase was due to the increase in the viscosity of CO_2 solution, which was within the expected (3-4) fold increase (Figure 21 and Figure 22). However, a series of pressure drop increases and decreases occurred raising the pressure drop up to 60 psi.

(3) After 5 PV of thickened CO_2 solution was injected, pressure drop increased from 30 psi to 45 psi, which is 6-fold increase in pressure drop, and continued increasing.

Experiment #2. Berea Sandstone

Thickened CO_2 solution was injected into a single core which was saturated with pure CO_2 (S_{CO2} = 100%). In this experiment, the PFA copolymer in CO_2 solution was injected into a relatively low permeability Berea sandstone, 125 mD, and the following observations and attempts were considered (Figure 29):

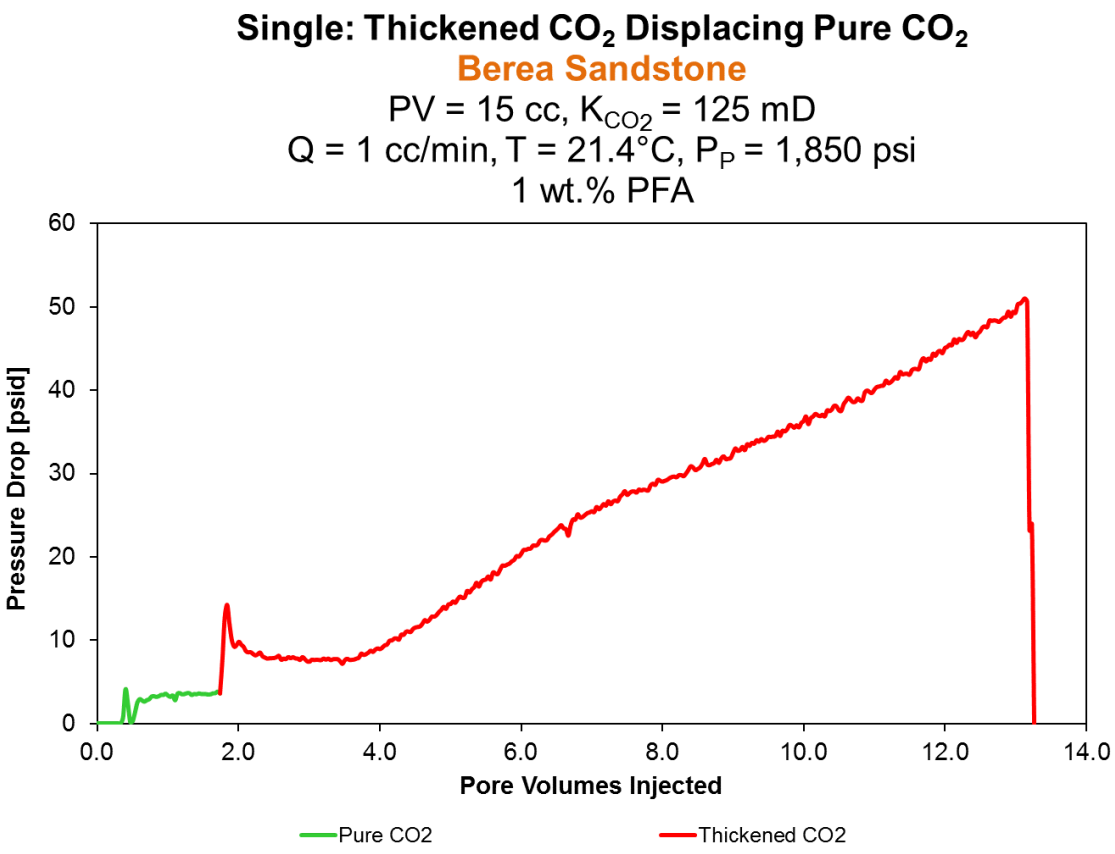

Figure 29. Single Core, Polymer Test, Pressure Performance (Experiment #2)

- *Observations:*

(1) Pure CO_2 was injected at 1 cc/min into the core and a baseline of 3.2 psi pressure drop was developed across the core.

(2) Next, thickened CO_2 solution, composed of pure CO_2 and the PFA, was injected at 1 cc/min, entered the core at 1.8 PV and a gradual increase in pressure drop was observed. After 2 PV of thickened CO_2 solution was injected, the pressure drop increased to 8 psi, which is 2.5-fold increase in pressure drop. Again, it was assumed that the pressure drop increase was due to the increase in the viscosity of

CO_2 solution, which was within the expected (3-4) fold increase. However, the pressure drop continued increasing up to 50 psi.

(3) After 5 PV of thickened CO_2 solution was injected, pressure drop increased from 8 psi to 24 psi, which is 7.5-fold increase, and continued increasing.

Based on (Experiment #1 and Experiment #2), it was important to realize that only pressure drop increases with roughly (3-4) fold increases can be attributed to the polymer's ability to increase the viscosity of CO_2 solution. The drastic pressure drop increases, beyond the (3-4) fold increase, were suspected to have come from some a different effect, such as adsorption, the presence of CO_2-insoluble solid impurities, or pore throat blocking by adsorbed or precipitated polymer. Moreover, despite that the polymer concentration slowly and continuously dropping below 1 wt.% during these displacements, the pressure drop continued to increase. This supported the notion that something other than an increase in viscosity was occurring within the core that was significantly decreasing its permeability (Figure 9 and Equation 7).

Experiment #3. Berea Sandstone

Thickened CO_2 solution was injected into a single core which was saturated with pure CO_2 (S_{CO2} = 100%). In this experiment, the PFA homopolymer in CO_2 solution was injected into the Berea sandstone, and the following observations and attempts were considered (Figure 30 and Table 7):

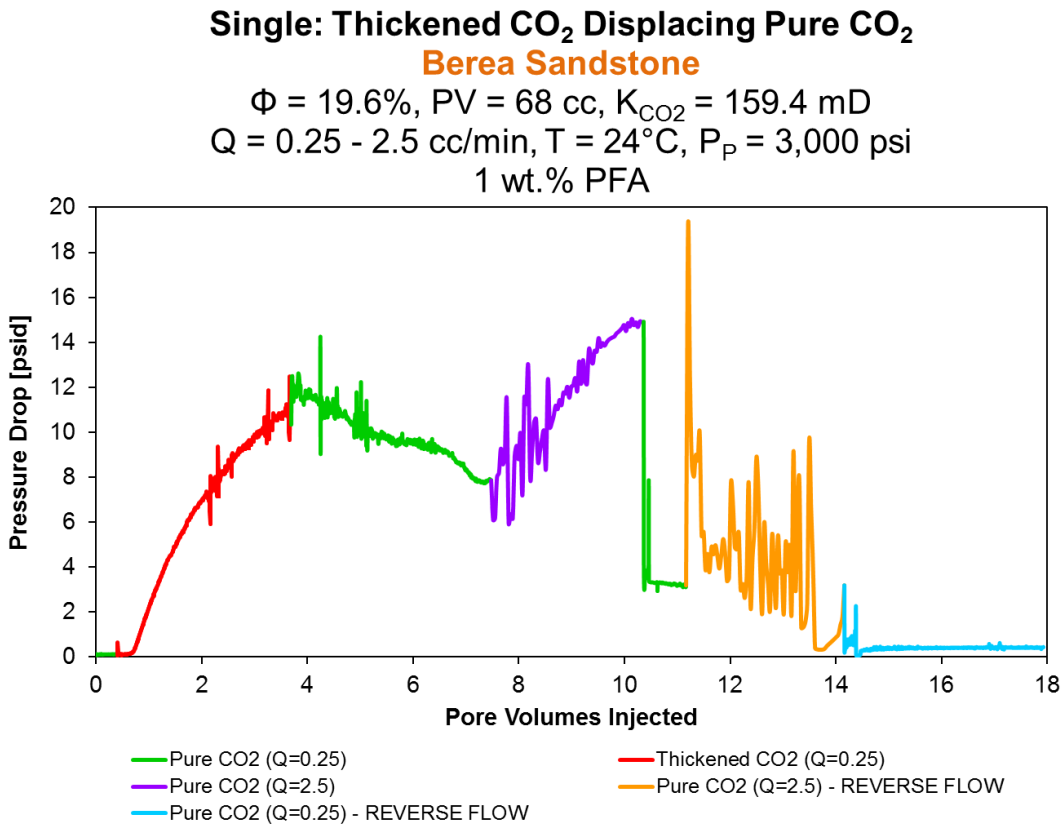

Figure 30. Single Core, Polymer Test, Pressure Performance (Experiment #3)

Table 7. (K) Fold Change on Single Core, Polymer Test, Pressure Performance (Experiment #3)

Q	ΔP	K	K, Fold Change	ΔP * K / Q
[cc/min]	[psi]	[mD]		[psi. mD / cc/min]
0.25	0.10	159.4	-	63.8
2.5	15	10.6	15	
0.25	3	5.3	30	
0.25	0.45	35.42	5	

- *Observations:*

(1) Pure CO_2 was injected at 0.25 cc/min into the core and a baseline of 0.1 psi pressure drop was developed across the core. The core sample was fully saturated with pure CO_2 and the permeability of the core sample was 159.4 mD.

(2) Next, thickened CO_2 solution, composed of CO_2 and 1 wt.% PFA, was injected at 0.25 cc/min, entered the core at 0.7 PV and a gradual increase in pressure drop was observed. After 3 PV of thickened CO_2 solution was injected, the pressure drop increased to 10 psi, which is 100-fold increase in pressure drop. In this experiment, the maximum pressure drop that can be attributed to thickened CO_2 solution was 0.4 psi.

(3) At this point of the study, the different parameters in previous experiments having produced similar pressure drop results provided sufficient evidence to consider three possible scenarios contributing to the overall pressure drop increases:

   a. The viscosity of CO_2 solution has increased.

   b. The polymer has strongly adsorbed onto the core surfaces.

   c. The polymer has been retained within the pores, and perhaps blocking the pores, in such a manner that the polymer can be removed by disruptions in the flow.

(4) To confirm and investigate further, a second pure CO_2 flood was injected at 0.25 cc/min. At this point the core sample is saturated with the highly viscous thickened CO_2 solution. And as the less viscous pure CO_2 is injected, it was expected to decrease the pressure drop considerably after few PV. However, after injecting 3 PV of pure CO_2, multiple pressure drop increases and decreases were observed, and the pressure drop decreased only slightly, slowly plateaued at 9 psi and finally decreased to 8 psi.

(5) Consequently, the third pure CO_2 flood injection increased to 2.5 cc/min, which was 10 times higher than the original pure CO_2 flood. According to Darcy's law, flow rate has a direct relationship with pressure drop and permeability. In other words, an increase in flow rate results in an increase in both pressure drop and permeability. And for a Newtonian fluid, increasing the flow rate 10 times results in a 10 times pressure drop and permeability increases. After increasing CO_2 injection rate from 0.25 to 2.5 cc/min, the pressure drop increased to 15 psi, which is a 150-fold increase in pressure drop. Therefore, the extreme pressure drop must have been the result of polymer particles either strongly or weakly adsorbing onto the core causing the permeability to decrease to 10.6 mD, which is a 15-fold decrease in permeability.

(6) In an attempt to instigate the removal of the weakly adsorbed or retained polymer particles, the fourth pure CO_2 flood was injected at 2.5 cc/min in the reverse direction, which is from the core's outlet to the inlet. The pressure drop increased and decreased drastically generating a general "noise|" trend. This was an indication that pure CO_2 was removing the weakly adsorbed or retained polymer particles, which resulted in a higher permeability, clearing the blocked pore throats, and eventually resulted in a gradual decrease in pressure drop (Figure 31).

(7) Finally, the last pure CO_2 flood injection decreased from 2.5 to 0.25 cc/min and the pressure drop decreased dramatically and plateaued at 0.45 psi, which is a 5-fold decrease in permeability from the original baseline pressure drop.

Based on (Experiment #3), the core's inlet face was not coated with any film-layer polymer particles suggesting that most of the polymer was accumulating inside the core and

within the core's pore throats, which caused a drastic decrease in the core's permeability (Figure 32 and Figure 33). Even though pressure drop increases, which exceeded the (3-4) fold increase, were considered to have blocked the core's pore throats, this experiment confirmed that the weakly adsorbed or retained polymer portion could be removed by reversing CO_2 flow, allowing for partial recovery of permeability.

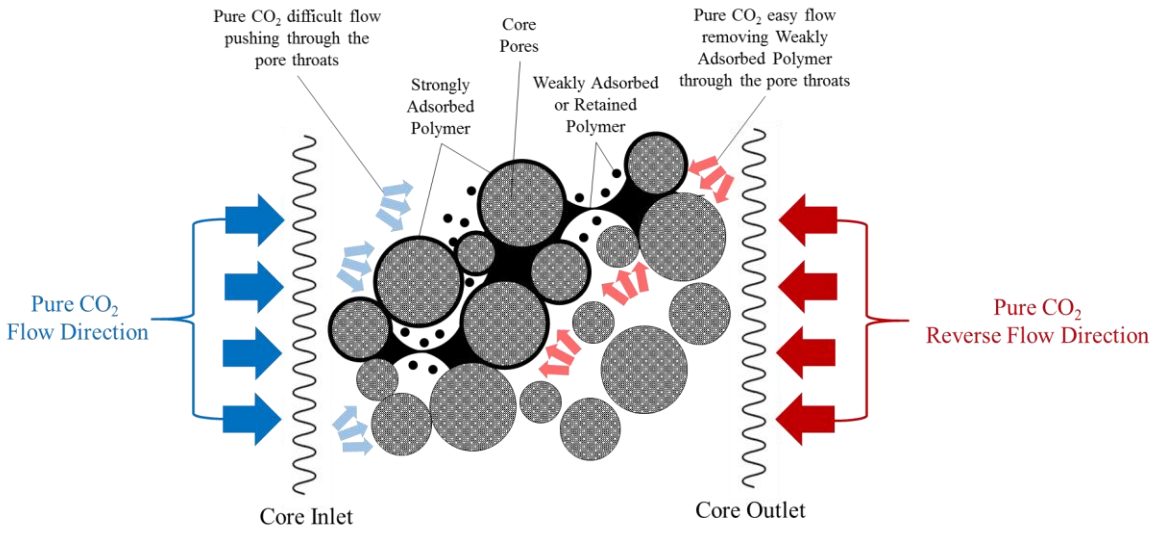

Figure 31. Polymer Particles Coating Pore Surfaces and Blocking a Core's Pore Throats

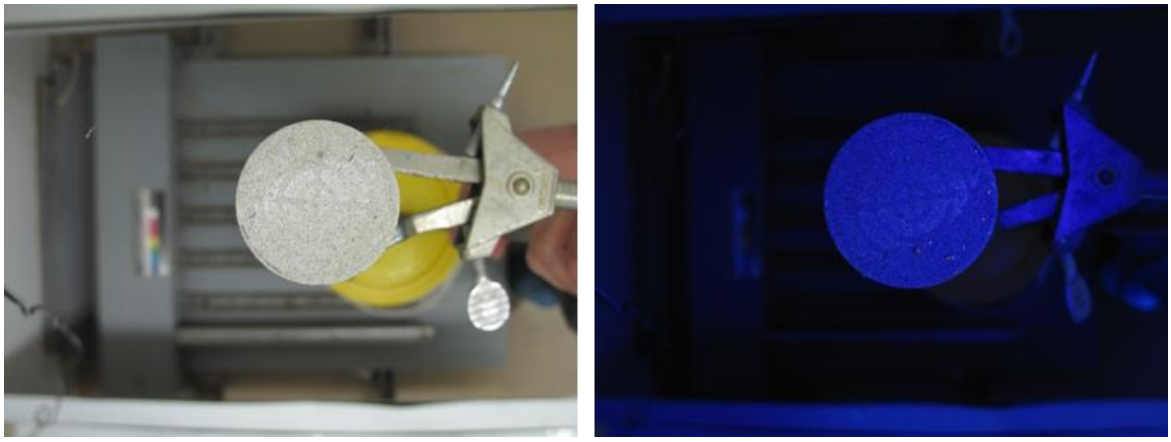

Figure 32. Inlet Face after Polymer Test in (Experiment #3)

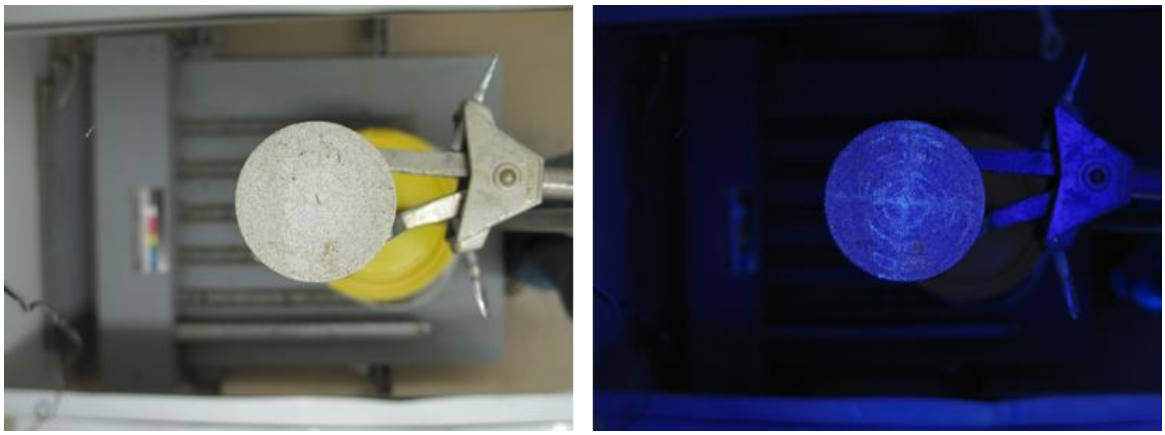

Figure 33. Outlet Face after Polymer Test in (Experiment #3)

Experiment #4. Berea Sandstone

Thickened CO_2 solution was injected into a single core which was saturated with pure CO_2 (S_{CO2} = 100%). In this experiment, the PFA homopolymer in CO_2 solution was injected into the Berea sandstone. Moreover, a microfiber filter was installed in front of the core sample with the hope to examine any particle impurities which could be encountered during core flooding tests (Figure 34). The following observations and attempts were considered (Figure 35 and Table 8):

Figure 34. Microfiber Filter used in Core Flooding

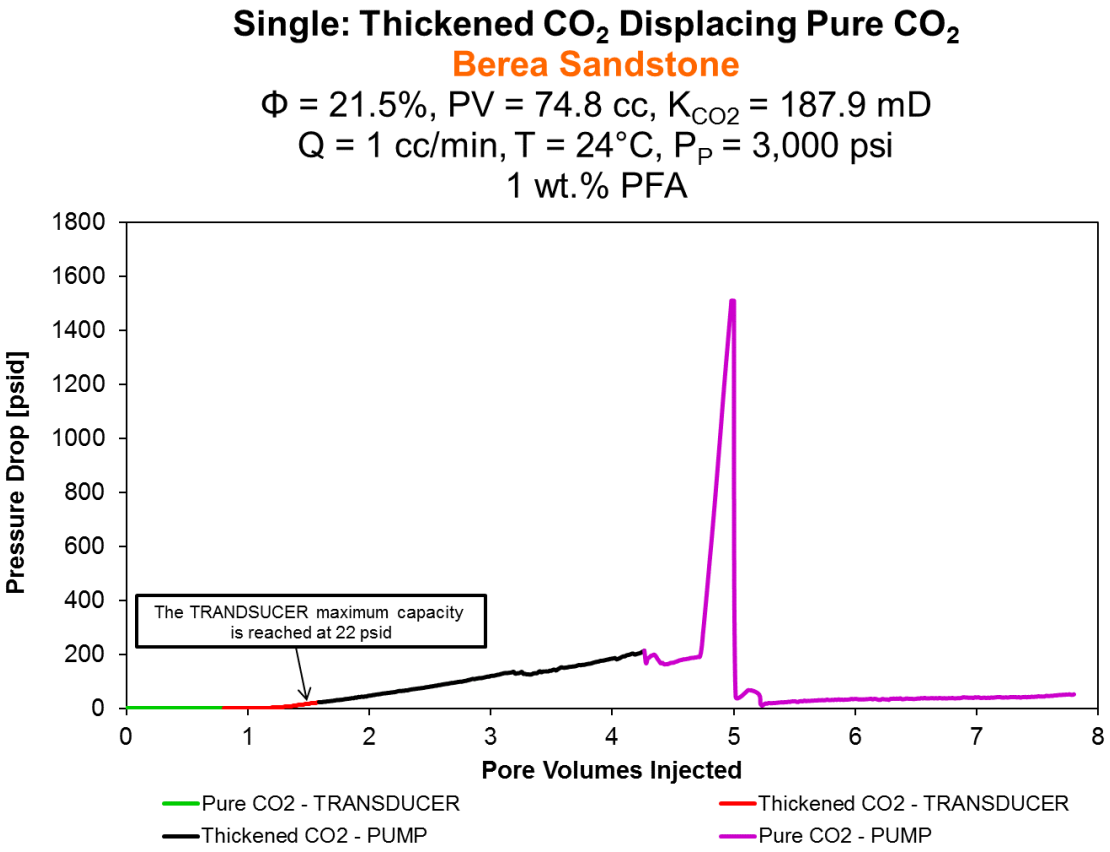

Figure 35. Single Core, Polymer Test, Pressure Performance (Experiment #4)

Table 8. (K) Fold Change on Single Core, Polymer Test, Pressure Performance (Experiment #4)

Q	ΔP	K	K, Fold Change	ΔP * K / Q
[cc/min]	[psi]	[mD]		[psi. mD / cc/min]
1	0.34	187.9	-	63.9
1	20	3.2	59	
1	200	0.3	588	
1	1500	0.04	4412	
1	40	1.6	118	

- *Observations:*

(1) Pure CO_2 was injected at 1 cc/min into the core and a baseline of 0.34 psi pressure drop was developed across the core. The core sample was fully saturated with pure CO_2 and the permeability of the core sample was 187.9 mD.

(2) Next, thickened CO_2 solution was injected at 1 cc/min, entered the core at 0.8 PV and a gradual increase in pressure drop was observed. At 1.58 PV of thickened CO_2 solution, the pressure drop increased to 20 psi, which is 200-fold increase in pressure drop. The transducer's measuring capacity was only up to 22 psi and, since the pressure continued to increase, another pump was installed with a higher capacity.

(3) After 3.46 PV of thickened CO_2 solution was injected at 1 cc/min, pressure drop gradually increased to 200 psi, which is a 2000-fold increase in pressure drop. In this experiment, the maximum pressure drop that can be attributed to thickened CO_2 solution was 1.36 psi.

(4) Pure CO_2 was injected at 1 cc/min, pressure drop plateaued at 200 psi for after 0.6 PV, sharply increased to 1500 psi, which is 4412-fold decrease in permeability.

(5) After 30 minutes of a resting period, pure CO_2 was injected at 1 cc/min and the pressure drop plateaued at 40 psi, which is a 118-fold decrease in permeability.

(6) At the end of this experiment, some polymer residue was found inside the mixer (Figure 36). There were three possible scenarios regarding the origin of that residue:

a. A portion of the polymer has strongly adsorbed on to the interior walls of the mixer and has never been displaced throughout the experiment.

b. A portion of the retained polymer has come out of the solution as the mixer's valve was opened and CO_2 was vented out of the mixer, losing its solvent strength, at the end of the experiment.

c. The quiescent pure CO_2 may have dissolved some of the weakly retained polymer, allowing for a partial recovery of permeability.

Figure 36. PFA Homopolymer inside Mixer after Polymer Test in (Experiment #4)

Experiment #5. Berea Sandstone

Thickened CO_2 solution was injected into a single core which was saturated with pure CO_2 (S_{CO2} = 100%). In this experiment, the PFA homopolymer in CO_2 solution was injected into the Berea sandstone. Again, the same microfiber filter used in (Experiment #4**)**, was installed for

the same purpose (Figure 34). The following observations and attempts were considered (Figure 37 and Table 9):

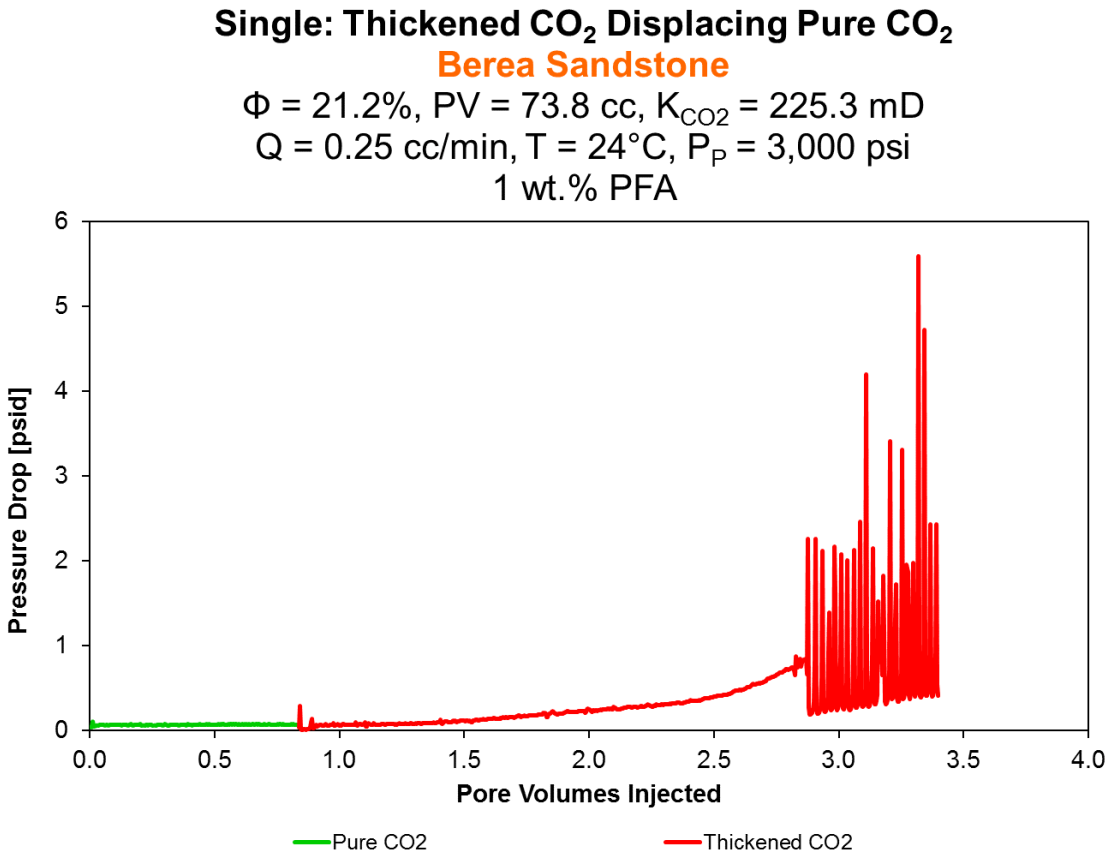

Figure 37. Single Core, Polymer Test, Pressure Performance (Experiment #5)

Table 9. (K) Fold Change on Single Core, Polymer Test, Pressure Performance (Experiment #5)

Q	ΔP	K	K, Fold Change	ΔP * K / Q
[cc/min]	[psi]	[mD]		[psi. mD / cc/min]
0.25	0.07	225.3	-	63.1
0.25	0.84	18.8	12	
0.25	2.5	6.3	36	

- *Observations:*

(1) Pure CO_2 was injected at 0.25 cc/min into the core and a baseline of 0.07 psi pressure drop was developed across the core. The core sample was fully saturated with pure CO_2 and the permeability of the core sample was 225.3 mD.

(2) Next, thickened CO_2 solution, composed of pure CO_2 and the polymer, was injected at 0.25 cc/min, entered the core at 0.9 PV and a gradual increase in pressure drop was observed. After 2 PV of thickened CO_2 solution was injected, the pressure drop increased to 0.84 psi, which is 12-fold increase in pressure drop. In this experiment, the maximum pressure drop that can be attributed to thickened CO_2 solution was 0.28 psi.

(3) After 2.2 PV of thickened CO_2 solution was injected, pressure drop increased from 0.84 psi to 2.5 psi, which is 36-fold decrease in permeability, and the pressure drop continued increasing.

Based on (Experiment #4 and Experiment #5), it was important to realize the change in permeability after thickened CO_2 flooding where pressure drop across the core continued to increase and the permeability was drastically reduced. There was no evidence of particle impurities on the fiber filter after both core flooding tests. Nonetheless, all subsequent experiments were to be conducted using either the AQ microfiber filter with 0.9µ liquid efficiency, or the 5M sintered stainless steel filter with 5µ liquid efficiency.

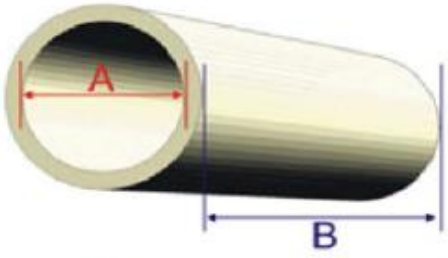

Part Number	ID	Length
050-03	1/2"	1"
050-05	1/2"	1-1/4"
050-015	1/2"	0.45"
050-07	1/2"	1-1/2"
050-11	1/2"	2-1/4"

Microfibre	Gas Efficiency	Liquid Efficiency
DX /DQ/ DXQ / DH	0.01µ at 93%	25µ at 98%
CX /CQ/ CXQ / CH	0.01µ at 98%	8µ at 98%
BX / BQ/BXQ / BH	0.01µ at 99.99%	2µ at 98%
AQ / AH	0.01µ at 99.9999%	0.9µ at 98%
AAQ	0.01µ at 99.99999%	0.3µ at 98%

Sintered SS	Gas Efficiency	Liquid Efficiency
00M	100µ Nominal	100µ Nominal
70M	70µ Nominal	70µ Nominal
40M	40µ Nominal	40µ Nominal
20M	20µ Nominal	20µ Nominal
10M	10µ Nominal	10µ Nominal
5M	5µ Nominal	5µ Nominal

Figure 38. Microfiber and Stainless Steel Filters Specifications

Experiment #6. Berea Sandstone

Thickened CO_2 solution was injected into a single core which was saturated with pure CO_2 (S_{CO2} = 100%). In this experiment, the PFAST-C6 copolymer in CO_2 solution was injected into the Berea sandstone, and the following observations and attempts were considered (Figure 39 and Table 10):

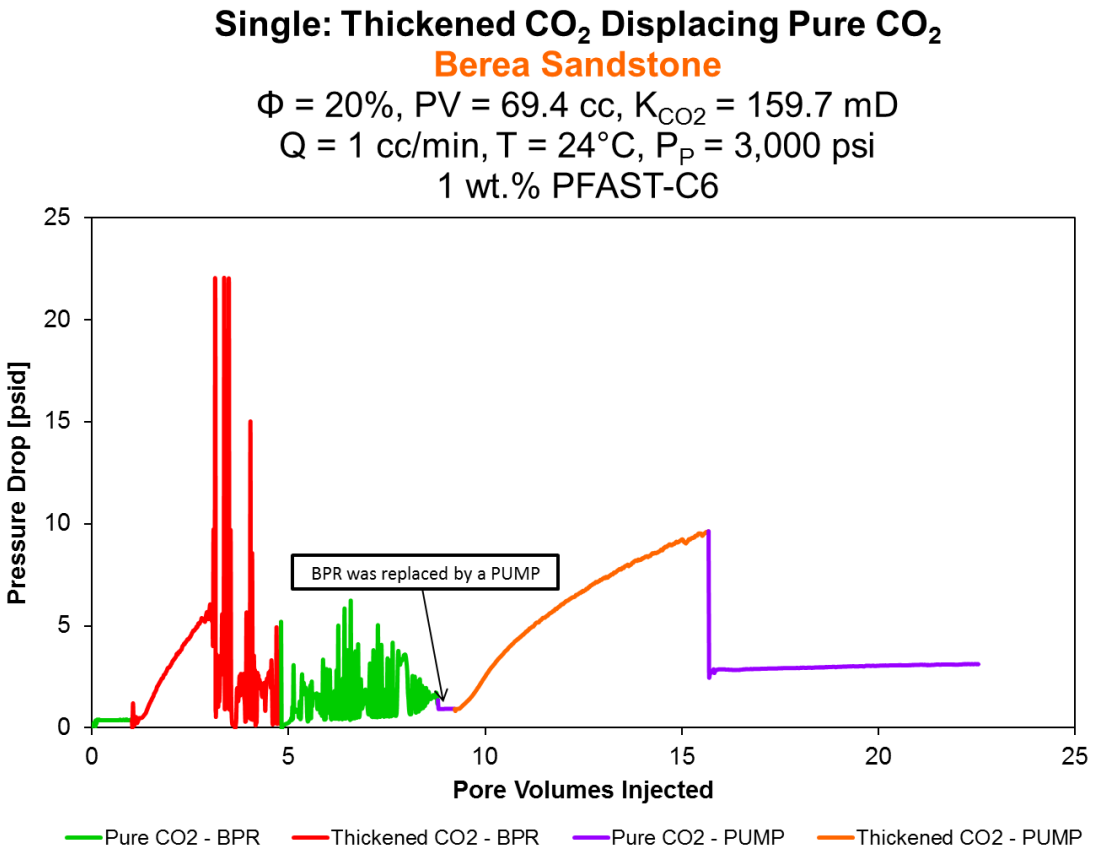

Figure 39. Single Core, Polymer Test, Pressure Performance (Experiment #6)

Table 10. (K) Fold Change on Single Core, Polymer Test, Pressure Performance (Experiment #6)

Q	ΔP	K	K, Fold Change	ΔP * K / Q
[cc/min]	[psi]	[mD]		[psi. mD / cc/min]
1	0.40	159.7	-	63.9
1	6	10.6	15	
1	1	63.9	3	
1	9	7.1	23	
1	3	21.3	8	

- *Observations:*

(1) Pure CO_2 was injected at 1 cc/min into the core and a baseline of 0.3 psi pressure drop was developed across the core. The core sample was fully saturated with pure CO_2 and the permeability of the core sample was 159.7 mD.

(2) Next, thickened CO_2 solution, composed of pure CO_2 and the polymer, was injected at 1 cc/min, entered the core at 1 PV and a gradual increase in pressure drop was observed. After 2 PV of thickened CO_2 solution was injected, the pressure drop increased to 6 psi, which is 15-fold increase in pressure drop. In this experiment, the maximum pressure drop that can be attributed to thickened CO_2 solution was 1.2 psi.

(3) Soon after injecting additional 2 PV of thickened CO_2, a series of sharp pressure drop increases and decreases were developed across the core. This was attributable to polymer coming out of the solution as the solution experienced a sharp pressure drop exiting the BPR. This deposit not only disrupted the seal of the BPR, hence the noise in the data, but also provided direct evidence that a portion of the polymer had indeed remained dissolved in the CO_2 and passed through the entire core.

(4) Even after injecting 3 PV of pure CO_2 was at 1 cc/min, pressure drop was still fluctuating. At this point, the back pressure regulator was replaced by a PD pump operating at the same flow rate but opposite direction as the CO_2 injection PD pump.

(5) Pure CO_2 was injected at 1 cc/min using the newly replaced pumps and a pressure drop plateau of 1 psi was developed across the core. It is important to note that the

pressure drop did not fall back to the original 0.3 baseline, which, again, indicated the existence of polymer particles adsorbing onto the core and blocking the core's pore throats.

(6) Then, thickened CO_2 solution, was injected at 1 cc/min, entered the core at 9.5 PV and a gradual increase in pressure drop was observed. After 5 PV of thickened CO_2 solution was injected, the pressure drop increased to 9 psi, which is 23-fold decrease in permeability.

(7) After 80 minutes of a resting period, the pressure drop sharply declined and plateaued at 3 psi, which is 8-fold decrease in permeability. Similar to (Experiment #4), once pure CO_2 was injected at 15.5 PV, the decrease in pressure drop was essentially instantaneous, which is most likely due to the resting period where the polymer dissolved back into the CO_2 solution.

(8) Then, the core sample was vented of pure CO_2 and was cut in half. The first half, which is close to the inlet, has a permeability of 61 mD, and the second half has a permeability of 122 mD. This indicates that most of the polymer adsorption and retention occurred near the core inlet.

(9) The mass of the core sample was measured before and after core flooding, and there was a 1.697 g increase. However, this data was not used in a PFA material balance because small fragments of the core can fall off of the core as it is removed from the core holder sleeve. Furthermore, it is difficult to remove the polymer that remains in the mixer and the polymer that accumulates in the reverse flow PD pump (or BPR if the BPR is used).

Experiment #7. Berea Sandstone

Thickened CO_2 solution was injected into a single core which was saturated with pure CO_2 (S_{CO2} = 100%). In this experiment, the PFA homopolymer solution in CO_2 solution was injected into the Berea sandstone, and the following observations and attempts were considered (Figure 40 and Table 11):

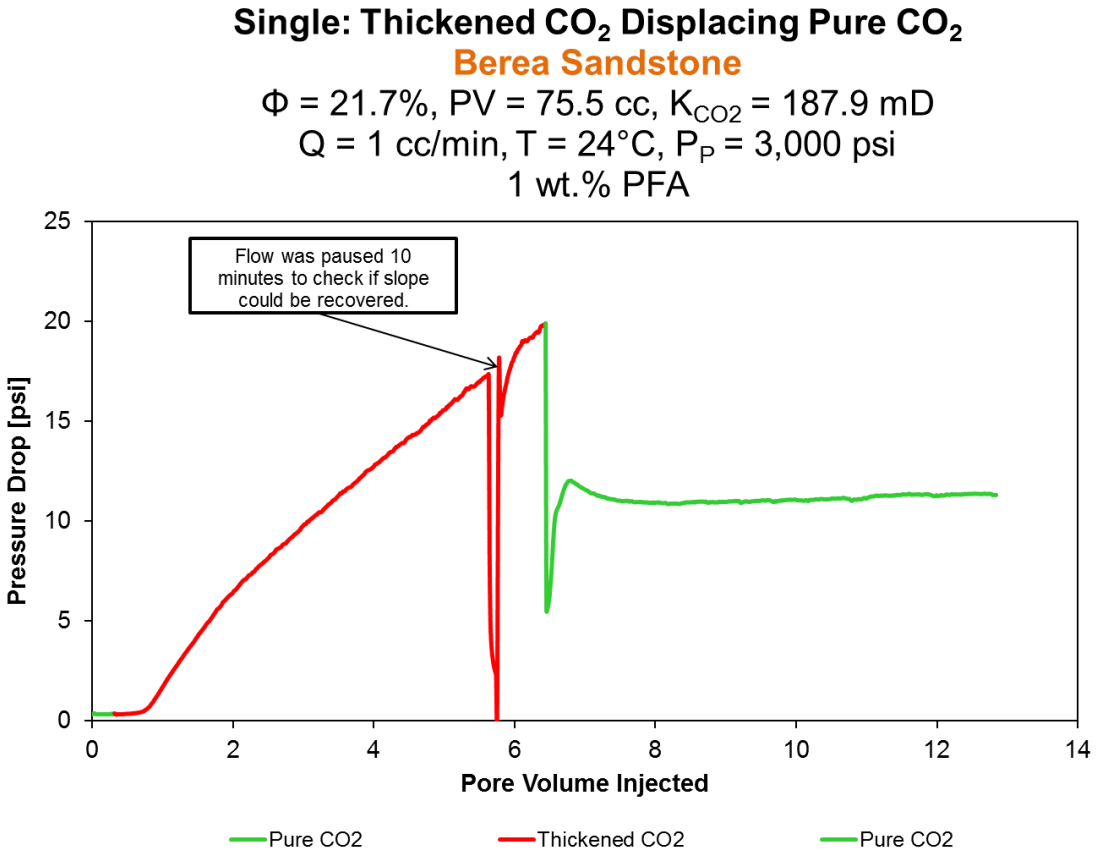

Figure 40. Single Core, Polymer Test, Pressure Performance (Experiment #7)

Table 11. (K) Fold Change on Single Core, Polymer Test, Pressure Performance (Experiment #7)

Q	ΔP	K	K, Fold Change	ΔP * K / Q
[cc/min]	[psi]	[mD]		[psi. mD / cc/min]
1	0.34	187.9	-	63.9
1	20	3.2	59	
1	11	5.8	32	

- *Observations:*

(1) Pure CO_2 was injected at 1 cc/min into the core and a baseline of 0.34 psi pressure drop was developed across the core. The core sample was fully saturated with CO_2 and the permeability of the core sample was 187.9 mD.

(2) Next, thickened CO_2 solution, composed of CO_2 and the polymer, was injected at 1 cc/min, entered the core at 0.4 PV and a gradual increase in pressure drop was observed. After 6 PV of thickened CO_2 solution was injected, the pressure drop increased to 20 psi, which is 60-fold increase in pressure drop. In this experiment, the maximum pressure drop that can be attributed to thickened CO_2 solution was 1.36 psi.

(3) Pure CO_2 was injected at 1 cc/min and pressure drop plateau of 11 psi was developed across the core, which is 32-fold decrease in permeability. Similar to (Experiment #7), the pressure drop did not fall back to the original 0.34 baseline, which, again, indicated the existence of the polymer altering the core permeability.

(4) Finally, the core sample was vented of pure CO_2 and was cut in half. The first half, which is close to the inlet, has a permeability of 11 mD, and the second half has a permeability of 152 mD. This again indicates that most of the polymer adsorption and retention occurred near the core inlet.

Experiment #8. Indiana Limestone

Thickened CO_2 solution was injected into a single core which was saturated with pure CO_2 (S_{CO2} = 100%). In this experiment, the PFA homopolymer in CO_2 solution was injected into the Indiana limestone, and the following observations and attempts were considered (Figure 41 and Table 12):

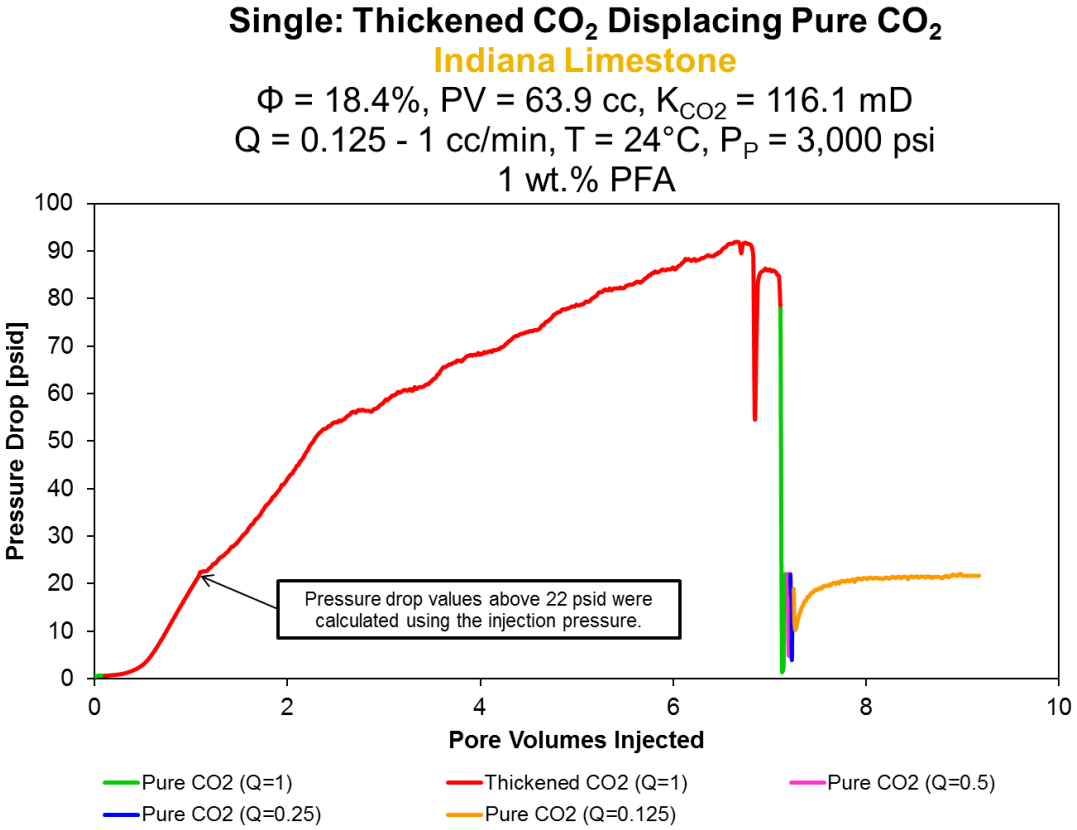

Figure 41. Single Core, Polymer Test, Pressure Performance (Experiment #8)

Table 12. (K) Fold Change on Single Core, Polymer Test, Pressure Performance (Experiment #8)

Q	ΔP	K	K, Fold Change	ΔP * K / Q
[cc/min]	[psi]	[mD]		[psi. mD / cc/min]
1	0.55	116.1	-	63.9
1	22	2.9	40	
1	90	0.7	164	
0.125	22	0.4	320	

- *Observations:*

(1) Pure CO_2 was injected at 1 cc/min into the core and a baseline of 0.55 psi pressure drop was developed across the core. The core sample was fully saturated with CO_2 and the permeability of the core sample was 116.1 mD.

(2) Next, thickened CO_2 solution, composed of pure CO_2 and the polymer, was injected at 1 cc/min, entered the core at 0.4 PV and a sharp increase in pressure drop was observed. After 1 PV of thickened CO_2 solution was injected, the pressure drop increased to 22 psi, which is 40-fold decrease in permeability. The pressure drop continued to increase to 90 psi, which is 164-fold increase in pressure drop. In this experiment, the maximum pressure drop that can be attributed to thickened CO_2 solution was 2.2 psi.

(3) Pure CO_2 was injected at 1, 0.5, 0.25 and 0.125 cc/min and the pressure drop was never able to reach 22 psi. It was only when pure CO_2 was injected at 0.125 cc/min that the pressure drop reached 22 psi, which is 320-fold decrease in permeability.

(4) Finally, the core sample was vented of pure CO_2 and was cut in half. The first half, which is close to the inlet, has a permeability of 2.8 mD, and the second half has a permeability of 23.5 mD.

Based on (Experiment #6, Experiment #7 and Experiment #8), there was an instantaneous pressure drop decrease after the resting period suggesting that some polymer particles have settled and dissolved back into the CO_2 solution. Again, similar to previous experiments, the

pressure drop across the core continued to increase and the permeability was greatly reduced. Moreover, the venting process of pure CO_2 increased the permeability of the cores perhaps by dislodging ore rearranging the polymer particles inside the core to be re-dissolve in CO_2 solution.

4.4.3.2 Lessons Learned

(1) Again, the polymer's concentration dropped exponentially below 1 wt.%; however, the pressure drop continued to increase. This was a clear indication that some polymer particles were not dissolved in the solution and worked against the expected pressure drop decrease due to the dilute polymer's concentration in CO_2 solution.

(2) There are three possible scenarios contributing to the overall pressure drop increase:

a. The polymer dissolved completely in CO_2 solution and flew entirely through the core as some portions of the polymer were stuck in the BPR.

b. The polymer adsorbed strongly to the core's surface as the core's permeability was greatly reduced.

c. The polymer was weakly absorbed retained to the core and can be removed by reversing the flow across the core, increasing the velocity of CO_2 injection or venting the core of CO_2.

Despite the increase in oil recovery and brine recovery associated with the PFA-thickened CO_2, the entire set of the above results indicated that the PFA is an ineffective agent for mobility control because: 1) high rates of polymer loss due to adsorption occur that will

reduce the thickening, and 2) extremely large reductions in permeability occur. However, the PFA appears to be a novel CO_2-soluble conformance control agent because a portion of the PFA strongly adsorbs on the core surfaces and a portion is more weakly retained; together these PFA losses to the core can greatly reduce the permeability of a rock. Therefore, the subsequent core flooding tests were designed to examine permeability reduction across the core.

4.4.4 Cores Flooded with Pure CO_2, Thickened CO_2 and Brine (No Oil)

4.4.4.1 Single: Pure CO_2 vs. Pure and Thickened CO_2 Displacing Brine

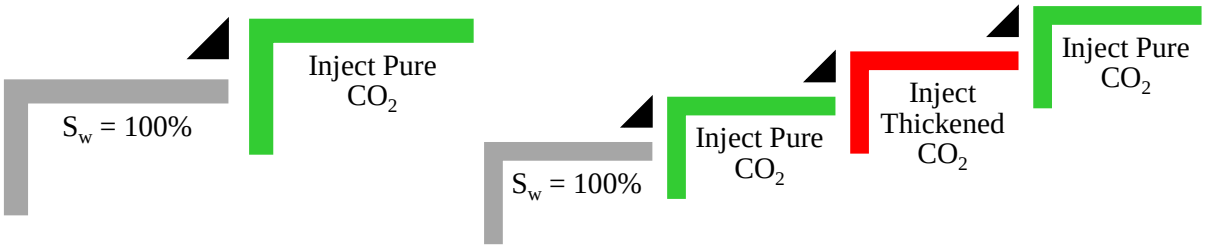

In this stage, a control test followed by a polymer test were conducted on brine water saturated single cores (S_w = 100%). The control test consisted of injecting pure CO_2, while the polymer test consisted of injecting both pure CO_2 and thickened CO_2, sequentially. In the following experiments, a 1 wt.% of the PFA homopolymer in CO_2 solution was injected into the Berea sandstone, Carbon Tan sandstone, Indiana limestone and Edwards Yellow limestone to investigate permeability change due to pressure drop increase during each core flooding. The following observations and attempts were considered:

Experiment #1. Berea Sandstone

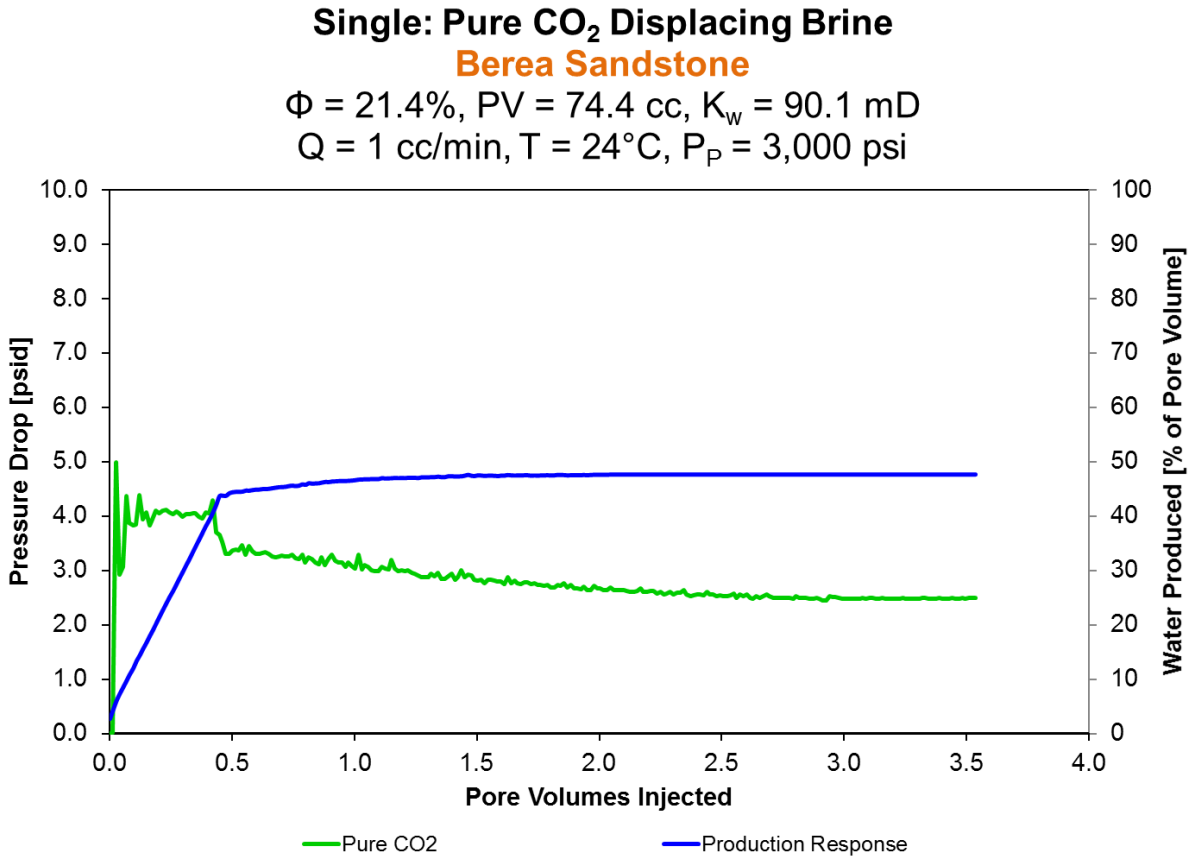

Figure 42. Single Core, Control Test, Pressure and Production Performances (Experiment #1)

- *Observations:*

(1) The effective permeability of the Berea sandstone to brine ($K_{e,w}$), when (S_w = 100%), was found to be 90.1 mD.

(2) After pure CO_2 flood, the effective permeability of the Berea sandstone to pure CO_2 (K_{e,CO_2}), when (S_w = 52.4%), was found to be 25.6 mD.

(3) Following the pure CO_2 flood, the effective permeability of the Berea sandstone to brine, when (S_w = 64.4%), was found to be 19.2 mD, which is a 4.7-fold decrease in the effective permeability of the Berea sandstone to brine (Figure 42).

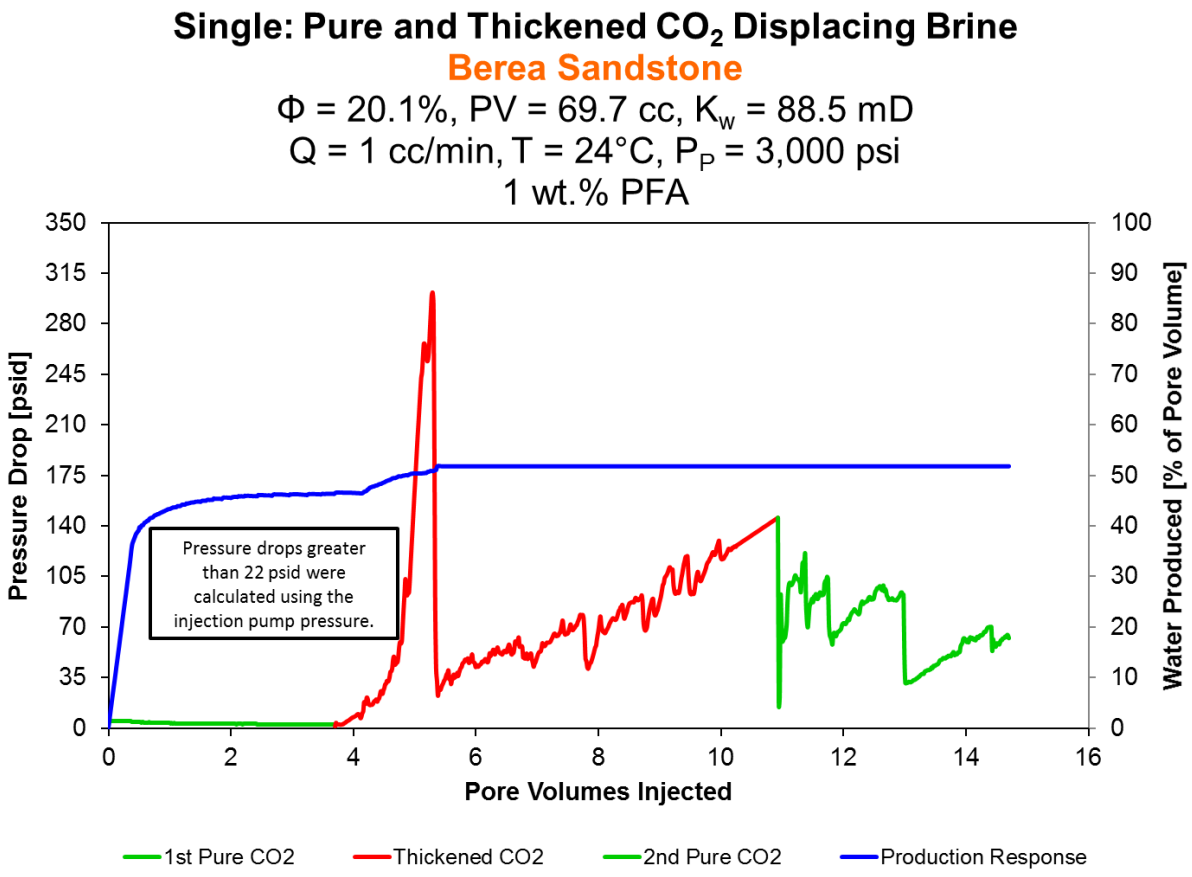

Figure 43. Single Core, Polymer Test, Pressure and Production Performances (Experiment #1)

- *Observations:*

(1) The effective permeability of the Berea sandstone to brine, when (S_w = 100%), was found to be 88.5 mD.

(2) After first pure CO_2 flood, the effective permeability of the Berea sandstone to pure CO_2, when (S_w = 53.6%), was found to be 25.6 mD.

(3) After thickened CO_2 flood, the effective permeability of the Berea sandstone to thickened CO_2, when (S_w = 48.2%), was calculated to be 0.44 mD, which is a 58-fold decrease in the effective permeability of the Berea sandstone to CO_2.

(4) After second pure CO_2 flood, the effective permeability of the Berea sandstone to pure CO_2, when (S_w = 48.2%), was calculated to be 0.91 mD, which is a 28-fold decrease in the effective permeability of the Berea sandstone to CO_2.

(5) Following the pure CO_2 flood, the effective permeability of the Berea sandstone to brine, when (S_w = 59.8%), was found to be 10.3 mD, which is an 8.59-fold decrease in the effective permeability of the Berea sandstone to brine (Figure 43).

Experiment #2. Carbon Tan Sandstone

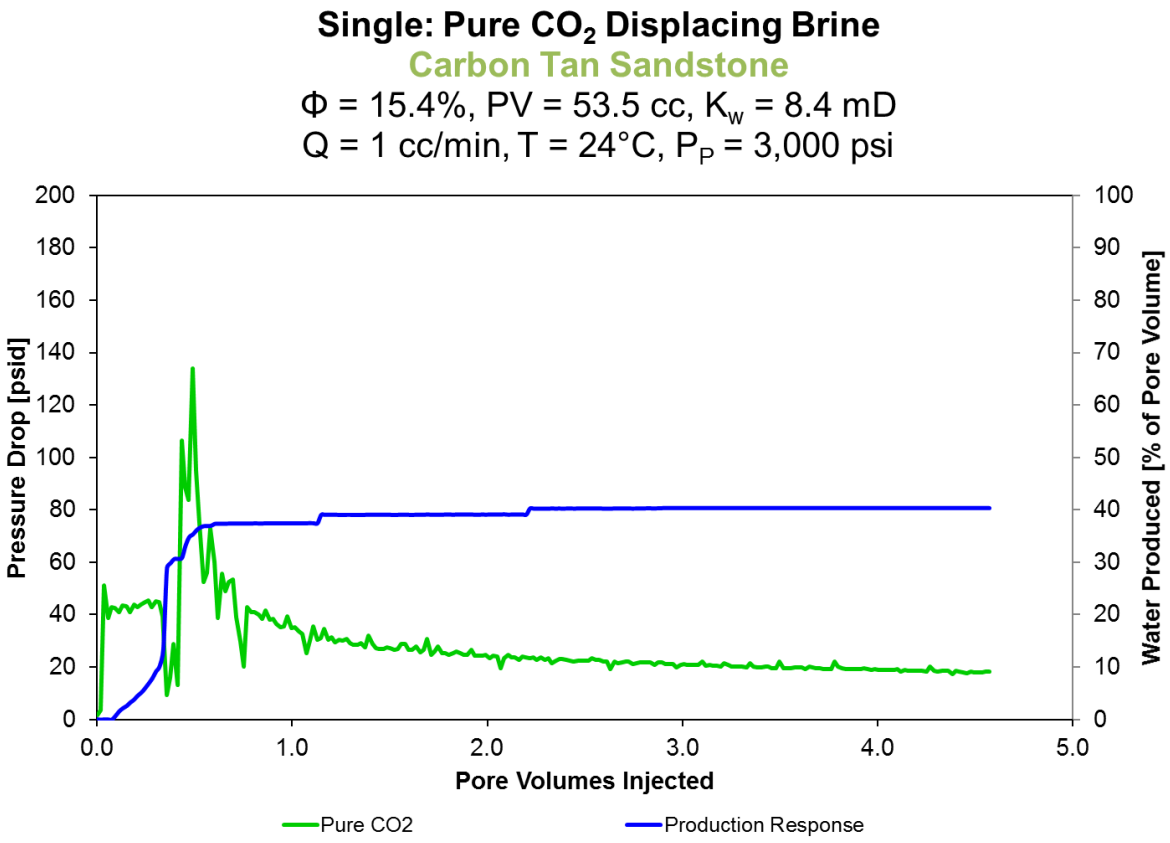

Figure 44. Single Core, Control Test, Pressure and Production Performances (Experiment #2)

- *Observations:*

(1) The effective permeability of the Carbon Tan sandstone to brine, when (S_w = 100%), was found to be 8.4 mD.

(2) After pure CO_2 flood, the effective permeability of the Carbon Tan sandstone to pure CO_2, when (S_w = 59.7%), was found to be 3.5 mD.

(3) Following the pure CO_2 flood, the effective permeability of the Carbon Tan sandstone to brine, when (S_w = 69.5%), was found to be 2.5 mD, which is a 3.4-

fold decrease in the effective permeability of the Carbon Tan sandstone to brine (Figure 44).

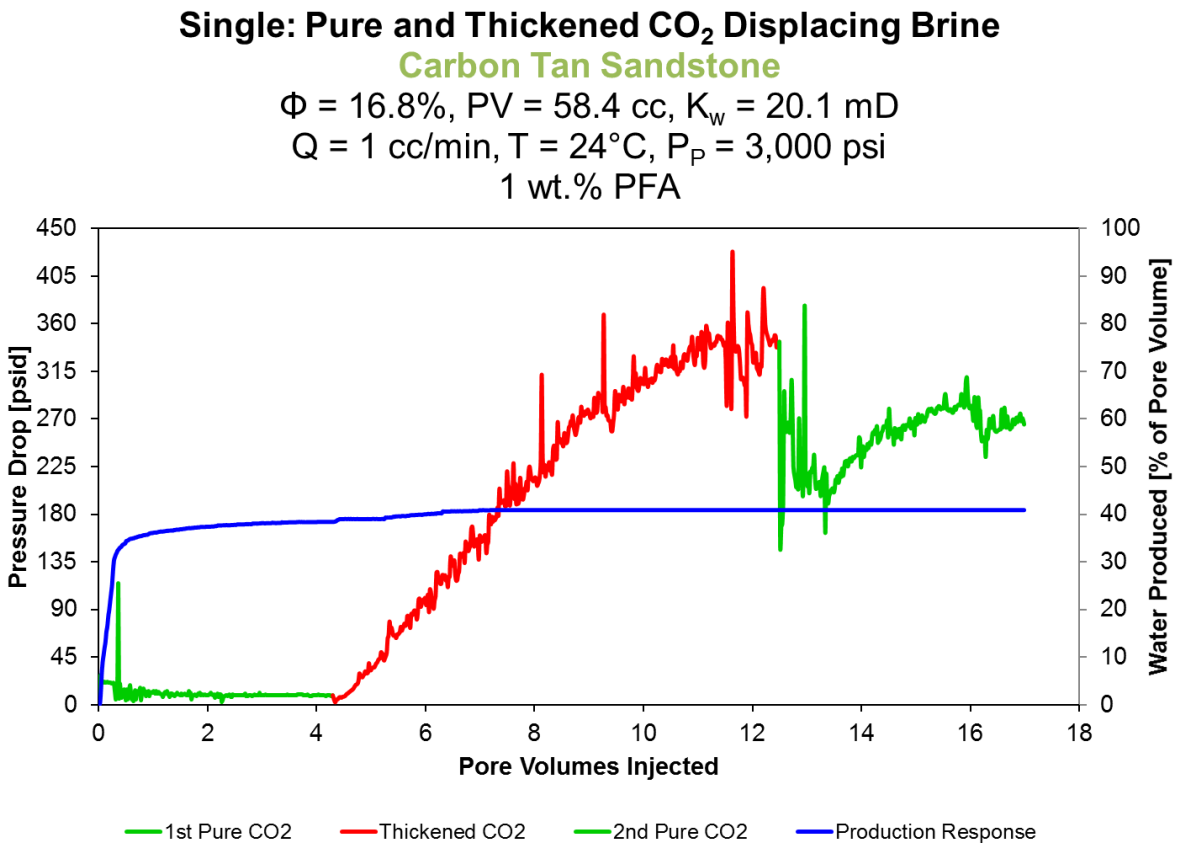

Figure 45. Single Core, Polymer Test, Pressure and Production Performances (Experiment #2)

- *Observations:*

(1) The effective permeability of the Carbon Tan sandstone to brine, when (S_w = 100%), was found to be 20.1 mD.

(2) After first pure CO_2 flood, the effective permeability of the Carbon Tan sandstone to pure CO_2, when (S_w = 61.7%), was found to be 7.3 mD.

(3) After thickened CO_2 flood, the effective permeability of the Carbon Tan sandstone to thickened CO_2, when (S_w = 59.2%), was calculated to be 0.18 mD, which is a 40-fold decrease in the effective permeability of the Carbon Tan sandstone to CO_2.

(4) After second pure CO_2 flood, the effective permeability of the Carbon Tan sandstone to pure CO_2, when (S_w = 59.2%), was calculated to be 0.24 mD, which is a 31-fold decrease in the effective permeability of the Carbon Tan sandstone to CO_2.

(5) Following the pure CO_2 flood, the effective permeability of the Carbon Tan sandstone to brine, when (S_w = 66.5%), was found to be 3.2 mD, which is a 6.28-fold decrease in the effective permeability of the Carbon Tan sandstone to brine (Figure 45).

Experiment #3. Indiana Limestone

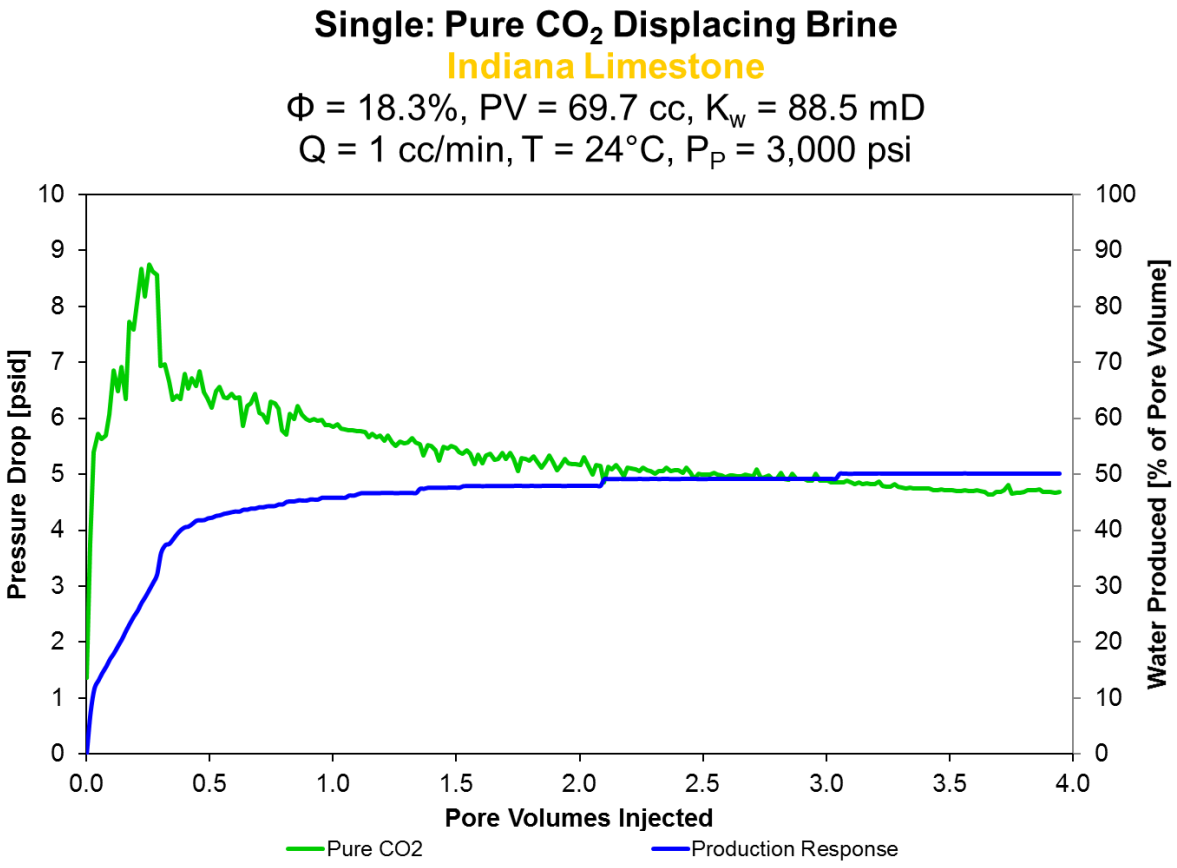

Figure 46. Single Core, Control Test, Pressure and Production Performances (Experiment #3)

- *Observations:*

(1) The effective permeability of the Indiana limestone to brine, when (S_w = 100%), was found to be 64.2 mD.

(2) After pure CO_2 flood, the effective permeability of the Indiana limestone to pure CO_2, when (S_w = 50%), was found to be 13.7 mD.

(3) Following the pure CO_2 flood, the effective permeability of the Indiana limestone to brine, when (S_w = 61.4%), was found to be 9.7 mD, which is a 6.6-fold

decrease in the effective permeability of the Indiana limestone to brine (Figure 46).

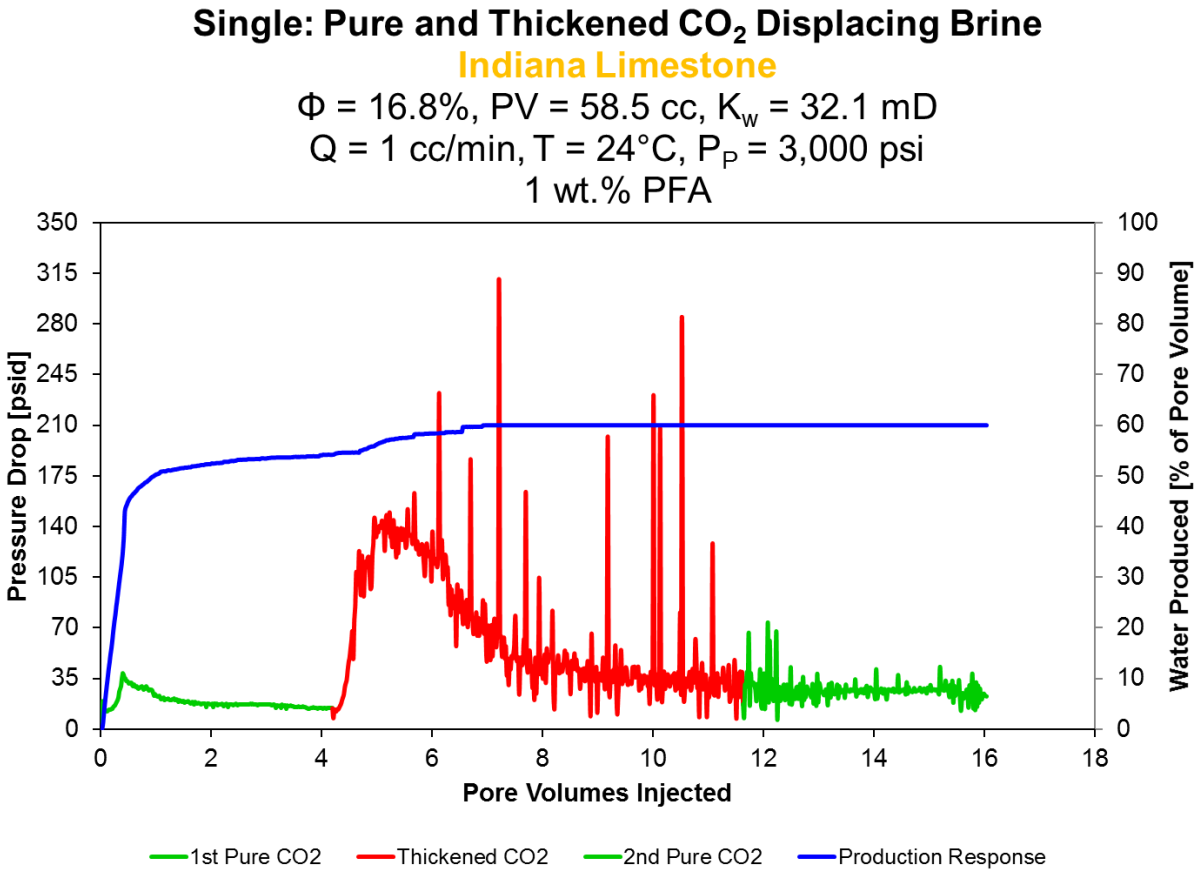

Figure 47. Single Core, Polymer Test, Pressure and Production Performances (Experiment #3)

- *Observations:*

(1) The effective permeability of the Indiana limestone to brine, when (S_w = 100%), was found to be 32.1 mD.

(2) After pure CO_2 flood, the effective permeability of the Indiana limestone to pure CO_2, when (S_w = 45.8%), was found to be 4.4 mD

(3) After thickened CO_2 flood, the effective permeability of the Indiana limestone to thickened CO_2, when (S_w = 40%), was calculated to be 2.1 mD, which is a 2.08-fold decrease in the effective permeability of the Indiana limestone to CO_2.

(4) After pure CO_2 flood, the effective permeability of the Indiana limestone to pure CO_2, when (S_w = 40%), was calculated to be 2.6 mD, which is a 1.67-fold decrease in the effective permeability of the Indiana limestone to CO_2.

(5) Following the pure CO_2 flood, the effective permeability of the Indiana limestone to brine, when (S_w = 51.6%), was found to be 3.3 mD, which is a 9.73-fold decrease in the effective permeability of the Indiana limestone to brine (Figure 47).

Experiment #4. Edwards Yellow Limestone

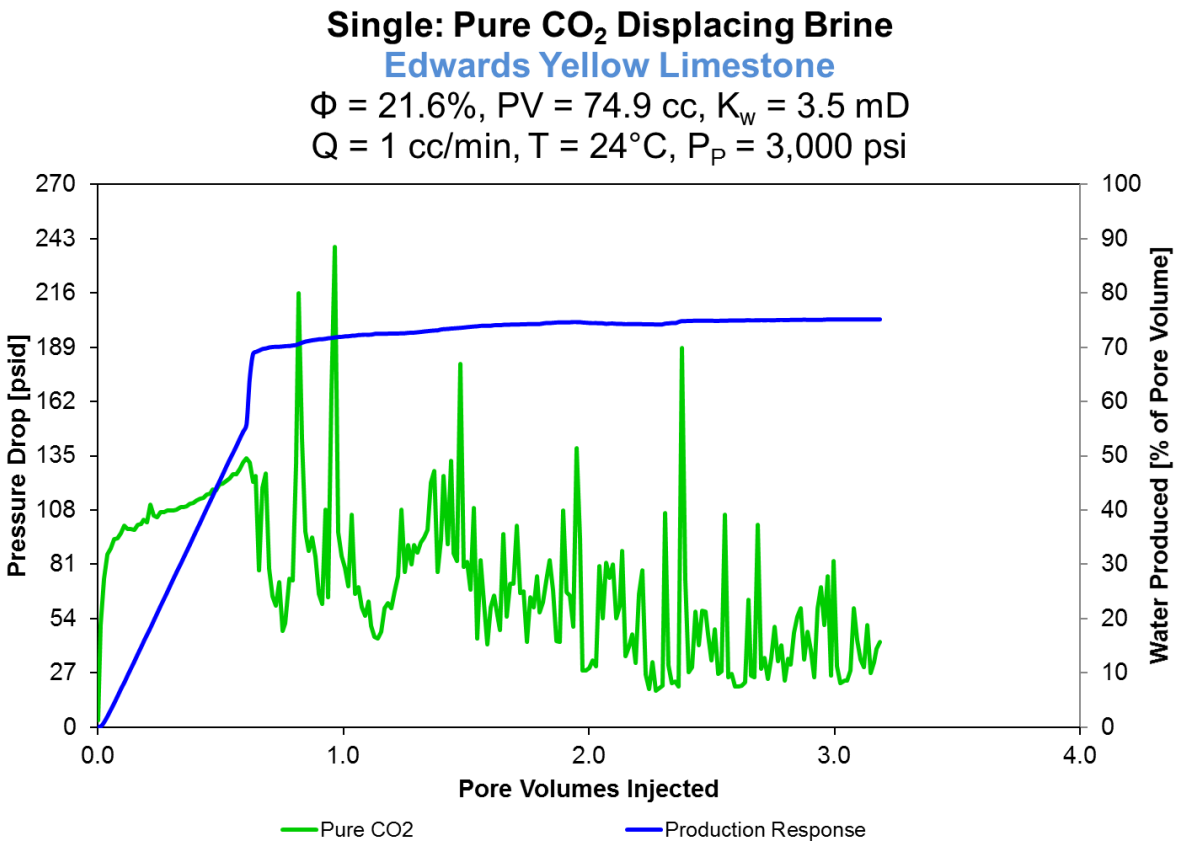

Figure 48. Single Core, Control Test, Pressure and Production Performances (Experiment #4)

- *Observations:*

(1) The effective permeability of the Edwards Yellow limestone to brine, when (S_w = 100%), was found to be 3.5 mD.

(2) After pure CO_2 flood, the effective permeability of the Edwards Yellow limestone to pure CO_2, when (S_w = 24.9%), was found to be 1.5 mD.

(3) Following the pure CO_2 flood, the effective permeability of the Edwards Yellow limestone to brine, when (S_w = 54.3%), was found to be 1.4 mD, which is a 2.5-

fold decrease in the effective permeability of the Edwards Yellow limestone to brine (Figure 48).

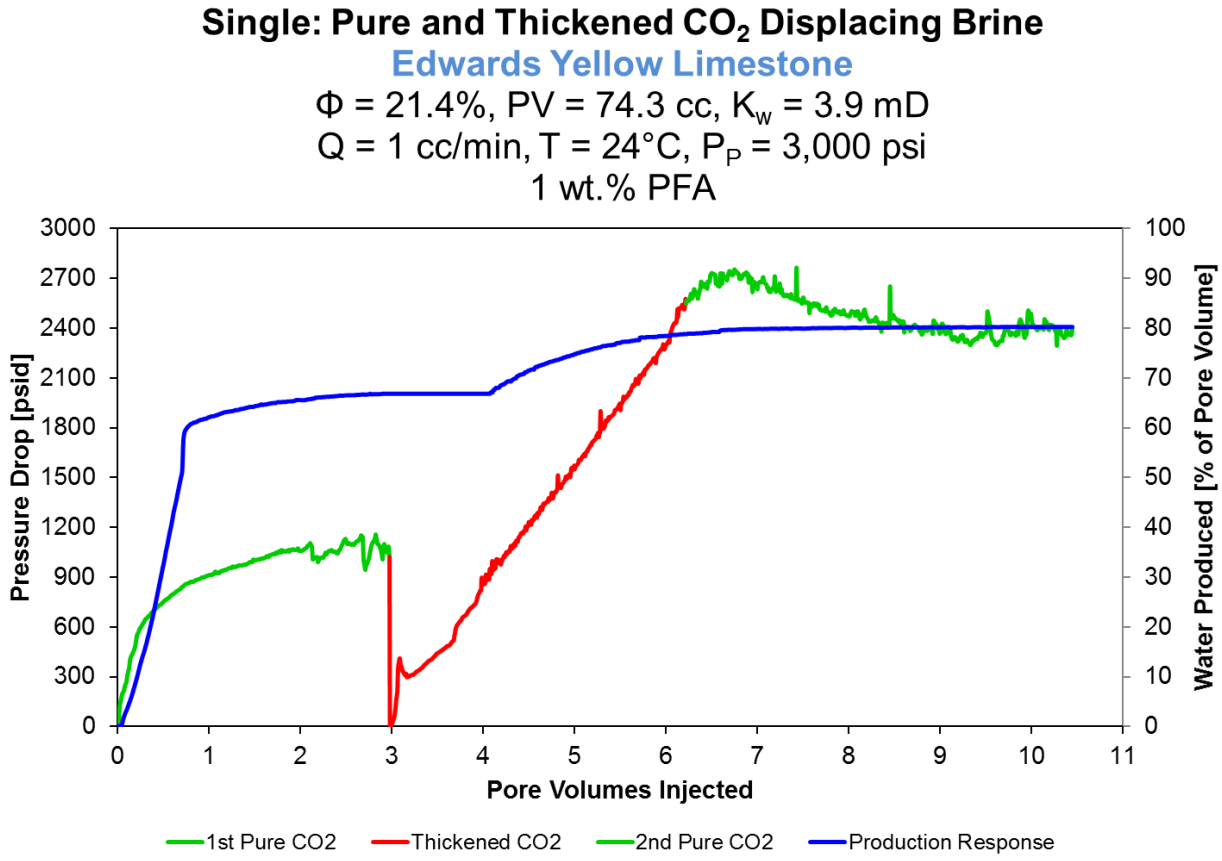

Figure 49. Single Core, Polymer Test, Pressure and Production Performances (Experiment #4)

- *Observations:*

(1) The effective permeability of the Edwards Yellow limestone to brine, when (S_w = 100%), was found to be 3.9 mD.

(2) After pure CO_2 flood, the effective permeability of the Edwards Yellow limestone to pure CO_2, when (S_w = 33.2%), was found to be 0.06 mD.

(3) After thickened CO_2 flood, the effective permeability of the Edwards Yellow limestone to thickened CO_2, when (S_w = 21.2%), was calculated to be 0.025 mD,

representing a 2.45-fold reduction in effective permeability of the Edwards Yellow limestone to CO_2.

(4) After pure CO_2 flood, the effective permeability of the Edwards Yellow limestone to pure CO_2, when (S_w = 19.8%), was calculated to be 0.026 mD, which is a 2.35-fold decrease in the effective permeability of the Edwards Yellow limestone to CO_2.

(5) Following the pure CO_2 flood, the effective permeability of the Edwards Yellow limestone to brine, when (S_w = 59.8%), was found to be 1.1 mD, which is a 3.55-fold decrease in the effective permeability of the Edwards Yellow limestone to brine (Figure 49).

Based on (Experiment #1, Experiment #2, Experiment #3 and Experiment #4), it is important to note that when cores were initially brine saturated, thickened CO_2 notably decreased the effective permeability of sandstone cores to CO_2. However, the reductions of effective permeability of limestone cores to CO_2 were quite modest.

4.4.4.2 Parallel: Pure CO_2 vs. Thickened CO_2 Displacing Brine

In this stage, a control test followed by a polymer test were conducted on brine water saturated parallel cores (S_w = 100%). In each case, the type of the rock (sandstone or limestone) was the

same for the two parallel cores, but they had a significant difference in permeability; the higher permeability core was representative of a thief zone. The control test consisted of injecting pure CO_2, while the polymer test consisted of injecting only thickened CO_2. In the following experiments, a 1 wt.% of the PFA homopolymer in CO_2 solution was injected into the Berea sandstone, Carbon Tan sandstone, Indiana limestone and Edwards Yellow limestone to investigate permeability change due to pressure drop increase during each core flooding. The following observations and attempts were considered:

Experiment #1. Berea Sandstone and Carbon Tan Sandstone

First, pure CO_2 was injected into the brine-saturated Berea sandstone and Carbon Tan sandstone. Production performance indicated that brine was recovered from the more permeable core, first, and then from the less permeable core. After 1 PV of injected pure CO_2, the Berea sandstone recovered 28% of brine followed by an additional 20% recovered by the Carbon Tan sandstone. Pressure drop performance showed that the pressure drop was fluctuating. But as additional CO_2 was injected, the pressure drop constantly decreased to almost 0.1 psi (Table 13, Figure 50 and Figure 51).

Table 13. Parallel Cores, Control Test, Production Performance (Experiment #1)

	Berea Sandstone	**Carbon Tan Sandstone**	
K_w	80.8	22.6	**mD**
Φ	20.2	17.53	**%**
PV	70.21	60.9	**cc**
S_{wi}	44.66	57.03	**%**

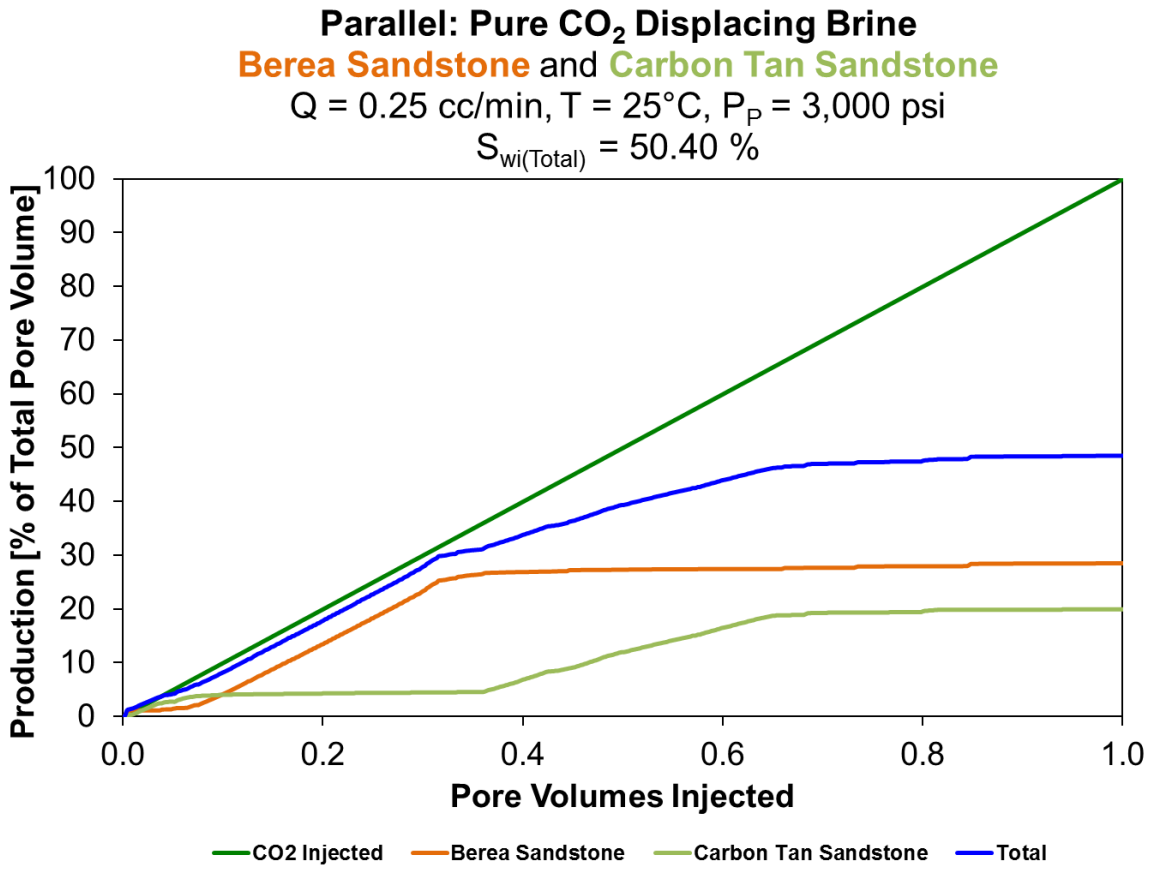

Figure 50. Parallel Cores, Control Test, Production Performance (Experiment #1)

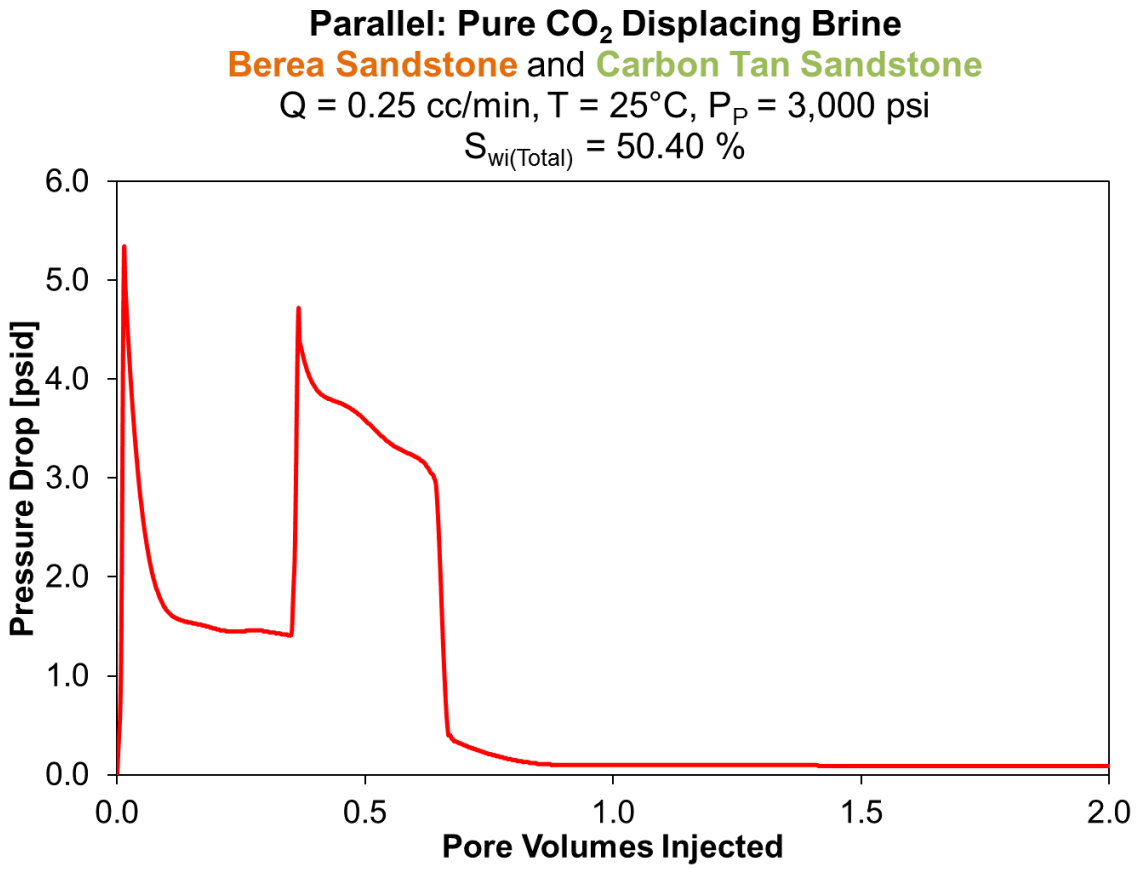

Figure 51. Parallel Cores, Control Test, Pressure Performance (Experiment #1)

Next, thickened CO_2, composed of the PFA in CO_2 solution was injected into the same Berea sandstone and Carbon Tan sandstone. Production performance indicated that brine was recovered simultaneously by both the permeable core and the less permeable core. After 1 PV of injected thickened CO_2, the Berea sandstone recovered 20% of brine and an additional 28% recovered by the Carbon Tan sandstone. It is important to note that the two cores recovered brine faster and the less permeable core produced more than the permeable core. Pressure drop performance showed that the pressure was fluctuating. But as additional thickened CO_2 was injected, the pressure drop constantly decreased to almost 5 psi (Table 14, Figure 52 and Figure 53).

Table 14. Parallel Cores, Polymer Test, Production Performance (Experiment #1)

	Berea Sandstone	Carbon Tan Sandstone	
K_w	80.8	22.6	**mD**
Φ	20.2	17.53	**%**
PV	70.21	60.9	**cc**
S_{wi}	60.54	41.47	**%**

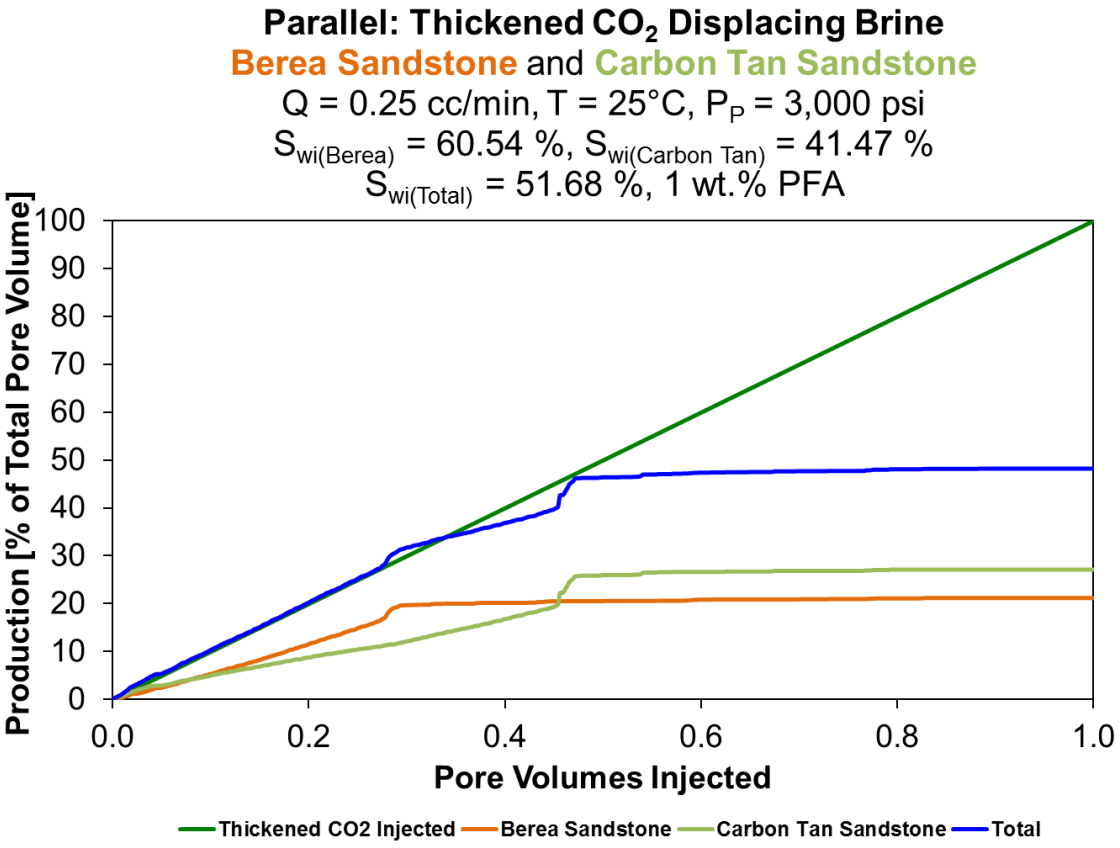

Figure 52. Parallel Cores, Polymer Test, Production Performance (Experiment #1)

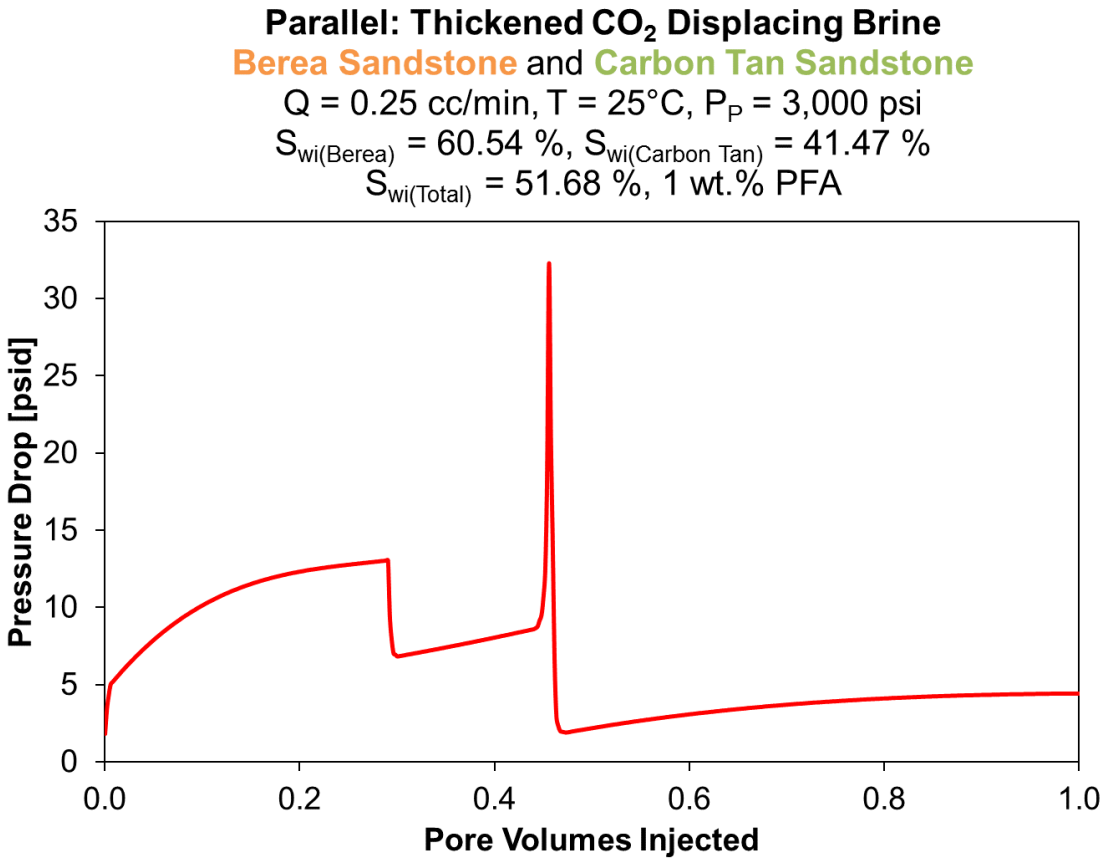

Figure 53. Parallel Cores, Polymer Test, Pressure Performance (Experiment #1)

Experiment #2. Indiana Limestone and Edwards Yellow Limestone

First, pure CO_2 was injected into the Indiana limestone and Edwards Yellow limestone. Production performance indicated that brine was recovered simultaneously by both the permeable core and the less permeable core with a slightly higher recovery rate from the permeable core. After 1 PV of injected pure CO_2, the Indiana limestone recovered 15% of brine followed by an additional 10%, in gradual increments, recovered by the Edwards Yellow limestone. It is important to note that the permeable core recovered brine much faster than the less permeable core which had a steady incremental recovery. Pressure drop performance

showed that the pressure was fluctuating. But as additional CO_2 was injected, the pressure drop constantly decreased to almost 1.2 psi (Table 15, Figure 54 and Figure 55).

Table 15. Parallel Cores, Control Test, Production Performance (Experiment #2)

	Indiana Limestone	Edwards Yellow Limestone	
K_w	34.2	6.2	**mD**
Φ	18.89	23.33	**%**
PV	65.63	81.06	**cc**
S_{wi}	66.04	50.49	**%**

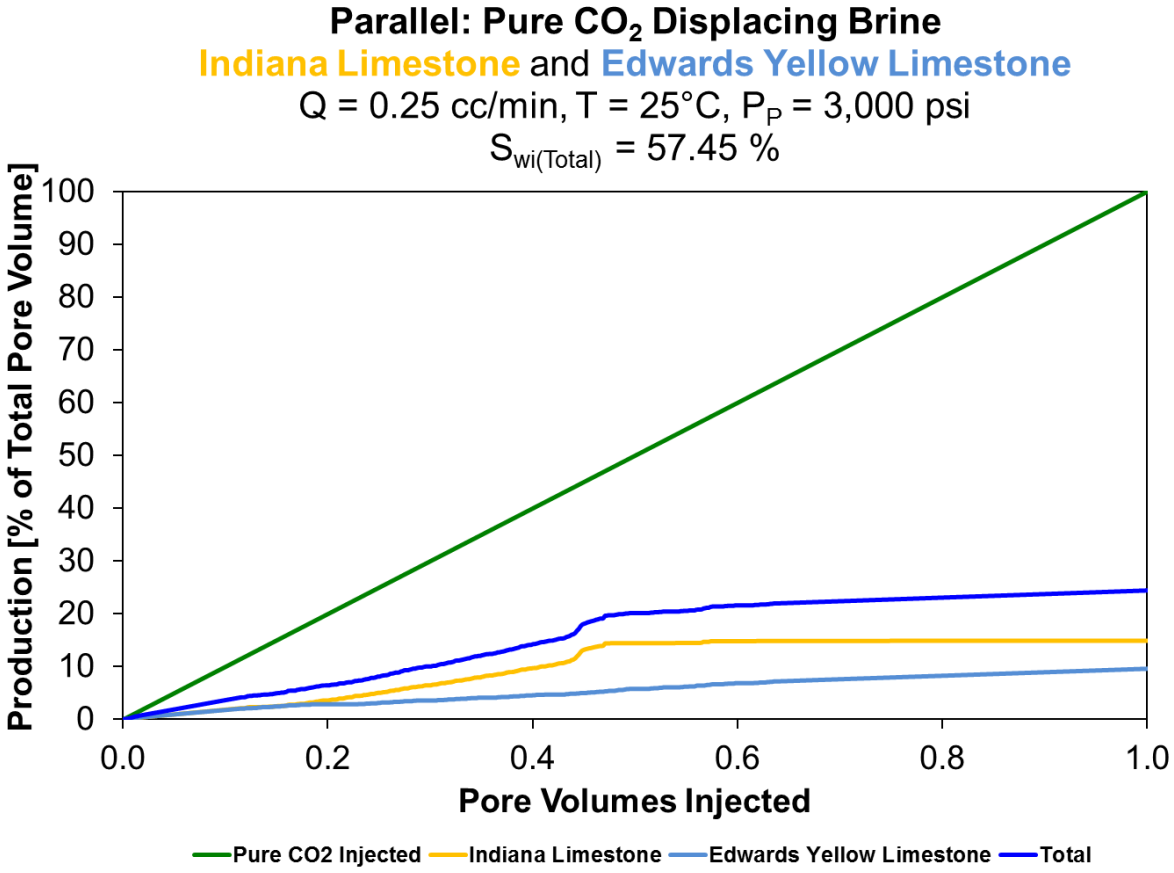

Figure 54. Parallel Cores, Control Test, Production Performance (Experiment #2)

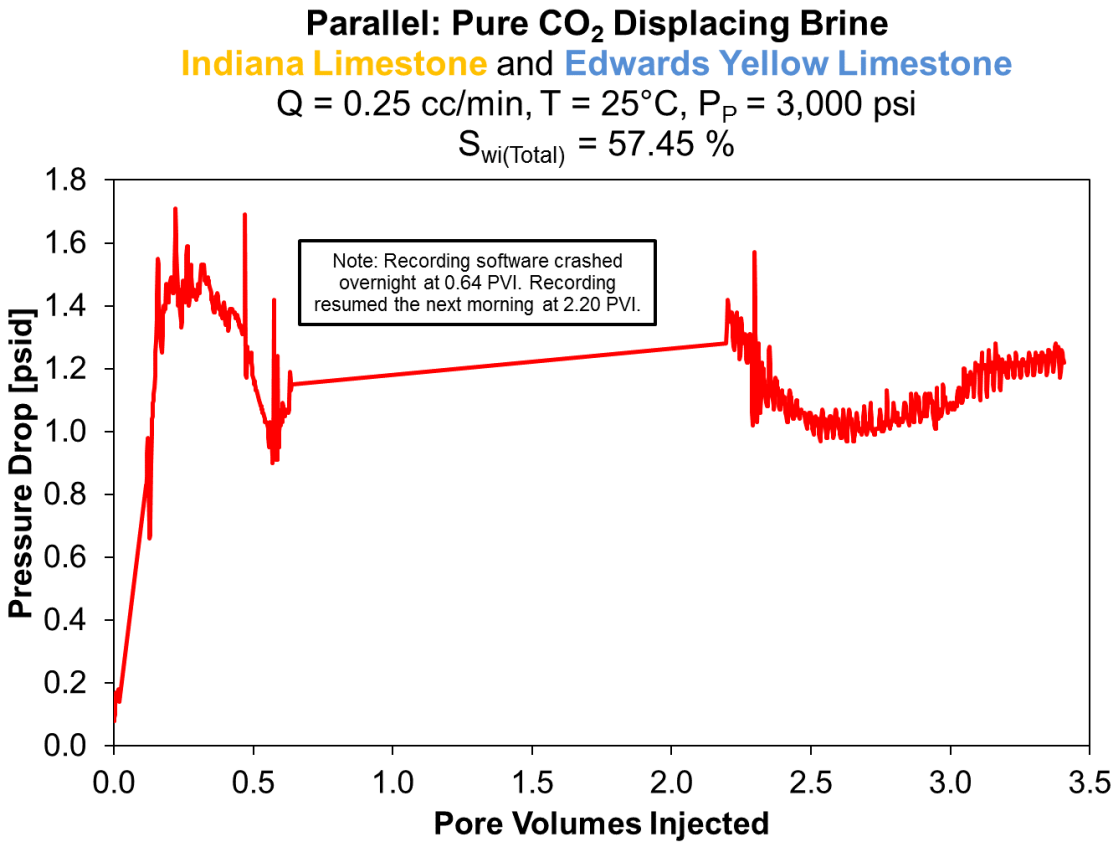

Figure 55. Parallel Cores, Control Test, Pressure Performance (Experiment #2)

Next, thickened CO_2, composed of the PFA in CO_2 solution, was injected into the same Indiana limestone and Edwards Yellow limestone. Production performance indicated that brine was recovered simultaneously by both the permeable core and the less permeable core. After 1 PV of injected thickened CO_2, the Indiana limestone recovered 20% of brine and an additional 20% recovered by the Edwards Yellow limestone. It is important to note that the two cores recovered brine faster and both the permeable and less permeable cores produced more brine. Pressure drop performance showed that the pressure was fluctuating. But as more thickened CO_2 was injected, the pressure drop sharply increased to almost 70 psi (Table 16, Figure 56 and Figure 57).

Table 16. Parallel Cores, Polymer Test, Production Performance (Experiment #2)

	Indiana Limestone	Edwards Yellow Limestone	
K_w	34.2	6.2	**mD**
Φ	18.89	23.33	**%**
PV	65.63	81.06	**cc**
S_{wi}	51.97	38.56	**%**

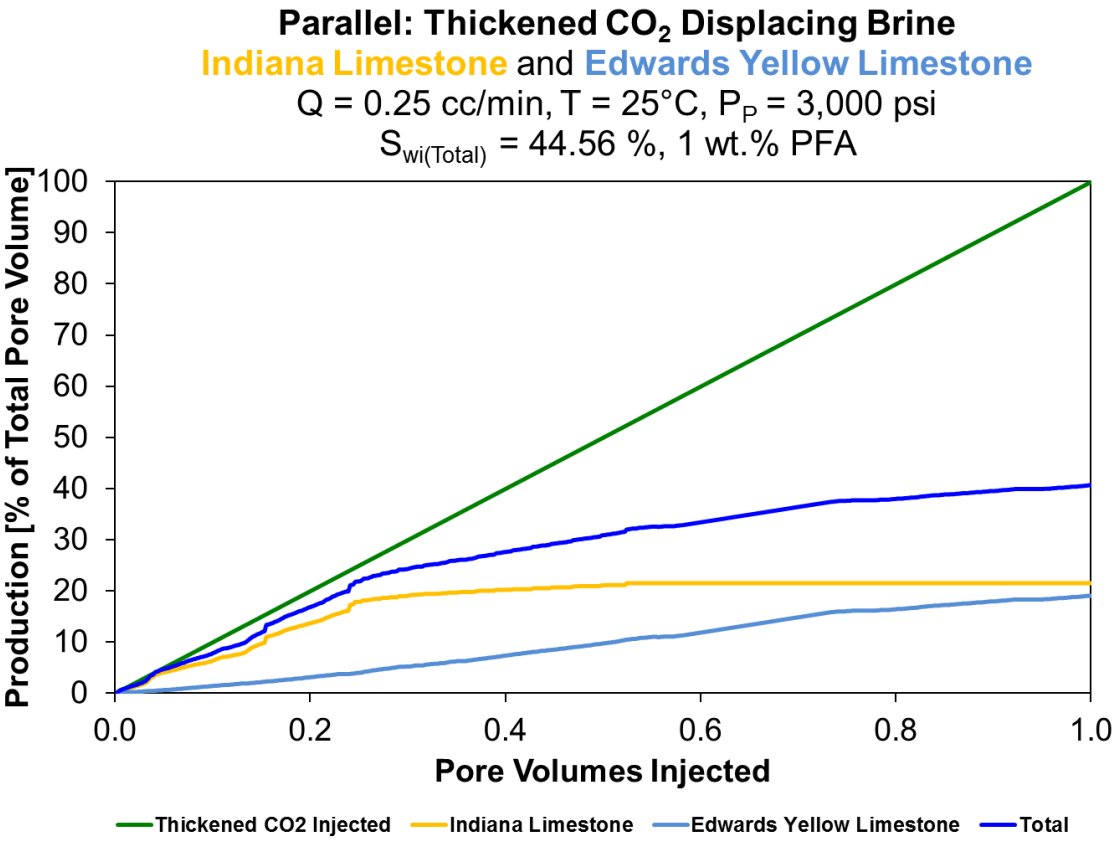

Figure 56. Parallel Cores, Polymer Test, Production Performance (Experiment #2)

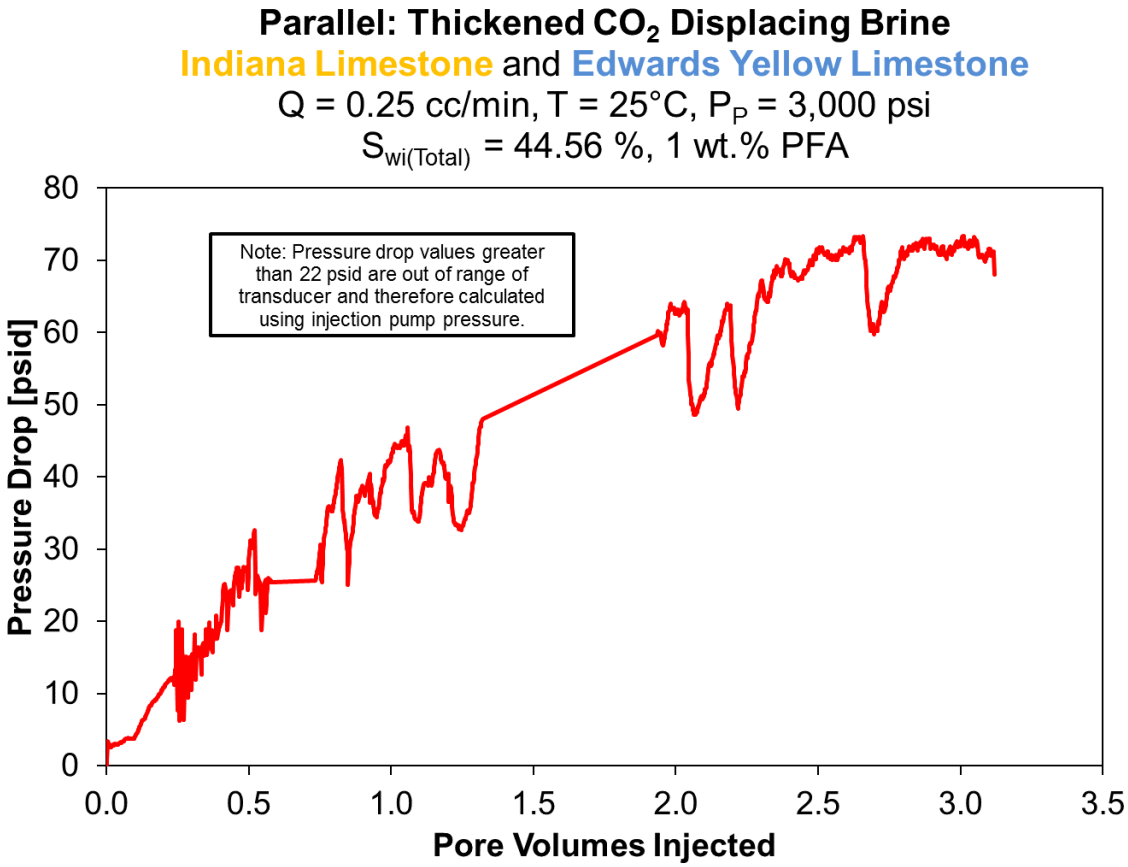

Figure 57. Parallel Cores, Polymer Test, Pressure Performance (Experiment #2)

4.4.4.3 Parallel: Pure CO_2 vs. Thickened CO_2 Displacing Brine (Thief Zone)

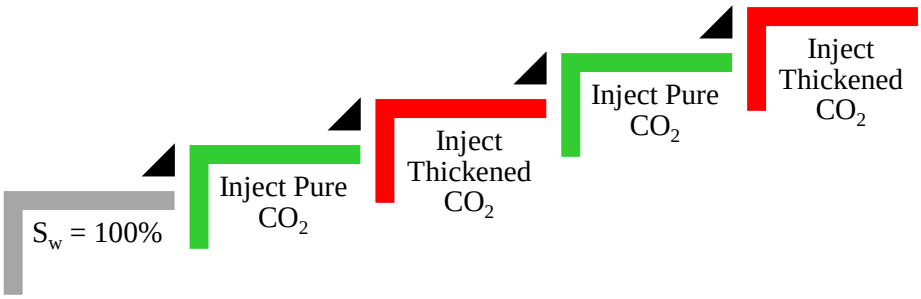

In this stage, one core was isolated to conduct a control test followed by a polymer test on brine water-saturated parallel cores (S_w = 100%). Again, in each case the type of rock (sandstone or

limestone) was the same for the two parallel cores, but they had a significant difference in permeability; the higher permeability core was representative of a thief zone. The control test consisted of injecting pure CO_2, while the polymer test consisted of injecting only thickened CO_2 or both pure CO_2 and thickened CO_2, sequentially. In the following experiments, a 1 wt.% of the PFA homopolymer in CO_2 solution was injected into the Berea sandstone, Carbon Tan sandstone, Indiana limestone and Edwards Yellow limestone to investigate permeability change due to pressure drop increase during each core flooding. The following observations and attempts were considered:

Experiment #1. Berea Sandstone and Carbon Tan Sandstone

First, pure CO_2 was injected only into the brine water-saturated Berea sandstone, and a 30% recovery was achieved solely by the permeable core; this was intended to better replicate the existence of a highly watered out zone that was subsequently flooded with significant amounts of CO_2 (the thief zone). Then, pure CO_2 was injected into the Berea sandstone and Carbon Tan sandstone in parallel; this was a mean to replicate the effects of simultaneously injecting CO_2 into a previously CO_2-flooded core in parallel with a core into which no CO_2 had invaded. Production performance indicated that the total recovery remained constant at 30% with no production from the less permeable core. Pressure drop performance showed a relatively constant pressure between (1.7-2) psi (Table 17, Figure 58 and Figure 59).

Table 17. Parallel Cores (Isolated Thief Zone), Control Test (Experiment #1)

	Berea Sandstone	**Carbon Tan Sandstone**	
K_w	56	25	**mD**
Φ	20.92	17.32	**%**
PV	72.71	60.18	**cc**
S_{wi}	42.66	100	**%**

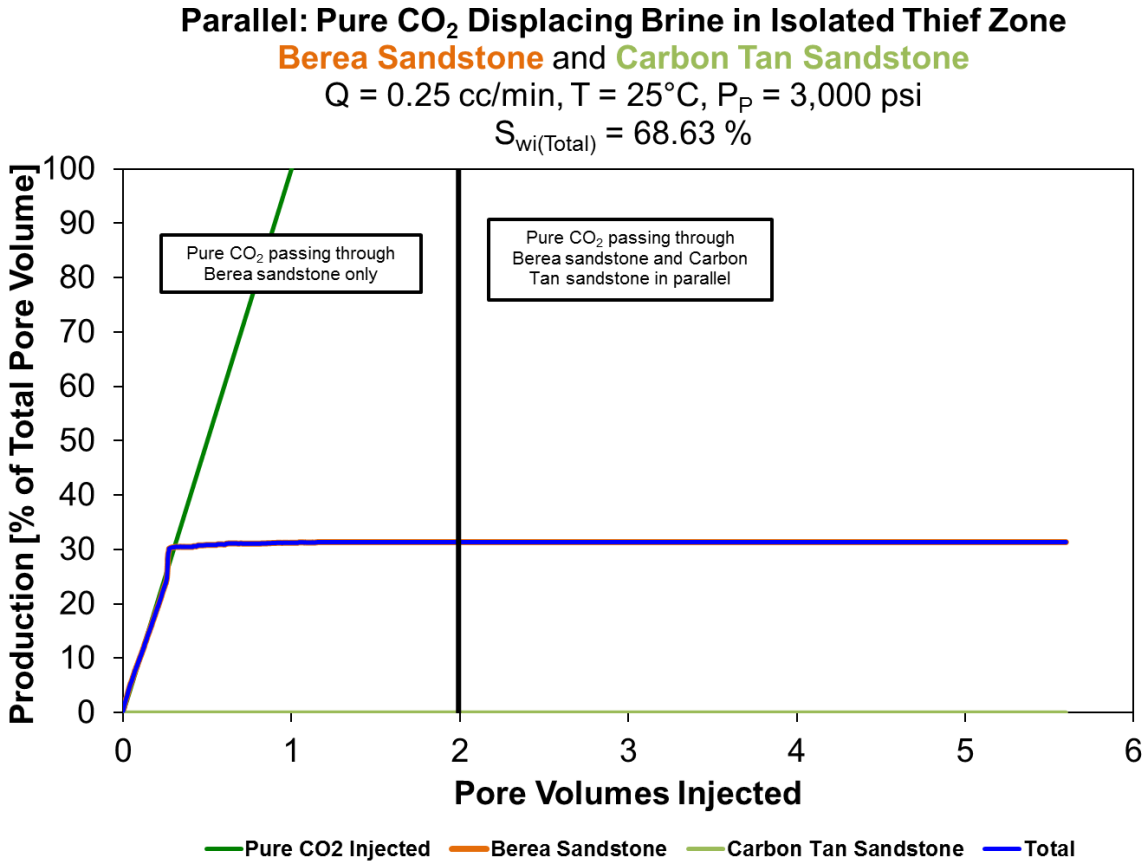

Figure 58. Parallel Cores (Thief Zone), Control Test, Production Performance (Experiment #1)

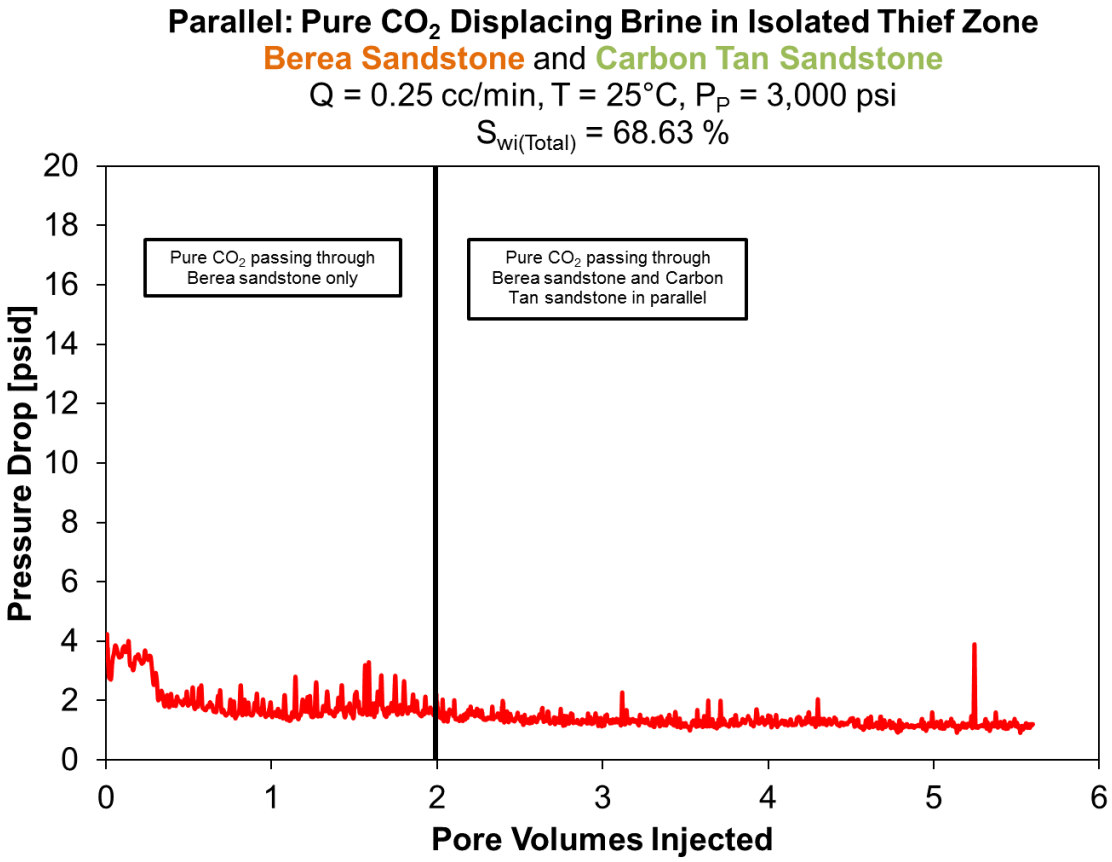

Figure 59. Parallel Cores (Thief Zone), Control Test, Pressure Performance (Experiment #1)

Next, pure CO_2, was injected only into the Berea Sandstone and, again, a 30% recovery is achieved solely by the permeable core. Then, the PFA-thickened CO_2 was simultaneously injected into both Berea sandstone and Carbon Tan sandstone. Production performance indicated a final total recovery of 61% which verified that thickened CO_2 was able to recover additional 8% of brine from the permeable core and 23% from the less permeable core. Pressure drop performance showed a relatively constant pressure between (7-8) psi (Table 18, Figure 60 and Figure 61).

Table 18. Parallel Cores (Thief Zone), Polymer Test #1 (Experiment #1)

	Berea Sandstone	Carbon Tan Sandstone	
K_w	56	25	**mD**
Φ	20.92	17.32	**%**
PV	72.71	60.18	**cc**
S_{wi}	30.92	56.89	**%**

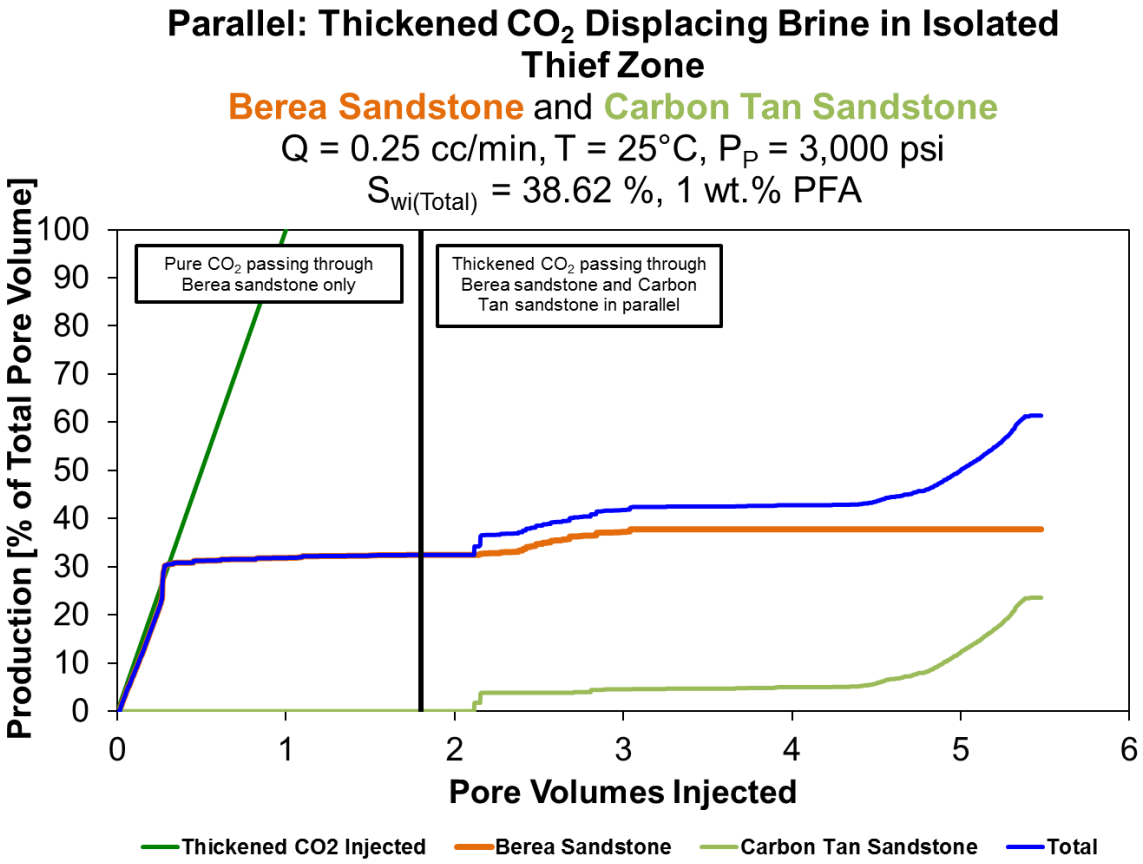

Figure 60. Parallel Cores (Thief Zone), Polymer Test #1, Production Performance (Experiment #1)

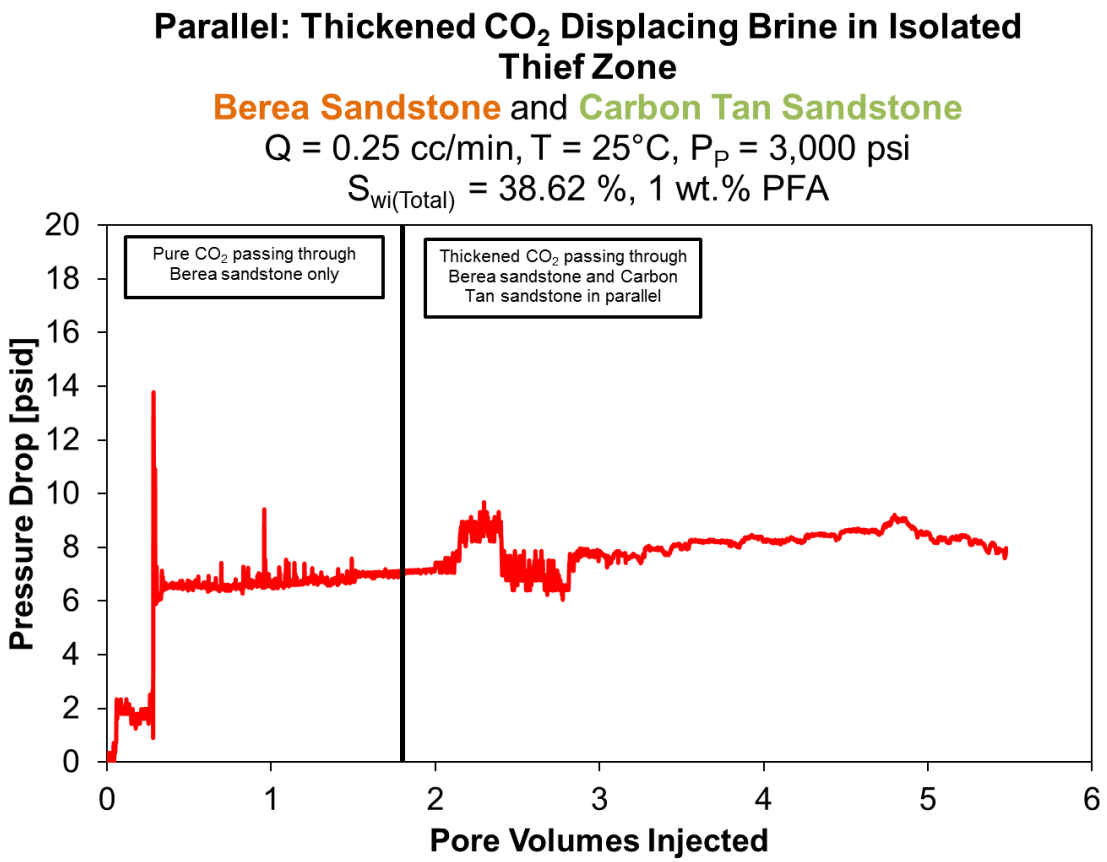

Figure 61. Parallel Cores (Thief Zone), Polymer Test #1, Pressure Performance (Experiment #1)

Finally, thickened CO_2 was injected only into the Berea sandstone and a 40% recovery is achieved solely from the permeable core; this step was meant to replicate the isolation of the thief zone and the injection of the conformance only in the offending layer. Then, pure CO_2 was simultaneously injected into the parallel Berea sandstone and Carbon Tan sandstone. Production performance indicated an additional 25% of brine recovery from the less permeable zone increasing a final total recovery to 65% with no flow of CO_2 entering the higher permeability zone. This is an ideal CO_2 conformance control result. Pressure drop performance showed a relatively constant pressure between (0.8-2) psi (Table 19, Figure 62 and Figure 63).

Table 19. Parallel Cores (Thief Zone), Polymer Test #2 (Experiment #1)

	Berea Sandstone	Carbon Tan Sandstone	
K_w	73	7.8	**mD**
Φ	19.94	15.23	**%**
PV	69.3	52.93	**cc**
S_{wi}	27.45	41.24	**%**

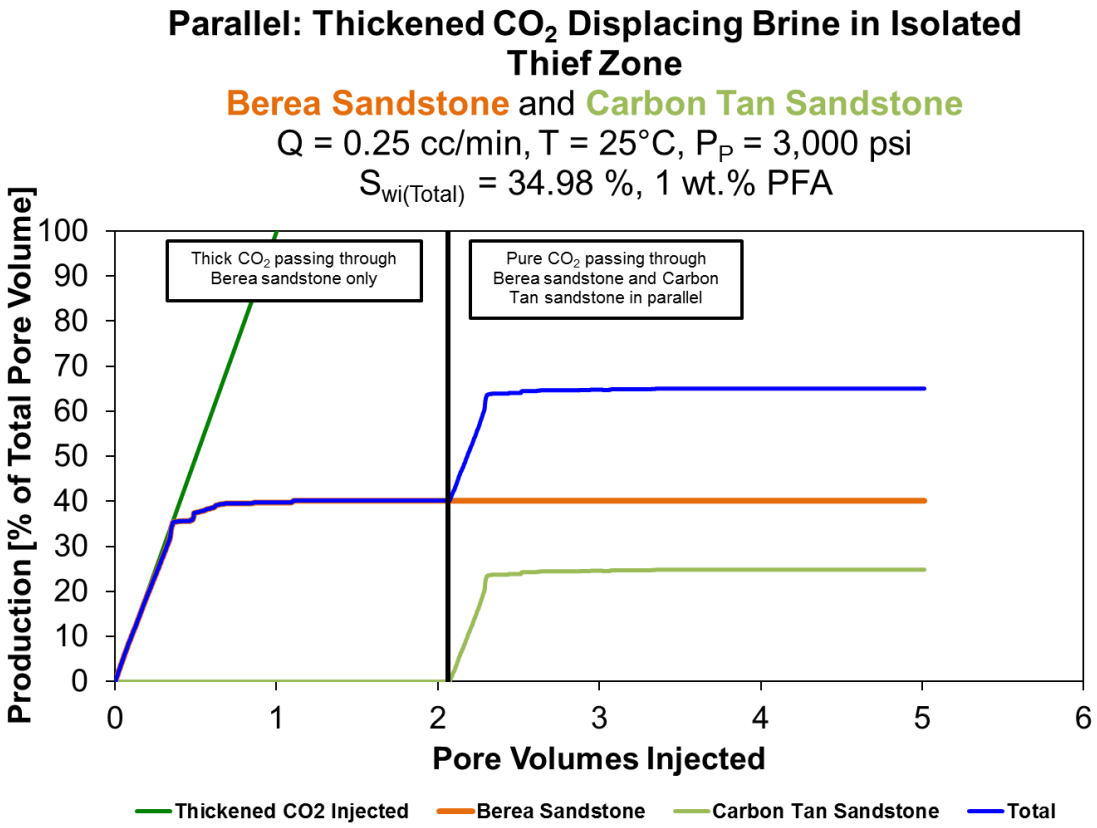

Figure 62. Parallel Cores (Thief Zone), Polymer Test #2, Production Performance (Experiment #1)

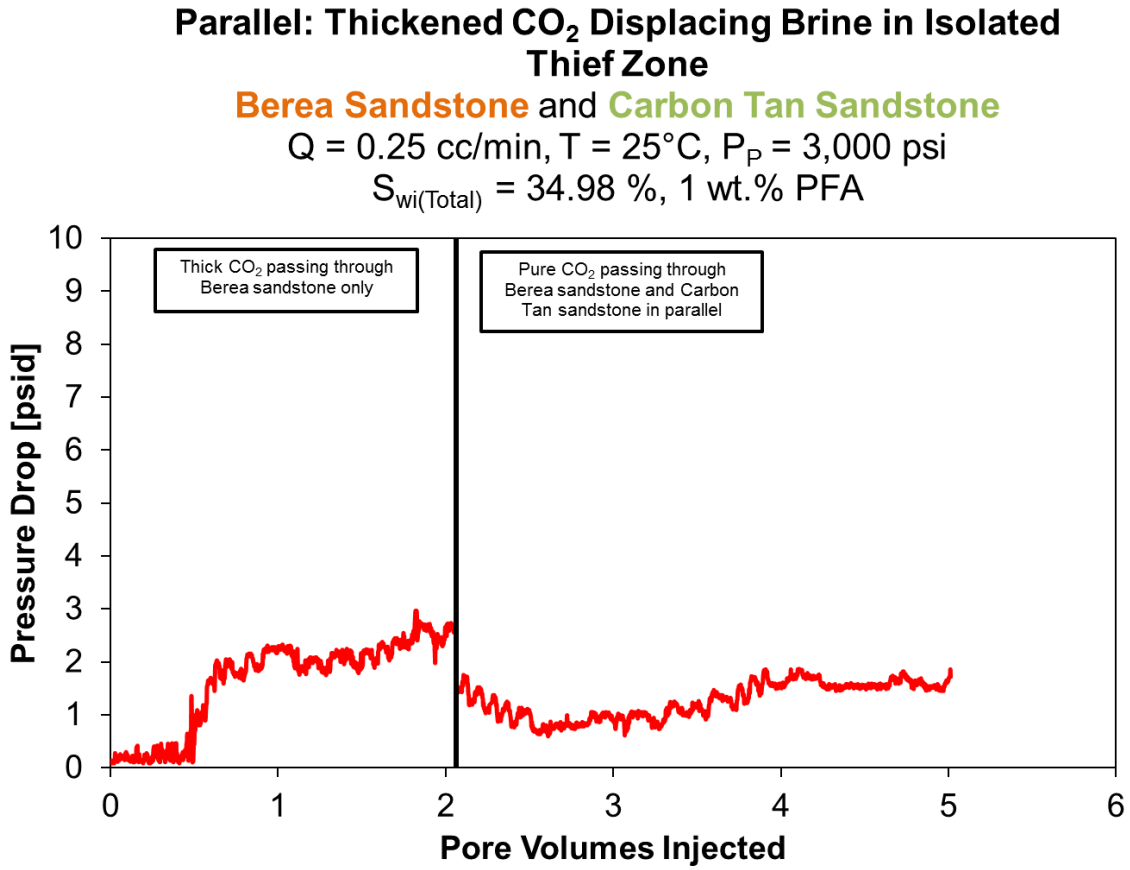

Figure 63. Parallel Cores (Thief Zone), Polymer Test #2, Pressure Performance (Experiment #1)

Experiment #2. Indiana Limestone and Edwards Yellow Limestone

First, pure CO_2 is injected only into the Indiana limestone and a 20% recovery is achieved solely by the permeable core. Then, pure CO_2 is injected into both Indiana limestone and Edwards Yellow limestone. Production performance indicated a total recovery remained constant at 25% with no production from permeable core and the additional 5% recovery from the less permeable core. Pressure drop performance showed a relatively constant pressure between (0.4-0.6) psi.

Finally, thickened CO_2 was injected only into the Indiana limestone and only 0.5% recovery is achieved solely by the permeable core. Then, pure CO_2 is injected into both Indiana limestone and Edwards Yellow limestone. Production performance indicated a total recovery of 28% which verified that pure CO_2 was able to recover additional 3% of brine only from the less permeable core. Pressure drop performance showed a relatively constant pressure between (1-1.2) psi (Table 20, Figure 64 and Figure 65).

Table 20. Parallel Cores (Thief Zone), Polymer Test (Experiment #2)

	Indiana Limestone	**Edwards Yellow Limestone**	
K_w	64	5.6	**mD**
Φ	17.55	23.17	**%**
PV	60.99	80.5	**cc**
S_{wi}	50.83	87.63	**%**

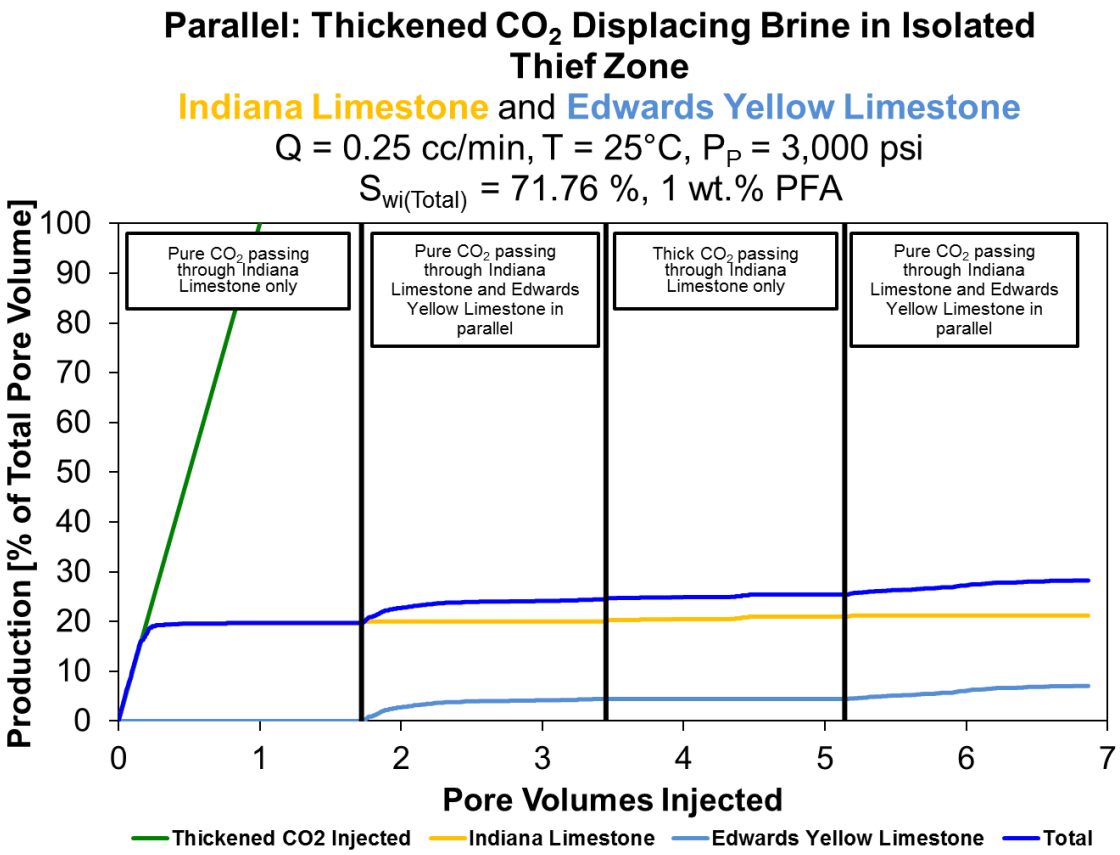

Figure 64. Parallel Cores (Thief Zone), Polymer Test, Production Performance (Experiment #2)

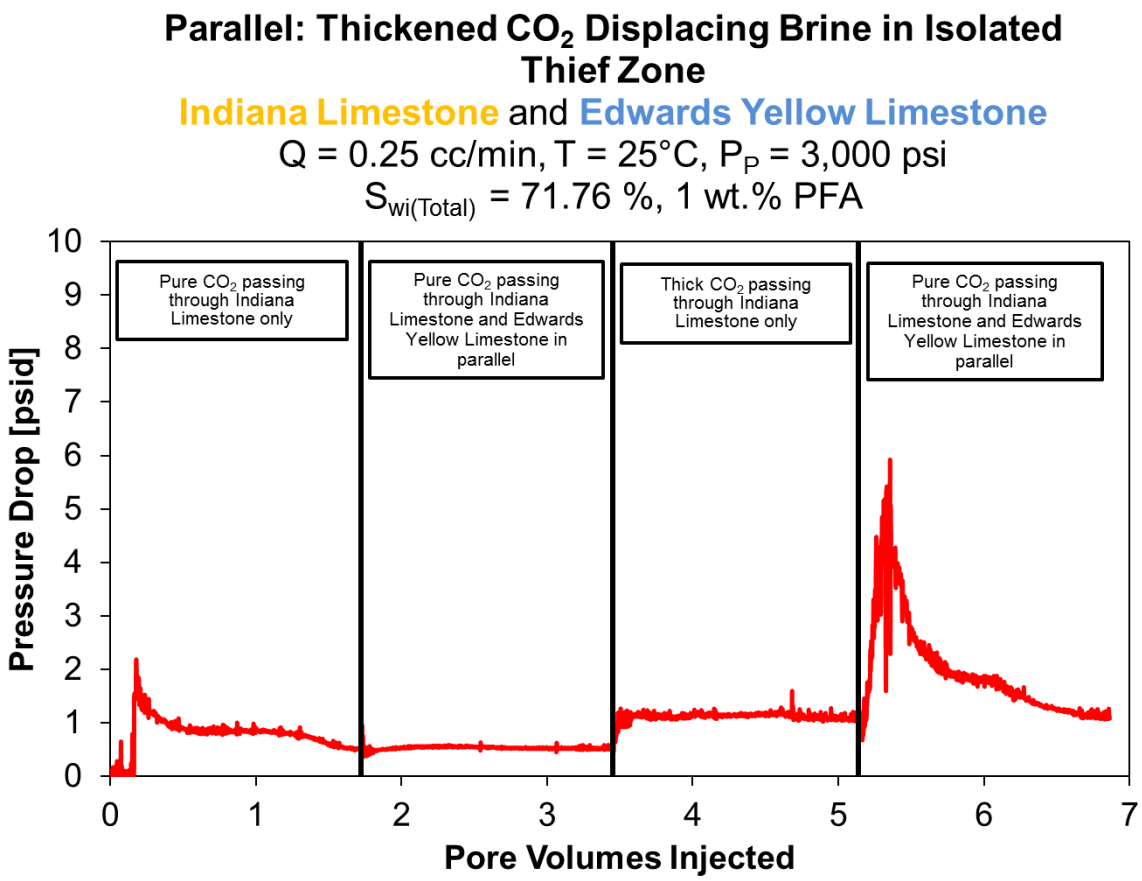

Figure 65. Parallel Cores (Thief Zone), Polymer Test, Pressure Performance (Experiment #2)

4.4.4.4 Lessons Learned

(1) Multiple cases were examined for the use of the PFA homopolymer to address the common EOR CO_2 conformance control problem where high permeability, watered-out, oil-depleted thief zones dominate the flow over low permeability, oil-rich zones.

(2) Single: Pure CO_2 vs. Pure and Thickened CO_2 Displacing Brine

a. The PFA homopolymer notably decreased the effective permeability of a single sandstone core to CO_2 (K_{e,CO_2}). However, the reductions of the effective permeability of a single limestone core to CO_2 were quite modest.

(3) Parallel: Pure CO_2 vs. Thickened CO_2 Displacing Brine

a. In the control test, 48% of the brine water was recovered, 28% and 20% of which were produced by the high permeability and low permeability sandstone cores, respectively. In the polymer test, the same total recovery of 48% was achieved. However, 28% and 20% of which were produced by the low permeability and high permeability sandstone cores, respectively. Moreover, the two sandstone cores reached the 48% recovery much faster.

b. In the control test, 25% of the brine water was recovered, 15% and 10% of which were produced by the high permeability and low permeability limestone cores, respectively. In the polymer test, a total recovery of 40% was achieved, 20% was produced by each of the limestone cores. Again, the two limestone cores reached the 40% recovery much faster.

c. The PFA homopolymer was much more effective in recovering more brine water in sandstone than in limestone.

(4) Parallel: Pure CO_2 vs. Thickened CO_2 Displacing Brine (Thief Zone)

a. First, sandstone cores were tested by implementing a control test followed by a polymer test. This case was driven by replicating the effects of simultaneously injecting CO_2 into a previously CO_2-flooded core in parallel with a core that is CO_2-uninvaded. In the control test, 30% of brine water was recovered, initially, by the high permeability sandstone core. Then, the recovery from both sandstone cores remained constant at 30% and was, still, solely dominated by the high permeability sandstone core. In the polymer test, 61% of brine water was recovered by injecting the PFA simultaneously into the parallel sandstone cores. The PFA homopolymer was able to recover additional 8% and 23% of brine from the high permeability and low permeability sandstone cores, respectively.

b. Second, sandstone cores were tested by implementing polymer test only. This case was driven by replicate the isolation of the thief zone and the injection of the conformance only in the offending layer. In the polymer test, 40% of brine water was recovered, initially, by the high permeability sandstone core. Then, 65% of brine water was recovered by injecting the PFA simultaneously into the parallel sandstone cores. The PFA homopolymer was able to recover additional 25% of brine coming only from the low permeability sandstone core.

c. For sandstone, an ideal conformance control was achieved by injecting thickened CO_2 only in the high permeability sandstone core

followed by the injection of pure CO_2 into both parallel sandstone cores. In this case, none of the subsequent pure CO_2 entered the PFA-treated sandstone core, which resulted in all of the pure CO_2 flowing into the low permeability sandstone core.

d. Third, limestone cores were tested by implementing a control test followed by a polymer test. Again, this case was driven by replicating the effects of simultaneously injecting CO_2 into a previously CO_2-flooded core in parallel with a core that is CO_2-uninvaded. In the control test, 20% of brine water was recovered, initially, by the high permeability limestone core. Then, the recovery from both limestone cores added an additional 5% from the low permeability limestone core and remained constant at 25% with no production from the high permeability limestone core. In the polymer test, only 0.5% of brine water was recovered by injecting the PFA into the high permeability limestone core. However, 28% of brine water was recovered by a subsequent injection of pure CO_2 simultaneously into the parallel limestone cores. The PFA homopolymer was able to recover additional 3% of brine from the low permeability limestone core.

e. Again, the PFA homopolymer was much more effective in recovering more brine water in sandstone than in limestone.

f. In both sandstone and limestone, pressure performance indicated that brine recovery is not solely attributed to the increase in CO_2

viscosity. One portion of the polymer is effectively increasing CO_2 viscosity, and the other portion is being adsorbed or retained by the core.

g. The effective permeability of all cores, which were fully saturated with brine water, to both CO_2 and water have been reduced during PFA-thickened CO_2 injection. However, the effective permeability of CO_2 decreased notably in sandstone compared limestone:

    i. For Berea sandstone, there was a 30-fold decrease in (K_{e,CO_2}) and an 8.9-fold decrease in ($K_{e,w}$).

    ii. For Indiana limestone, there was a 1.6-fold reduction in (K_{e,CO_2}) and a 9.7-fold decrease in ($K_{e,w}$).

h. The PFA homopolymer was much more suitable in sandstone than in limestone as it induced drastic reductions in the (K_{e,CO_2}) of high permeability, watered out, thief zones.

At this point, results indicated that the PFA could, indeed, be used for conformance control, especially if the (CO_2+PFA) solution can be injected only in the high permeability thief zone.

4.5 WETTABILITY

When a liquid drop is placed onto a solid surface, its behavior depends on the wetting forces between the liquid and the solid surface. A contact angle method was used to determine the

wettability of the core samples using a sessile drop method. The liquid drop is released from a tip of a needle and an image of the drop is recorded using a camera, and the contact angle was measured using a contour-shape analysis software. In wettability tests, the solid surface is the surface of any desired core sample. And in order to examine the wettability forces between the liquid drop and the core sample, both water and oil were used to distinguish wetting from non-wetting behaviors. Moreover, the polymer was mixed with both water and oil for further observation. After core flooding, a core sample was cut in half in order to examine wettability and permeability changes across the core (Table 21, Table 22, Table 23 and Figure 66).

Table 21. Fluid Properties used during Core Flooding Tests

Fluid	Density [g/cc]	Interfacial Tension [dynes/cm]	Temperature [°C]
Distilled Water	1.0	70.03	23.8
Oil	0.8314	21.24	23.8

Table 22. Plugs Details after Core Samples are cut in half

Core Sample	Plug	Polymer	Details
Berea Sandstone	1A	PFAST-C6	Inlet half used in (Experiment #6)
Berea Sandstone	1B	PFAST-C6	Outlet half used in (Experiment #6)
Berea Sandstone	2A	PFA	Inlet half used in (Experiment #7)
Berea Sandstone	2B	PFA	Outlet half used in (Experiment #7)
Indiana Limestone	A	PFA	Inlet half used in (Experiment #8)
Indiana Limestone	B	PFA	Outlet half used in (Experiment #8)

Table 23. Wettability Change after Core Samples are cut in half

Core Sample	Fluid	θ_c	Details
Berea Sandstone	Brine	35-65°	Inlet half used in (Experiment #6)
	Oil	35-50°	
Berea Sandstone	Brine	35-65°	Inlet half used in (Experiment #7)
	Oil	35-50°	
Indiana Limestone	Brine	35-65°	Inlet half used in (Experiment #8)
	Oil	35-50°	

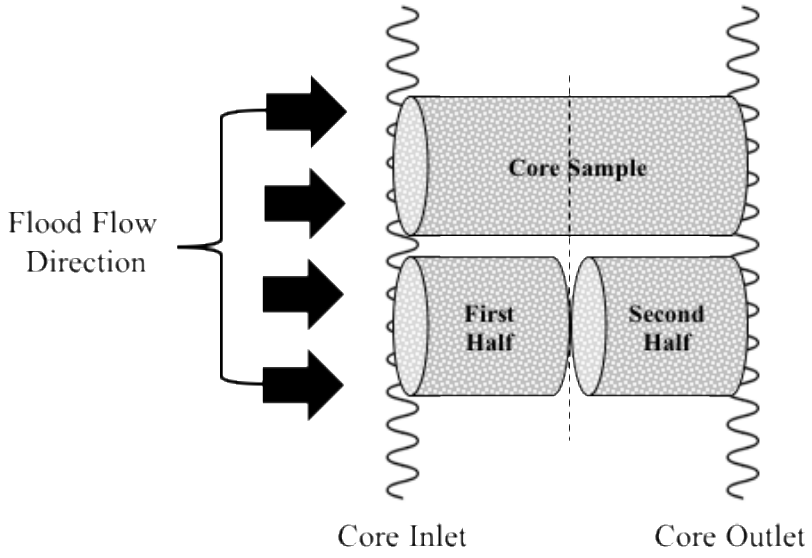

Figure 66. Core Sample Cut in half

Based on the strength of the wetting forces, the shape of the liquid drop will exhibit a contact angle (θ_c), which can be measured from the solid surface through the end of the liquid drop interface. If the wetting forces between a water drop and the solid surface are attractive, the water drop spreads along the solid surface where ($\theta_c < 90°$). This type of surface is called "hydrophilic," which means water loving. If the wetting forces are repellent, the water drop retains its spherical shape without spreading along the solid surface, where ($\theta_c > 90°$). This type of surface is called "hydrophobic," which means water hating (Figure 67). If oil drop is used instead of water drop, the terms will change to "oleophilic" and "oleophobic" accordingly.

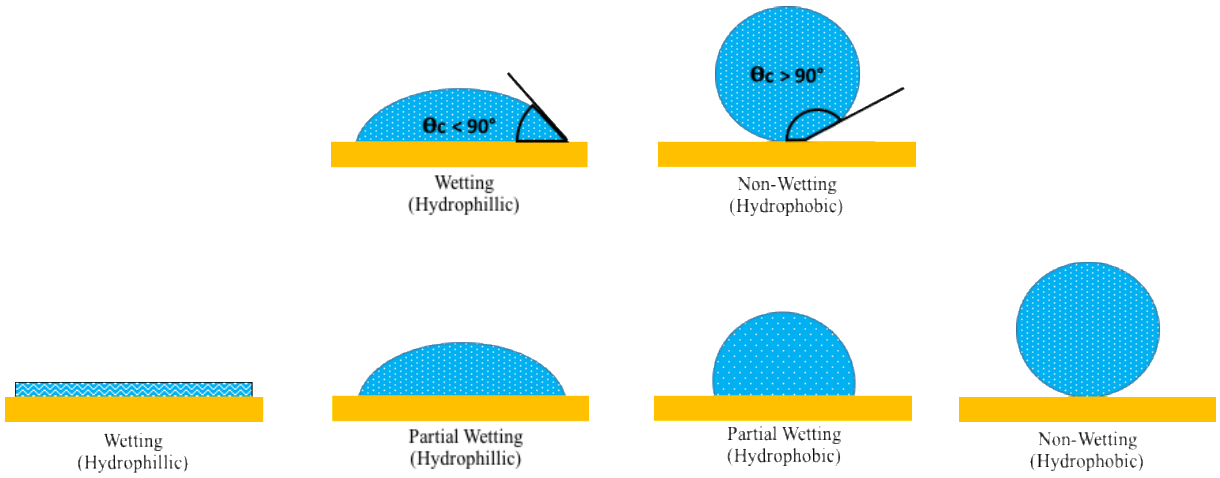

Figure 67. Contact Angle measured within Liquid Drop in Wetting and Non-Wetting Phases

Before core flooding tests, a fresh Berea sandstone core sample exhibited a wetting (strongly hydrophilic) behavior. However, after polymer flooding, a Berea sandstone core sample, previously saturated with the PFA, exhibited a non-wetting (strongly hydrophobic and slightly oleophobic) behavior which indicated that the PFA must have altered the wettability of the core (Figure 68, Figure 69 and Figure 70).

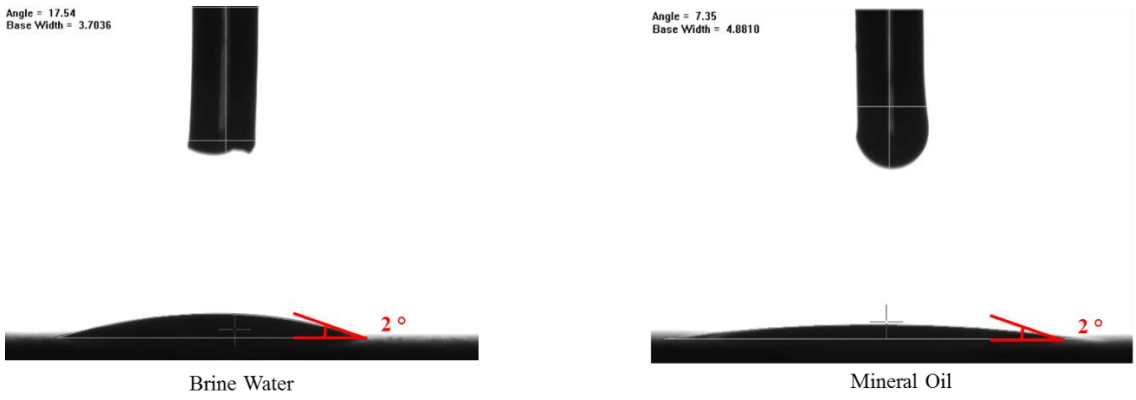

Figure 68. 5 s after drop placement on fresh Berea sandstone (Strongly hydrophilic)

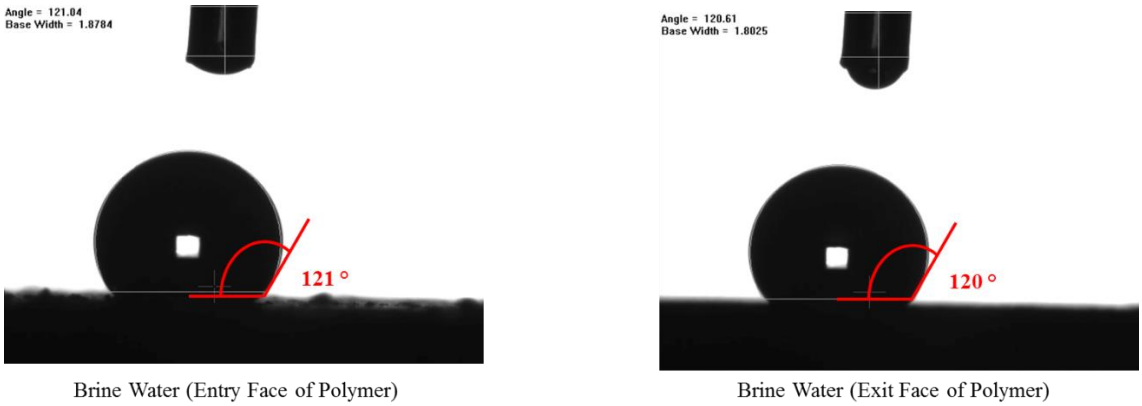

Figure 69. 12 s after drop placement on polymer saturated Berea sandstone (strongly hydrophobic)

Figure 70. 14 s after drop placement on polymer saturated Berea sandstone (slightly oleophobic)

4.6 POLYMER CHARACTERISTICS

In all materials, the arrangement of molecules exists in three physical states: solid, liquid or gas. For polymeric materials, a glass transitioning temperature (T_g) is an important factor in determining the physical state of a polymer. It is defined as the temperature at which a polymer's molecules gain just enough energy to move freely and then changes the polymer's condition from brittle and "glassy" to softer and "rubbery." At room temperature, most polymers are in an amorphous solid state where molecules are randomly arranged with no repeating polymer chains. However, it is important to note that amorphous solid is not the same as crystalline solid where molecules are well arranged and structured with repeating polymer chains. At temperatures below the (T_g), the polymer becomes hard and brittle, like glass, where molecules do not inhibit enough energy to move. At temperatures above the (T_g), the polymer becomes soft and flexible, like rubber, where molecules inhibit enough energy to move freely.

For the PFA, (T_g) was reported by the manufacturer as -6 °C. At a very low temperature, the polymer is brittle and has a glassy condition. At high temperature, the polymer is softer and has a rubbery condition. However, the polymer has no crystalline contents and therefore it is believed to be in an amorphous solid state, which was confirmed in several ways:

(1) At room temperature, the PFA has a white color. But when stretched, it was apparent that the polymer was transparent but filled with small bubbles that made the polymer appear white.

(2) Using DSC (Differential Scanning Calorimeter) Test to observe the thermal transitions of the PFA when exposed to heat. The polymer had no evidence of a melting point transition up to 240 °C (Figure 71). Instead, it absorbed the increase

in temperature gradually with no distinct peak. This indicates the absence of a crystalline region in this completely amorphous polymer.

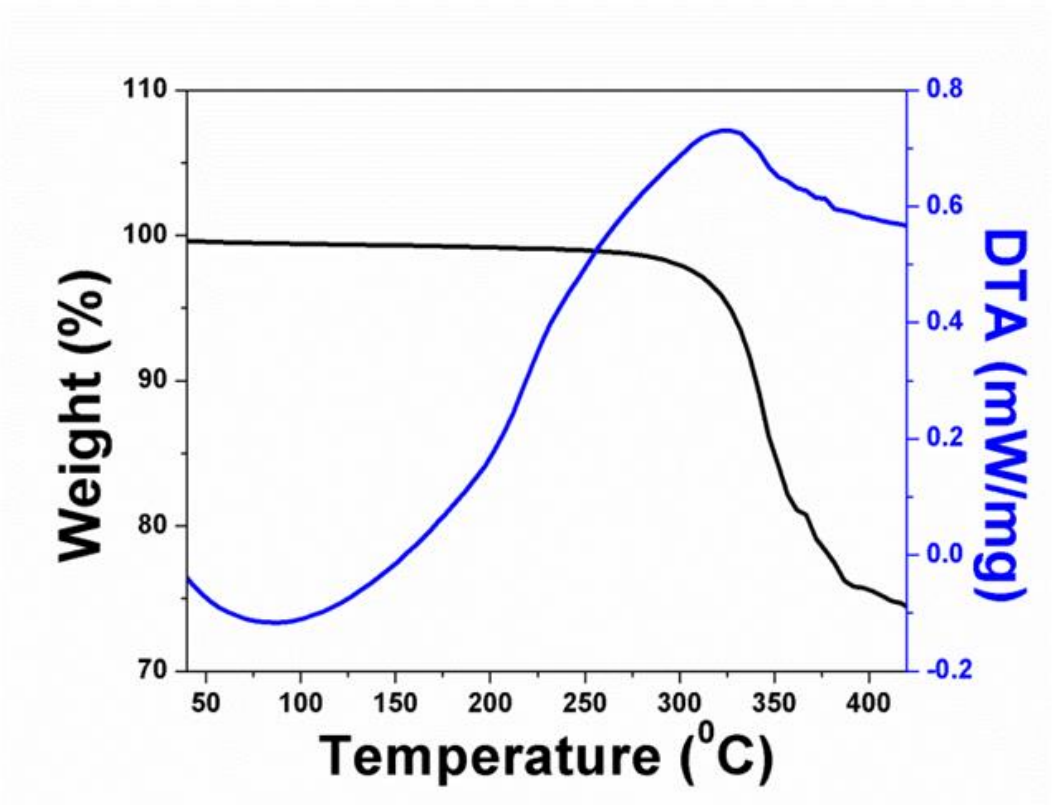

Figure 71. PFA Homopolymer DSC Test

5.0 CONCLUSION

The initial focus of this study was to improve mobility control by decreasing CO_2 mobility. In order to achieve this end, the PFA homopolymer has to increase the viscosity of CO_2 and maintain it throughout the flood front at a far distance from the wellbore. If the polymer comes out of the solution, then CO_2 viscosity will constantly decrease at the leading edge of the flood and the polymer will continuously precipitate behind the flood front. The following points are several conclusions drawn from that initial approach:

(1) Two independent viscosity measurements confirmed that the PFA is expected to increase the viscosity of CO_2 by (3-4) fold, which is directly related to a (3-4) fold increase in pressure drop (based on Darcy's law).

(2) Core flooding results on sandstones and limestone showed pressure drop increases that exceeded the (3-4) fold increase, which could not be attributed solely to an increase in the CO_2 viscosity. Therefore, the following factors contributed to the overall pressure drop increase:

   a. A portion of the dissolved polymer remained in the solution, flew through the core and increased the viscosity of CO_2.

   b. A portion of the polymer strongly adsorbed onto the surface of the core, altered its wettability (strongly hydrophobic and slightly

oleophobic), reduced its effective permeability and ultimately reduced its relative permeability.

c. A portion of the polymer weakly adsorbed onto the core and can be removed and re-dissolved in CO_2 solution by reversing CO_2 flow direction, increasing the pressure of CO_2 flowing into the core (especially with a "resting" period), increasing the velocity of the CO_2 flowing into the core or venting the core of CO_2.

(3) Due to the polymer adsorption and retention, the pressure drop across the core increased continually during polymer flooding, even as the concentration of the polymer in the CO_2 solution dropped rapidly.

(4) Several concerns associated with the use of the PFA for mobility control, include the polymer's solubility in light alkane CO_2-rich phase, its modest increase in the viscosity of CO_2, its low adsorption and retention, and its deep propagation into the core's formation.

(5) The initial results indicated that the PFA is an ineffective mobility control agent due to high rates of polymer loss, attributed to adsorption, and extreme reductions in permeability.

Following the conclusions associated with the pressure drop increase (a, b and c) highlighted above, it became evident that such a reduction in permeability would be more suitable in attaining conformance control than in attaining mobility control. In order to improve conformance control, the PFA homopolymer has to decrease the relative permeability of CO_2, resulting in a uniform flood front, at a short distance from the wellbore. When pure CO_2 is

injected, a thief zone with high permeability would dominate the flow and, therefore, have a high CO_2 saturation with irreducible water saturation. If the polymer is injected into that thief zone, the relative permeability of CO_2 will decrease such that the subsequent CO_2 flood will cause a much lower CO_2 relative permeability. The following points address the final conclusions drawn from the latter approach:

(6) The PFA homopolymer notably decreased the effective permeability of a single sandstone core to CO_2 (K_{e,CO_2}). However, the reductions of the effective permeability of a single limestone core to CO_2 were quite modest.

(7) In single and parallel sandstone and limestone cores, the PFA homopolymer induced drastic reductions in the effective permeability of a watered out core to water ($K_{e,w}$) and CO_2 (K_{e,CO_2}).

   a. The effective permeability reductions are significant for Berea sandstone, especially for CO_2: a 30-fold decrease in (K_{e,CO_2}) and an 8.9-fold decrease in ($K_{e,w}$).

   b. The effective permeability reductions are modest for Indiana limestone, especially for CO_2: a 1.6-fold decrease in (K_{e,CO_2})and a 9.7-fold decrease in ($K_{e,w}$).

(8) There is no concern with the PFA polymer coming out of the solution when light alkane concentrations become significant in CO_2-rich phase since the thief zones are depleted of oil; even if the polymer did precipitate it would enhance the conformance control.

(9) The PFA appears to be a novel CO_2-soluble conformance control agent because a portion of the PFA strongly adsorbs on the core surfaces and a portion is more weakly retained; together these PFA losses to the core can greatly reduce the permeability of a rock.

(10) There have been extensive studies conducted involving the use of CO_2-soluble polymers as a mobility control agent, but none involved their use as a conformance control agent. The PFA homopolymer may, however, be the first example of a CO_2-soluble conformance control agent that can be used to block high permeability oil-depleted thief zones and diverting subsequently injected CO_2 into low permeability oil-rich zones.

APPENDIX A

POLYMERIC CO_2 THICKENERS

Table 24. CO_2 Thickeners' Details from Literature Review Research

Researcher	**Heller**	**Zhang**	**Zhang**	**Bullen**	**Bae**	**McClain**
Abbrev.	-	PVEE	P1D	-	PDMS	PFA
Type	-	Polymer	Polymer	Copolymer	Polymer	Polymer
[wt.%]	0.24-1.1	0.6-0.8	0.5-0.8	1.5-3	4	3.7
[g/mol]	< 1000	3800	910	20,000-150,000	197,000	1,400,000
[psi]	1700-3100	2030-2900	2030-2900	1450–3625	4500	4500
[°C]	20-58	56	56	22	50	50
[Fold]	-	13-14	13-14	3-4	30	2.5

Table 25. CO_2 Thickeners' Details from Enick and coworkers Research

Researcher	**Enick**	**Enick**
Abbrev.	PolyFAST	PolyBOVA
Type	Copolymer	Polymer
[wt.%]	1-1.5	3.7
[g/mol]	540,000	1,400,000
[psi]	1885-2175	9300
[°C]	24	25
[Fold]	19	1.8

APPENDIX B

RELATIVE VISCOSITY CALCULATIONS

For a ball, sphere, with an area of $(\frac{\pi {d_b}^2}{4})$ and a volume of $(\frac{\pi {d_b}^3}{6})$

$$W - F_B - F_D = 0 \tag{1}$$

$$F_D = C_D A \frac{\rho {V_t}^2}{2} \tag{2}$$

Assuming (Re) is less than 1 (creeping flow), then

$$C_D = \frac{24}{Re} \tag{3}$$

$$Re = \frac{\rho V_t d_b}{\mu} \tag{4}$$

Substituting (3) and (4) into (2)

$$F_D = \left(\frac{24\mu}{\rho V_t d_b}\right)\left(\frac{\pi {d_b}^2}{4}\right)\frac{3\rho {V_t}^2}{2}$$

$$F_D = 3\pi\mu V_t d_b \tag{5}$$

Substituting (5) into (1)

$$(\frac{\pi {d_b}^3}{6})\rho_b - (\frac{\pi {d_b}^3}{6})\rho_f - 3\pi\mu V_t d_b = 0 \tag{6}$$

$$3\pi\mu V_t d = \left(\frac{\pi {d_b}^3}{6}\right)(\rho_b - \rho_f)$$

$$\mu = \frac{{d_b}^2(\rho_b - \rho_f)}{18V_t}$$

Since (d_b) is constant

$$\mu = K\frac{(\rho_b - \rho_f)}{V_t}, \text{ (K is negative)} \tag{7}$$

Assuming the dilute concentration of polymer does not affect fluid density of the two fluids (pure CO_2 solution and thickened CO_2 solution), then relative viscosity can be written as

$$\text{Relative Viscosity} = \frac{\mu_{sol}}{\mu_o} = \frac{\rho_s}{V_{t,sol}} * \frac{V_{t,o}}{\rho_s}$$

$$\text{Relative Viscosity} = \frac{\mu_{sol}}{\mu_o} = \frac{V_{t,o}}{V_{t,sol}} \tag{8}$$

BIBLIOGRAPHY

Alabdulkarem, A., Hwang, Y., R.Radermacher, & Maryland, U. o. (2012). New Energy Efficient CO2 Pressurization Strategies for Enhanced Oil Recovery Applications. *CMTC-151639*.

Bae, J., & Irani, C. (1993). A Laboratory Investigation of Viscosified CO2 Process. *SPE 20467-PA*.

Bae, J., & Irani, C. (1995). Viscosified CO2 Process: Chemical Transport and Other Issues. *SPE 28950-MS*.

Broseta, D., Medjahed, F., Lecourtier, J., & Robin, M. (1995). Polymer Adsorption/Retention in Porous Media: Effects of Core Nettability and Residual Oil. *SPE 24149*.

Bullen, R., Mzik, J., & Richard, J. (1987, Oct 20). *United States Patent No. 4,701,270.*

Doffin, J., Perrault, R., & Garnaud, G. (1984). Blood viscosity measurements in both extensional and shear flow by a falling ball viscometer. *Biorheology (Suppl. 1)*, 89–93.

Dupuis, G., Rousseau, D., Tabary, R., & Grassl, B. (2010). Flow of Hydrophobically Modified Water-Soluble-Polymer Solutions in Porous Media: New Experimental Insights in the Diluted Regime. *SPE-129884*.

Enick, R., & Olsen, D. (2012). Mobility and Conformance Control for Carbon Dioxide Enhanced Oil Recovery (CO2-EOR) via Thickeners, Foams, and Gels – A Detailed Literature Review of 40 Years of Research. *National Energy Technology Laboratory (NETL)* .

Enick, R., & Tapriyal, D. (2008). *Poly(vinyl acetate), Poly((1-O-(vinyloxy) ethyl-2,3,4,6-tetra-O-acetyl-β-D-glucopyranoside) and Amorphous Poly(lactic acid) are the Most CO2-soluble Oxygenated Hydrocarbon-Based Polymers* (Vol. 46). J. Supercritical Fluids.

Enick, R., & Xu, J. (2001). Thickening Carbon Dioxide with the Fluoroacrylate-Styrene Copolymer. *SPE 71497*.

Enick, R., Beckman, E., Huang, Z., Shi, C., & Kilic, S. (2000). Enhancement of the Viscosity of Carbon Dioxide Using Styrene/Fluoroacrylate Copolymers. *SPE, 33*(15), 5437-5442.

Enick, R., Dhuwe, A., Klara, A., Sullivan, J., Lee, J., Cummings, S., . . . Perry, R. (2016, May 20). Assessment of solubility and viscosity of ultra-high molecular weight polymeric

thickeners in ethane, propane and butane for miscible EOR. *Journal of Petroleum Science and Engineering*.

Enick, R., Lee, J., Cummings, S., Dhuwe, A., Beckman, E., University of Pittsburgh, . . . General Electric Global Research. (2014). Development of Small Molecule CO2 Thickeners for EOR and Fracturing. *SPE 169039-MS*.

Enick, R., Lee, J., Dhuwe, A., Cumming, S., Beckman, E., Dohetry, M., . . . McClendon, T. (2016, April 11-13). Polymeric and Small Molecule Thickeners for CO2, Ethane, Propane and Butane for Improved Mobility Control. *SPE-179587-MS*.

Enick, R., Xu, J., & Walschin, A. (2003). Thickening Carbon Dioxide With the Fluoroacrylate-Styrene Copolymer. *SPE*, 85-91.

Ennin, E., Grigg, R. B., Center, P. R., & Technolog, N. M. (2016, Jun 13-15). CO2 Flooding and Minimum Miscibility Pressure Study in Texas Farnsworth Field. *SPE-180854-MS*.

Ghahfarokhi, R., Pennell, S., Matson, M., Linroth, M., & Kinder, M. (2016, Apr 11-13). Overview of CO2 Injection and WAG Sensitivity in SACROC. *SPE-179569-MS*.

Heller, J., & Dandge, D. (1987, Feb 4–6). Polymers for Mobility Control in CO2 Floods. *SPE 16271*.

McClain, J., Betts, D., Canelas, D., Samulski, E., DeSimone, J., Landona, J., & Wignall, G. (1996). *ACS Mtg, Div. Polym. Mat.* New Orleans, LA.

Meister, J. J., Pledger Jr., H., Hogen-Esch, T. E., Butler, G. B., & Florida, U. (1980). Retention of Polyacrylamide by Berea sandstone, Baker dolomite, and sodium kaolinite During Polymer Flooding . *SPE 8981*.

Mungan, N. (1970). Water Flooding With Polymer Solutions . *SPE 3172*.

Ogunberu, A. L., & Asghari, K. (2005). Water Permeability Reduction Under Flow-Induced Polymer Adsorption. *JCPT*.

Pricharda, T. D., Thomasb, R. R., Kauschb, C. M., & Vogta, B. D. (2011, Feb 11). Solubility of non-ionic poly(fluorooxetane)-block-(ethylene oxide)-block-(fluorooxetane) surfactants in carbon dioxide. *The Journal of Supercritical Fluids*.

Rogers, J., & Grigg, R. (2000). A Literature Analysis of the WAG Injectivity Abnormalities in the CO2 Process. *SPE 59329*.

Rousseau, D., Renard, S., Prempain, B., Fejean, C., & Betoulle, S. (2012, April 14-18). CO2 Mobility Control With Dissolved Polymers: A Core-Scale Investigation Of Polymer-Rock and Polymer-Oil Interactions. *SPE 154055*.

Verma, M. (2015). Fundamentals of Carbon Dioxide-Enhanced Oil Recovery (CO2-EOR)—A Supporting Document of the Assessment Methodology for Hydrocarbon Recovery Using CO2-EOR Associated with Carbon Sequestration. *U.S. Geological Survey*.

Wallace, M., & Kuuskraa, V. (2014, Apr 7). Near-Term Projections of CO2 Utilization for Enhanced Oil Recovery. *(ESPA), Energy Sector Planning and Analysis, National Energy Technology Laboratory (NETL)*.

Wang, G., & Alabama, U. o. (1986, Apr 2-4). A Study of Crude Oil Comosition During CO2 Extraction Process. *SPE 15085*.

Zaitoun, A., & Chauveteau, G. (1998). Effect of Pore Structure and Residual Oil on Polymer Bridging Adsorption. *SPE 39674*.

Zaitoun, A., & Kohler, N. (1987). The Role of Adsorption in Polymer Propagation Through Reservoir Rocks. *SPE 16274*.

Zaitoun, A., Chauveteau, G., & Denys, K. (2002). New Insight on Polymer Adsorption Under High Flow Rates. *SPE 75183*.

Zaitoun, A., Zitha, P., & Chauveteau, G. (1995). Permeability-Dependent Propagation of Polyacrylamides Under Near-Wellbore Flow Conditions. *SPE 28955*.

Zhang, S., She, Y., & Gu, Y. (2011). Evaluation of Polymers as Direct Thickeners for CO2 Enhanced Oil Recovery. *Journal of Chemical and Engineering Data*.